WIND LOADS ON LOW-SLOPE ROOFS OF LOW-RISE AND MID-RISE BUILDINGS WITH LARGE PLAN DIMENSIONS

Murad Aldoum

A Thesis
In
The Department
of
Building, Civil and Environmental Engineering

Presented in Partial Fulfillment of the Requirements
for the Degree of Master of Applied Science (Building Engineering)
at
Concordia University
Montréal, Quebec, Canada

August 2018

© Murad Aldoum, 2018

i

CONCORDIA UNIVERSITY

School of Graduate Studies

This is to certify that this thesis prepared

By: Murad Aldoum

Entitled: Wind Loads on Low-slope Roof of Low-rise and Mid-rise buildings with
            Large Plan Dimensions

and submitted in partial fulfillment the requirements for the degree of

Master of Applied Science (Building Engineering)

complies with the regulations of the University and meets the accepted standards with
respect to originality and quality.

Signed by the final Examining Committee:

_____	Chair
Dr. A. Bagchi	
_____	Examiner
Dr. H. D. Ng	External (to program)
_____	Examiner
Dr. L. Tirca	
_____	Supervisor
Dr. T. Stathopoulos	

Approved by _____
            Dr. Fariborz Haghighat, GPD
            Department of Building, Civil and Environmental Engineering

            _____
            Dr. Amir Asif, Dean
            Faculty of Engineering and Computer Science

Date   _____

ABSTRACT

WIND LOADS ON LOW-SLOPE ROOFS OF LOW-RISE AND MID-RISE BUILDINGS WITH LARGE PLAN DIMENSIONS

Murad Aldoum

The present study examines wind loads on low-slope roofs of low-rise and mid-rise buildings with large plan dimensions (118 m) to investigate the suitability of wind provisions of the North American codes and standards to such buildings. Examination of such buildings is necessary since the wind provisions of the North American codes and standards were established based on wind tunnel studies involved in the determination of wind loads on buildings with common plan dimensions, i.e. less than 60 m.

The size of roof pressure zones and the magnitude of pressure coefficients on low-sloped roofs of low-rise and mid-rise buildings with large spans have been examined experimentally in the wind tunnel of Concordia University. Three building models were constructed at a length scale of 1:400 with identical plan dimensions (118 m x 118 m) and different heights (5 m, 10 m, and 20 m). The models were tested in simulated open country and suburban exposures for 7 wind directions: 0°, 15°, 30°, 45°, 60°, 75° and 90°. The pressure measurements have been presented in terms of contours of enveloped pressure coefficients, local pressure coefficients, and area-averaged pressure coefficients. The results of the current study have been compared with previous studies, full-scale data and the wind provisions of the North American codes.

It was found that the magnitude of external peak pressure coefficients recommended by ASCE 7-16 for low-slope roofs of low-rise buildings are much higher than the experimental findings and using those recommended by ASCE 7-10 is safe and more economical for large low-rise buildings.

iii

Also, for buildings of 8 m height or more, the corner zone should be sized according to ASCE 7-10 and NBCC 2015; and shaped based on ASCE 7-16.

Moreover, for large low-rise building with low heights, say 5 m, it was found that wind loads on the roof corner are approximately equal to those on the edge zone. Exceptions for low-rise buildings with large configurations and low-slope roofs are proposed for ASCE 7 and NBBC regarding roof pressure zones and the magnitude of cladding and components external peak pressure coefficients.

Acknowledgment

I would like thank Dr. Ted Stathopoulos for his valuable support and generous assistance during the last two years, it has been an honor to work under his supervision. This work would not have been completed without his superb guidance.

I cannot fully express my gratitude to my parents, brothers and sisters for their continuous support, generosity and encouragement to make this dream come true.

My gratitude to all my friends in Canada, UAE and Jordan for the motivation they provided to me during the Master program. Finally, I would be remiss if I did not mention my gratitude to my soulmate Hatem Alrawashdeh for his exceptional help.

To my father, Mohammed, and my mother, Alia.

TABLE OF CONTENTS

LIST OF TABLES

LIST OF FIGURES

xiv

LIST OF SYMBOLS

A_i — Tributary area of the ith pressure tap

a, z — End-zone width

B, L, D, W — Plan dimensions

C_e, K_z — Exposure factors

C_g, G — Gust factors

C_p — Mean pressure coefficient

$C_{p,A}(t)$ — Area-averaged pressure coefficient at instant (t) for tributary area (A)

$C_p C_g, GC_p$ — Peak pressure coefficients

$C_{pi}(t)$ — Pressure coefficient at instant (t) for the ith pressure tap

C_t, K_{Zt} — Topographic factors

g — Acceleration of gravity

H — Mean roof height

h — Eave height

I_u — Longitudinal turbulence intensity

I_w — Importance factor

K_e — Ground elevation factor

K_d — Directionality factor

L_u^x — Longitudinal integral length scale in the longitudinal direction

n — Frequency

N — Number of pressure taps

P	Static pressure
P_i	Wind-induced pressure on the ith pressure tap
P_o	Atmospheric pressure
q_z	Dynamic pressure at Height (Z)
R_e	Reynold's number
$R_u(\tau)$	Auto-covariance function of the fluctuation velocity
$S(n)$	Spectral density function for longitudinal component
u_*	Friction velocity
V	Basic wind velocity
$\bar{V}$	Mean wind velocity
$\bar{V}_g$	Mean wind velocity at gradient height
$\bar{V}_Z$	Mean wind velocity at height (Z)
$\bar{V}_{10}$	Mean wind velocity at height of 10 m
$\bar{V}'$	Wind velocity fluctuation
Z	Height from ground
Z_g	Gradient height
z_o	Roughness length
α	Mean speed exponent
β	Gust speed exponent
ρ	Air density
σ	Standard deviation

Ѳ   Wind azimuth

Chapter 1

Introduction

1.1 General

Wind is our friend and enemy at the same time. It is a friend when employed in energy production through wind turbines, at which the kinetic energy of wind is converted to mechanical power, which in turn is used to generate electricity. The installed power generation was greater than 440 GW in 2017, and it is anticipated to increase in 2020 and surpass 720 GW (Blaabjerg and Ma, 2017). Another advantage of the wind is its ability to diffuse the air pollutants produced by industrial factories through their chimneys away from the urban areas, which makes the breathed air healthy and pleasant. The wind has also been used, in the mists of the time, to assist sailors to move with their ships across seas and oceans.

On the other hand, the wind flow impacts buildings and structures and induces loads on their components, such as roofs and walls; and hits at the street level and may cause discomfort for the pedestrians. In these cases, the wind is an enemy and it should be accounted for in the design of buildings and other types of structures, as well as, in urban planning.

Design criteria for buildings vary depending on the height, whether it is a low-rise building or a high-rise building. In fact, the prediction of wind load patterns and magnitudes is more complicated for low-rise, because buildings with low heights are situated in the lower part of the atmospheric boundary layer where the wind velocity gradient, wind turbulence and wind flow unsteadiness are high.

Furthermore, most of the existing buildings around the world are low-rise buildings and wind damages of low-rise buildings cost a lot. This highlights the necessity and the importance of investigating the wind loads on low-rise buildings in order to provide safe and economical design for such buildings. Figure 1-1 presents roof damage of relatively new low-rise buildings in Tasmania caused by a wind storm in April 2017. Figure 1-2 shows severe roof damage of a gabled roof building caused by heavy winds in Chicago's Park, April 2016.

Figure 1-1: Roof damage of a new building due to a wind storm in Tasmania, April 2017 (http://www.abc.net.au/news/2017-04-27/the-roof-peeled-back-from-a-house-in-kings-meadows/8475332).

Figure 1-2: Large roof damage of gabled roof building caused by heavy winds in Chicago's Park, April 2016 (http://www.skylinenewspaper.com/wind-storm-rips-roof-from-apartment-building/).

1.2   Problem statement

Low-rise buildings are constructed widely with a regular plan size (up to 60 m or 200 ft) for residential, industrial and commercial purposes. However, numerous low-rise buildings are built with large plan dimensions (more than 60 m or 200 ft) for specific purposes at which large areas are required to satisfy the function of the building. Large buildings are constructed with low-slope roofs ($0° <$ slope $< 7°$) or flat roofs. Examples are grain storage buildings, commercial poultry breeding buildings, and large shopping centers. Most often, large low-rise buildings are constructed with low-slope roofs.

To design these types of low-rise buildings against wind loads, the structural designer should follow the guidelines and recommendations of the current codes and standards. However, wind provisions of the current codes and standards were established based on extensive wind tunnel studies concentrated on testing regular sized low-rise building models, and none of the studies had investigated the wind effects on low-rise buildings of large dimensions.

The necessity of examining wind loads on buildings of large plan dimensions arises since wind provisions of the North American codes were constructed based on studies conducted on buildings of regular size. An elaborated wind tunnel study should be conducted on large roof models to assess the suitability of wind provisions in the North American codes and standards for large low-rise buildings regarding the economic aspect and the structural safety.

1.3   Scope and objectives

The main scope of the present study is to compare the experimental findings of the present study with the North American codes and standards for low-slope roofs of low-rise and mid-rise buildings with large configurations. Detailed objectives of the present study can be summarized as follows:

1.   To compare the wind provisions of low-slope roofs of low-rise and mid-rise buildings in the North American codes, including ASCE 7-10, ASCE 7-16 and NBCC 2015; regarding the roof zonal systems and the recommended wind loads.

2.   To examine the spatial distribution of wind loads on low-slope roofs of low-rise and mid-rise buildings of large plan size.

3.   To evaluate local and area-averaged wind loads on low-slope roofs of low-rise and mid-rise buildings of large plan size.

4. To compare the experimental findings of the present study with the full-scale measurements of wind pressures on an experimental building of Duro-Last roofing Inc. in Iowa site carried out by NRC.

5. To compare the results of the present study with the recommended wind design provisions for low-slope roofs of low-rise and mid-rise buildings in ASCE 7-10, ASCE 7-16 and NBCC 2015.

6. To assess the suitability of roof zonal systems and design wind pressure coefficients of the North American codes and standards to low-slope roof buildings of large plan dimensions.

1.4 Outline

Chapter 2 presents the wind engineering basics including wind speed, atmospheric boundary layer, turbulence, wind spectrum, and boundary layer wind tunnel. Also, the contribution of past studies in the characterization and identification of the wind effects on buildings and structures is presented.

Chapter 3 introduces and compares the wind provisions of low-slope roofs in the North American codes: NBCC 2015, ASCE 7-10 and ASCE 7-16. The roof zonal systems of low-rise and mid-rise buildings provided by each code are presented, and the factors that contribute to the design pressure calculations are presented as well. Further, a comparison between the components and cladding pressure coefficients recommended by each code is presented.

In Chapter 4, the boundary layer wind tunnel of Concordia University is described in detail, and the simulation of terrain exposures in the wind tunnel is presented, as well as, the measurement techniques of wind speed and the characteristics of wind speed profile for each terrain exposure.

5

A full description of the building models is included. Also, the pressure measurement system used to record the wind pressures on the roofs of the models is described. In addition, the methodology followed to analyze the recorded wind pressures is described.

In Chapter 5, the results of the present study are presented in terms of contours of enveloped pressure coefficients, local pressure coefficients, and area-averaged pressure coefficients. Also, comparisons with previous studies and full-scale data are presented.

Chapter 6 presents comparisons between the results of the present study and the wind provisions of NBCC 2015, ASCE 7-10, and ASCE 7-16. The comparisons were performed for the area-averaged pressure coefficients for all the pressure zones specified by each code. Additionally, the spatial distribution of wind loads over the roof obtained from the present study was compared with the roof zonal systems of the North American codes.

Finally, Chapter 7 provides the concluded remarks of the present study and addresses future work recommendations.

Chapter 2

Literature review

2.1 Wind

Wind is the movement of air at large scales from high-pressure areas toward areas of low pressure. It is well known that the solar radiation received by earth surface is very high at the equator and decreases from the equator toward the poles. As a result, temperature differences occur, which in turn generate pressure gradients, which consequently cause movement of large air masses to form the atmospheric circulations or simply the "wind". This is the basic process at which the wind is generated, however, other factors contribute to wind configuration, including temperature changes during the four seasons, geological and topographic effects and rotation of the earth about its own axis. The latter affects the wind direction by causing a deflection in wind path to the right in the northern hemisphere and to left in the southern hemisphere, because of Coriolis force.

In literature, wind speed is best quantified using the well-known Beaufort scale. Table 2-1 presents the classification of wind according to wind speed range and the corresponding Beaufort number. Also, the description and the effect of wind are stated for each type, for instance, for Beaufort number 2, the wind is classified as a light breeze (1.1 - 2.3 m/s), at which the wind is felt on the face.

There is a confusion in winds names, however, wind can be divided into two main categories; planetary winds and periodic winds. Planetary winds are the air circulations which blow continuously all the year over continents and oceans, and include three types: trade winds, westerlies, and polar easterlies. Planetary winds are also called primary winds or permeant winds. Periodic winds blow at a particular time of the day or a particular season, such as land and sea breezes, mountain and valley breezes, hurricanes, tornados, and monsoons.

7

Table 2-1: Beaufort scale, after Baniotopoulos, C.C. et al. (2011)

Beaufort number	Description	Wind speed at 1.75 m height (m/s)	Effect
0	Calm	0.0 – 0.1	
1	Light air	0.2 – 1.0	No noticeable wind
2	Light breeze	1.1 – 2.3	Wind felt on face
3	Gentle breeze	2.4 – 3.8	Hair disturbed, clothing flaps, newspaper difficult to read
4	Moderate breeze	3.9 – 5.5	Raises dust and loose paper, hair disarranged
5	Fresh breeze	5.6 – 7.5	Force of wind felt on body, danger of stumbling when entering a windy zone
6	Strong breeze	7.6 – 9.7	Umbrellas used with difficulty, hair blown straight, difficult to walk steadily, sideways wind force about equal to forward walking force, wind noise on ears unpleasant
7	Near gale	9.8 – 12.0	Inconvenience felt when walking
8	Gale	12.1 – 14.5	Generally impedes progress, great difficulty with balance in gusts
9	Strong gale	14.6 – 14.1	People blown over by gusts

2.2   Wind engineering

Wind engineering is best described as the rational treatment of the interaction between wind in the atmospheric boundary layer and man and his works on the surface of earth (Cermak, 1975).

Wind engineering mainly concerns in evaluating wind-induced pressures on structures, hence, two elements are involved in calculating these loads; wind, a gaseous fluid, and structures. Therefore, fluid and structural mechanics are needed to comprehend wind engineering and understand the interaction between wind flow and civil engineering structures including buildings, chimneys, signboards etc., or mechanical engineering structures, such as planes and cars.

Naturally, wind flow near the earth surface is a turbulent flow because of exposure roughness, and the turbulence is magnified when the wind hits obstacles, such as buildings or trees and separates to cause extra unsteadiness in the wind flow regime, which in turn generates high fluctuating wind-induced pressures on structures. As a result, the wind flow regime becomes very complex and impossible to be quantified. This makes the evaluation of wind-induced pressures on buildings using computer models, which is known as computational fluid dynamics (CFD), untrusted. The best proxy to obtain reliable estimates of wind-induced pressures is accomplished by either full-scale measurements of wind pressures or testing building models in boundary layer wind tunnels since these techniques reflect and simulate the actual wind flow regime and its interaction with buildings.

Wind provisions in the current national codes and standards were formulated based on extensive wind tunnel experiments conducted on various types of structures.

2.3   Atmospheric boundary layer

In the 1870s, the English engineer William Froude conducted experiments in his laboratory by towing a thin plate in still water to figure out the effect of the frictional resistance of the moving

plate on the still water, Froude's work brought the concept of the boundary layer to the science field. The boundary layer term was introduced by the German scientist Ludwig Prandtl for the first time in 1905, after his extensive experimental work on low viscosity fluid flow to a solid boundary.

"In the atmospheric context, it has never been easy to define precisely what the boundary layer is. Nevertheless, a useful working definition identifies the boundary layer as the layer of air directly above the Earth's surface on time scale less than a day, and in which significant fluxes of momentum, heat or matter are carried by turbulent motion on a scale of the order of the depth of the boundary layer or less" (Garratt, 1994).

"While dealing with a flow, the latter is divided into two parts interacting on each other; on one side we have the "free fluid", which is dealt with as if it was frictionless, according to the Helmholtz vortex theorems, and on the other side the transition layers near the solid walls. The motion of these layers is regulated by the free fluid, but they for their part give to the free motion its characteristic feature by the emission vortex sheets" (Prandtl, 1905).

In other words, the atmospheric boundary layer may be simplified as the part of air circulation that passes directly above the earth surface, which is affected by the friction of the ground roughness to produce a layer of wind with a varying speed. The layer starts with almost zero wind speed at a point very near to the ground surface, i.e. height = 0, and ends with a value equal to the speed of the unaffected wind stream at a height far from the surface of the earth.

Figure 2-1 depicts the vertical mean wind speed profile in the atmospheric boundary layer. As shown, the mean wind speed is zero at the earth surface and increases exponentially with the height (Z) until the air stream is no longer influenced by the ground roughness at a height known as the gradient height (Z_G), and the mean wind velocity at the gradient height is called gradient velocity ($\bar{V}_{Z_G}$). Gradient height can be defined as the limit that separates the air flow affected by ground roughness and the free stream. Mean wind velocity above the gradient height is assumed to be constant and equals to the gradient velocity.
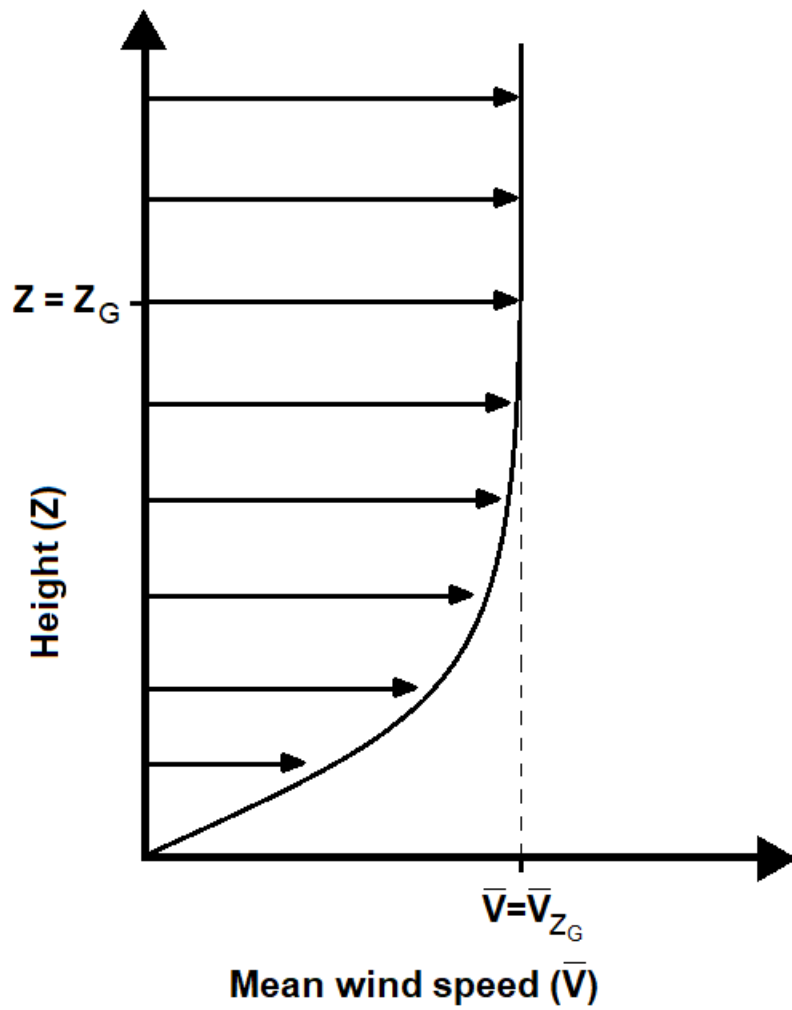
Figure 2-1: Vertical wind speed profile in the atmospheric boundary layer.

2.4 Wind velocity and turbulence in the atmospheric boundary layer

2.4.1 Wind velocity

As explained in the previous section, wind velocity in the atmospheric boundary layer varies with height up to the gradient height, therefore, atmospheric boundary layer could be visualized as a curve that shows the variation of wind velocity and bounded above by the gradient height and below by the earth surface.

Gradient height and variation of wind velocity depend on the ground roughness or the exposure. Exposure could be very smooth, i.e. oceans, or very rough, such as city centers and industrial areas. Wind velocity is estimated using the power law by some engineers - it is an empirical formula and has the following form for mean wind speed:

$$\frac{\bar{V}_Z}{\bar{V}_{Z_G}} = \left(\frac{Z}{Z_G}\right)^{\alpha} \tag{2.1}$$

where $\bar{V}_Z$ is the mean wind speed at height Z and α is the mean speed exponent, Table 2-2 presents typical values of parameters in the wind speed profile for different terrain exposures. The gust speed exponent β is used instead of α in equation 2.1 when the gust wind speed is concerned. It should be noted that both the gradient height and the speed exponent are higher for the rougher terrain exposure. This indicates that wind speed at height near the earth surface, say at 10 m, is higher in smooth terrain exposure than wind speed in rough terrain exposure.

Equation 2.2 presents the logarithmic law, which had been established based on physics and used widely by engineers and meteorologists to estimate the wind speed. The logarithmic law is valid in the bottom of the boundary layer (up to 30% of the atmospheric boundary layer).

$$\bar{V}_Z = 2.5 \cdot u^* \ln\frac{Z}{z_o} \tag{2.2}$$

where u^* is the friction velocity which is equal to $1 - 2\ m/s$ for extreme winds, and z_o is the roughness length which is defined as the height from earth surface at which the speed of the wind is no longer zero. Roughness length is a function of terrain exposure and higher for the rougher terrain.

Table 2-2: Typical wind speed profile parameters, from Stathopoulos and Baniotopoulos (2007).

Terrain category	Terrain description	Gradient height, Z_G(m)	Roughness length, z_o(m)	Mean speed exponent α	Gust speed exponent β
1	Open sea, ice, tundra, desert	250	0.001	0.11	0.07
2	Open country with low scrub or scattered trees	300	0.03	0.15	0.09
3	Suburban areas, small towns, well wooded areas	400	0.3	0.25	0.14
4	Numerous tall buildings, city centers, well developed industrial areas	500	3	0.35	0.2

2.4.2 Turbulence

"Turbulence is an irregular motion which in general makes its appearance in fluids, gaseous or liquid, when they flow past solid surfaces or even when neighboring streams of the same fluid flow past or over one another" Taylor (1937).

The turbulence in the atmospheric boundary layer results from frictional forces between wind flow and roughness of terrain exposure, as well as, the shear forces that developed within the flow itself; this is called mechanical turbulence. However, meteorological turbulence (convective air movements) contributes to the overall wind turbulence but it is minor at high wind speeds in the atmospheric boundary layer.

Wind turbulence is greater for the rougher terrain exposure, for instance, the turbulence of wind flow passes over urban terrain exposure is higher than turbulence of wind flow that passes over open country exposure. From the height aspect, turbulence decreases with height since the effect of ground roughness is mitigated as moving far from the earth surface.

Figure 2-2 shows the wind speed when recorded for 10 seconds in the wind tunnel of Concordia University at height of 5 centimeters in the wind tunnel scale. It can be observed that wind speed varies due to wind fluctuations caused by turbulence; the dashed line represents the mean wind speed over 10 seconds. As shown, wind speed at any instant is equal to the mean wind speed plus wind speed fluctuation V'. Furthermore, the maximum wind speed occurred over the 10 seconds is called gust peak speed within the 10 seconds.
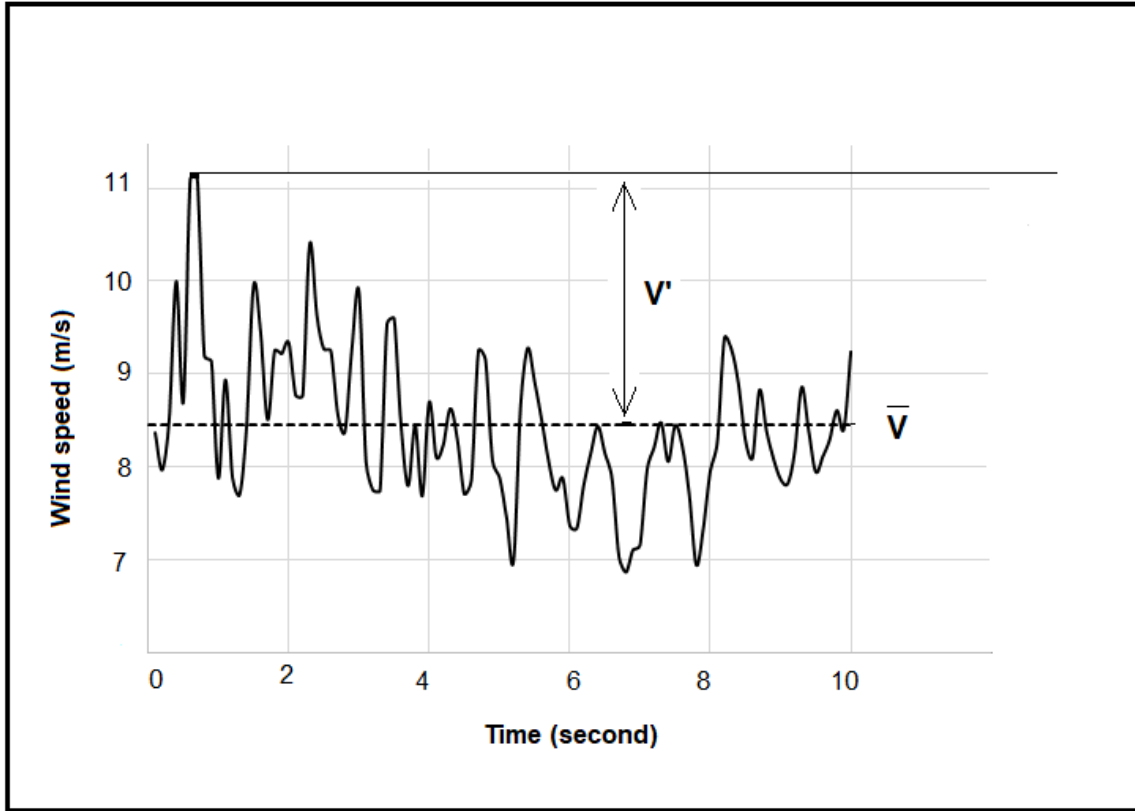
Figure 2-2: Wind speed recorded over a period of 10 seconds in the wind tunnel of Concordia University at height of 5 cm in the wind tunnel scale.

Wind turbulence can be quantified by the turbulence intensity which can be defined as the standard deviation value of the fluctuating speed with respect to the mean wind speed. Mean wind speed has three components when considered in the Cartesian coordinate; longitudinal (x) (parallel to wind direction), vertical (y) and lateral (z), the last two components are very small. Accordingly, vertical and lateral turbulence intensities may be negligible, whereas longitudinal turbulence intensity is major and takes the form of equation 2.3.

$$I_u(Z) = \sigma_u(Z)/\bar{V}_Z \tag{2.3}$$

where:

$I_u(Z)$: the longitudinal turbulence intensity at height Z.

$\sigma_u(Z)$: standard deviation of fluctuating velocity at height Z.

$\bar{V}_Z$: mean wind speed.

In addition to turbulence intensity, turbulent flow may be described by the gust size or the so-called integral length scale, which represents the average size of large vortices in wind flow. Integral length scale can be evaluated in three dimensions: longitudinal (parallel to wind direction), vertical and transverse. Gust size in vertical and transverse directions is very small, on the other hand, longitudinal integral length scale is significant and of great influence on the assessment of wind-induced loads on buildings and can be calculated in accordance with equation 2.4.

$$L_u^x = \frac{\int_0^\infty R_u(\tau)d\tau}{\sqrt{\bar{V}_Z^2}}$$
(2.4)

Where:

L_u^x: longitudinal integral length scale in the longitudinal direction.

$R_u(\tau)$: auto-covariance function of the fluctuation velocity.

"Theoretical analysis and prediction of turbulence have been, and to this date still is, the fundamental problem of fluid dynamics, particularly of computational fluid dynamics (CFD). The major difficulty arises from the random or chaotic nature of turbulence phenomena" (Celik, 1999).

Obviously, turbulence is very complicated and varies with place and time, therefore, it can not be quantified by deterministic equations, the available turbulence models are considered as approximations of the turbulence process. The absence of precise turbulence models makes Computational fluid dynamics (CFD) untrusted methodology to estimate wind loads.

2.5 Wind spectrum

Wind spectrum represents the frequency content of wind speed variations. Equation 2.5 presents the wind turbulence spectrum model of Von Karman, Von Karman spectrum gives a good description of wind turbulence spectrum in wind tunnels.

$$\frac{nS(n)}{\sigma^2} = \frac{4\frac{nL_u^x}{\bar{V}}}{\left(1+70.8\left(\frac{nL_u^x}{\bar{V}}\right)^2\right)^{5/6}}$$

2.5

where

n: frequency.

S(n): spectral density function for longitudinal component.

In addition, the following are proposed models of wind turbulence spectra:

- Kaimal's wind spectrum model:

$$\frac{nS(n)}{\sigma^2} = \frac{4\frac{nL_u^x}{\bar{V}}}{\left(1+6\frac{nL_u^x}{\bar{V}}\right)^{5/3}}$$

2.6

17

- Davenport's wind spectrum model:

$$\frac{nS(z,n)}{k\bar{V}_{10}} = \frac{4\left(\frac{nL_u^x}{\bar{V}_{10}}\right)^2}{\left(1+\left(\frac{nL_u^x}{\bar{V}_{10}}\right)^2\right)^{4/3}}$$

2.7

where $\bar{V}_{10}$ is the mean speed at 10 m height, k is the surface drag coefficient and L_u^x is the longitudinal integral length scale and can be approximated to 1200 m.

- Harris wind spectrum model:

$$\frac{nS(z,n)}{\bar{V}_{10}} = \frac{4\left(\frac{nL_u^x}{\bar{V}_{10}}\right)^2}{\left(1+\left(\frac{nL_u^x}{\bar{V}_{10}}\right)^2\right)^{4/3}}$$

2.8

Where L_u^x equals to 1800 m.

Figure 2-3 shows the full wind spectrum after the work of Van der Hoven (1957). In the figure, spectral density function is plotted versus frequency/period, and wind energy is observed in two main humps, the first is at period = 1 min, which is due to turbulence (wind gustiness) and the second at 4 days – this is associated to various weather systems. Between the two humps, there is a gap with low wind energy. This gap clearly distinguishes between mean speed and gusts. Also, if the averaging time for mean wind speed is specified to be between 10 min and 1 hr, stable values would be obtained. Furthermore, wind energy is high at a frequency of 0.01 Hz and attenuated significantly at frequencies greater than 1 Hz, which means that buildings with fundamental frequency more than 1 Hz would be subjected to negligible resonance, if any occurs.

2.6 Boundary layer wind tunnel

At the outset, wind effects on structures and machines were evaluated using aeronautical wind tunnels at which the tested model receives the same wind speed on all its components. This technique fails to estimate the actual wind effects on structures since it does not represent the actual wind flow above the earth surface. "The correct model test for phenomena in the wind must be carried out in a turbulent boundary layer, and the model-law requires that this boundary layer be to scale as regards the velocity profile" Jensen (1958). Eminent research of Jensen emphasized the need for more accurate simulation of natural wind in the atmospheric boundary layer, as opposed to using the uniform flow in aeronautical wind tunnels.

"Simulation of turbulence characteristics of the flow should include the intensities, probability distributions and spectra (both shape and scale) of the individual components of turbulence and their higher order correlations (Reynolds stresses)" Davenport and Isyumov (1967). Definitely, simulation of wind profile does not only mean to satisfy the similarity of vertical wind speed distribution in the wind tunnel and the natural wind, also, the turbulence characteristics should be similar as well.
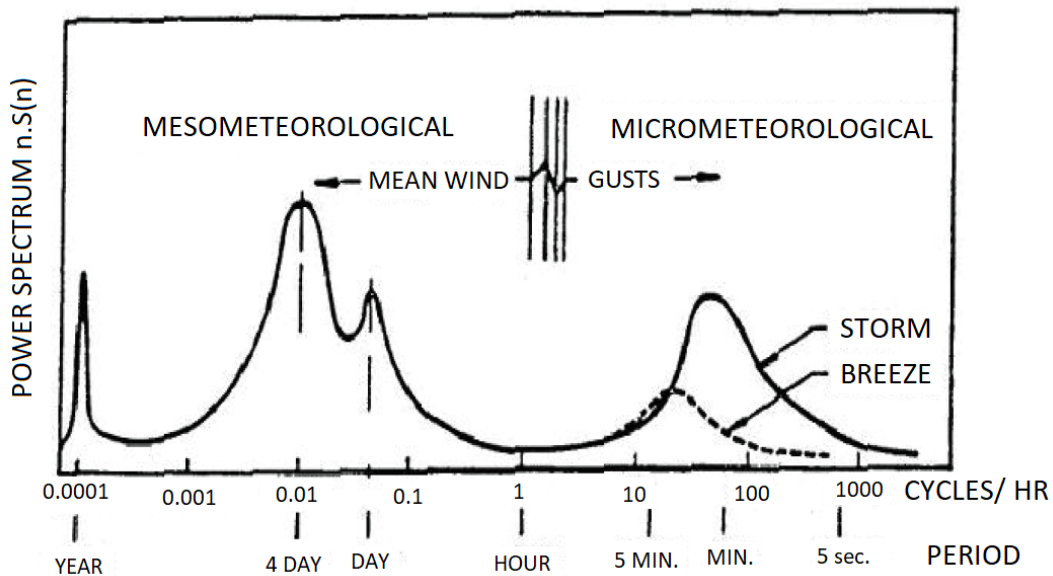
Figure 2-3: Wind spectrum after Van der Hoven (1957).

In all kinds of wind tunnels, whether it is closed-circuit or open-circuit, more advantage would be accounted for the longer wind tunnels, however, cost and space availability play a significant role in restricting the dimensions of wind tunnels. In order to have an effective wind tunnel, the distance from the wind blower to the testing section should be long enough to develop a wind flow at the testing section that would be representative to the full-scale flow. Also, the cross-section dimensions of the wind tunnel should be determined such that the frictional forces between wind flow and ceiling and both sidewalls would have negligible effects on the wind flow at the tested model.

Testing buildings in wind tunnels requires having a building model scaled with appropriate length scale factor, such that the length scale, time scale and velocity scale of the wind tunnel would satisfy the full-scale condition. Also, the terrain exposure should be simulated, and that can be achieved by furnishing the wind tunnel floor with suitable roughness elements. For instance, to simulate open country terrain exposure, the floor of the wind tunnel is furnished with a rough carpet to reflect the effect of an unobstructed land.

The function of Boundary layer wind tunnels is to produce realistic information about wind and wind effects on structures, such as wind pressure on buildings, wind speed, and wind patterns. The development of boundary layer wind tunnels has enriched the knowledge in wind engineering field and provided the structural engineers with the necessary information regarding wind loads to design safe and economic buildings.

2.7 Component and cladding wind loads on low-slope roofs of low-rise buildings.

A large percentage of the existing residential and industrial buildings are low-rise buildings, the height of which does not exceed 20 m (65 ft), and therefore, they are immersed in the bottom of the atmospheric boundary layer where the wind turbulence is extremely high. This fact indicates

the complexity of calculating wind loads of low-rise buildings. Furthermore, the variety of low-rise building shapes and sizes magnifies the difficulty of evaluating wind pressures on their components. "In several aspects, however, the determination of wind loads on low-rise buildings is more difficult than in the case of tall buildings. This is due to the variety of geometrical configurations of these buildings and their surroundings and to the increased turbulence and wind speed gradient to which they are exposed because of their low height" Stathopoulos (1982).

"Wind loads on components and cladding (C&C) are larger than those acting on the main structural system. Because of the combination of turbulence in the wind and the nature of building aerodynamics, high magnitude pressures can occur over the relatively small areas associated with building components. In contrast, the main structural system responds to pressures acting on multiple surfaces such that the highly-localized, intense pressure fluctuations are attenuated by the lack of full spatial and temporal correlations" Kopp and Morrison (2018).

2.7.1 Wind loads

It is very difficult to quantify the wind load in terms of a force at a specific point on a structure. Wind loads are calculated in terms of wind pressure at a certain area of the structure which can be defined as the wind-induced forces upon an area on a structure after the wind impacts the structure. According to Bernoulli's principle, for inviscid, steady and irrotational flow, the total pressure has the same value at any point within the wind flow (see equation 2.9).

$$P + \frac{1}{2}\rho V^2 + \rho g Z = constant \qquad\qquad 2.9$$

where ρ is the density of air, P is the static pressure, the middle term is known as the velocity pressure or the dynamic pressure, and the last term is called the elevation pressure.

Wind flow separates when it impacts sharp edges buildings known as bluff bodies in traditional aerodynamics. The separation happens at windward corners as shown in Figure 2-4, which presents wind flow around a rectangular building. This phenomenon divides the wind flow into two regions: the inner flow (wake) where the flow is viscous and the outer domain flow where viscosity has no

21

effects and Bernoulli's law is applicable. The two regions are separated by small vortices layer known as shear layer.

Dynamic pressure is zero at the middle of the windward wall, which produces, according to Bernoulli's equation, the maximum compressive pressure; this point is known as stagnation point. At the windward corner (point 2), the wind flow is accelerated, and the static pressure becomes lower than the static pressure at the stagnation point, i.e. negative pressure, to produce suction pressure at the corner.
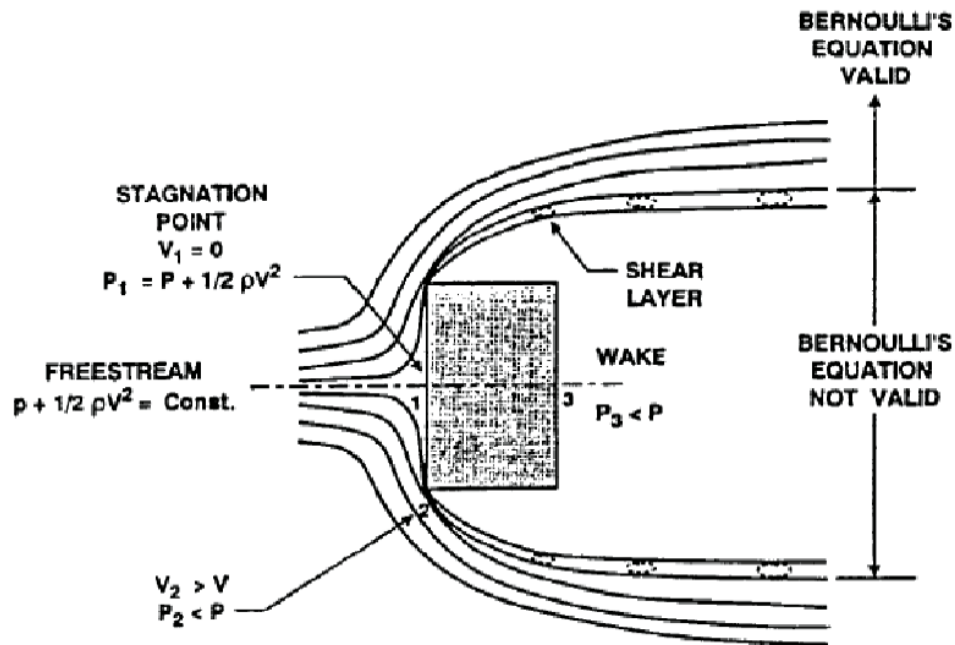
Figure 2-4: Flow around rectangular building, from Stathopoulos (2007).

In wind engineering and most of standards and codes of practice, e.g. ASCE 7, wind-induced pressures are presented using a dimensionless number known as pressure coefficient (C_P) which can be defined as the wind-induced pressure normalized with respect to the dynamic pressure of

the free stream. The wind-induced pressure is the difference between the pressure on the building and the atmospheric pressure. Based on Bernoulli's equation, the total pressure at a point in the free stream is equal to the total pressure at point 1 in Figure 2-4, and Bernoulli's equation becomes:

$$P + \frac{1}{2}\rho V^2 + \rho g Z = P_1 + \frac{1}{2}\rho V_1^2 + \rho g Z_1 \qquad 2.10$$

Considering the same level for the two points and knowing that the velocity is zero ($V_1 = 0$) at point 1 (stagnation point), Equation 2.10 becomes:

$$\frac{1}{2}\rho V^2 = P_1 - P = \triangle P \qquad 2.11$$

Finally, the pressure difference is normalized by the dynamic pressure of the free stream to obtain the pressure coefficient defined in Equation 2.12.

$$C_P = \frac{\triangle P}{\frac{1}{2}\rho V^2} \qquad 2.12$$

During wind flow and due to wind speed fluctuations, wind pressure varies accordingly, and two values of pressure coefficient are considered; mean pressure coefficient ($C_{P_{mean}}$) and peak pressure coefficient ($C_{P_{peak}}$), defined as follows:

$$C_{P_{mean}} = \frac{\triangle P_{mean}}{\frac{1}{2}\rho V^2} \qquad 2.13$$

$$C_{P_{peak}} = \frac{\triangle P_{peak}}{\frac{1}{2}\rho V^2} \qquad 2.14$$

2.7.2 Spatial distribution of wind loads on low-slope roofs of low-rise buildings.

Generally, as wind flow passes over a building, it produces suction pressures on its roof. High suctions occur at locations near flow separation because very high wind speeds and gradients are generated leading the wind pressure into extremely high negative pressure or suction (according to Bernoulli's equation).

For a rectangular building, wind separation happens at roof edges and corners. Consequently, large suctions occur on the areas near the windward edges and corners on the roof. On the other hand, low negative pressure is developed within the middle area of the roof. According to the wind flow nature over the roof, the pressure is assumed to be considered in three zones: corner zone, edge zone, and interior zone. Figure 2-5 shows the pressure zones on the roof with two different shapes: the L-shaped corner and the square corner. However, wind pressure is the highest in the corner zone, whereas wind pressure is high in the edge zone but lower than the pressure developed in the corner zone. The lowest wind pressure occurs in the interior zone.

The size of the pressure zones depends on the dimensions of the building, i.e. height, width, and length, and it is usually expressed as a fraction of the building dimensions. A recent study by Kopp and Morrison (2018) concluded that the roof pressure zones solely depend on building height for buildings with low-slope roofs, and the study was adopted by the ASCE 7-16. On the other hand, most of the previous studies concluded that the plan dimensions are significant factors; they affect the distribution of pressure on the roof and indeed affect the size of the pressure zones.

For curved buildings, such as circular tanks and chimneys, wind separation points are difficult to be located; they depend on a dimensionless parameter known as Reynolds number, R_e, (ratio of the inertia forces to the viscous forces in the fluid flow).
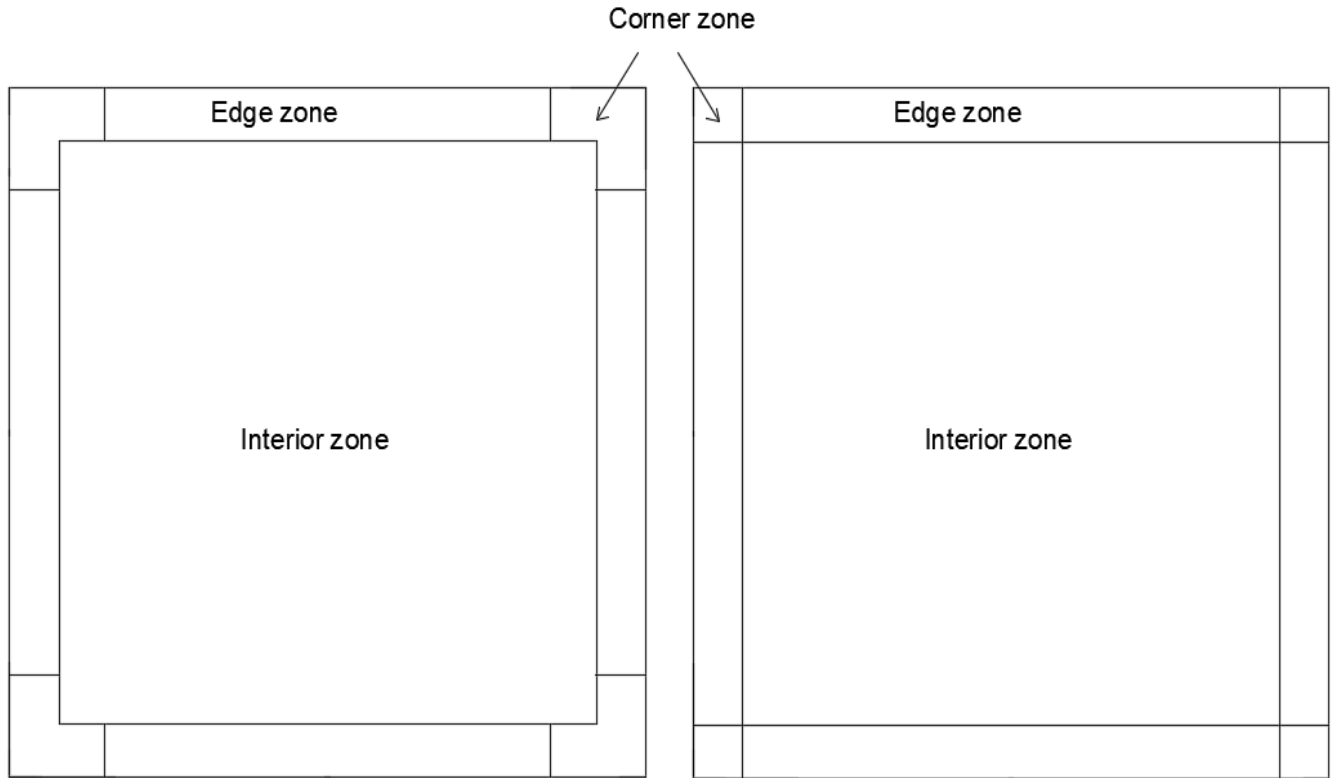
Figure 2-5: Roof pressure zones.

2.7.3 Previous research and studies

In the 1970s, a legendary and comprehensive research in the field of wind effects on buildings was performed in the boundary layer wind tunnel of University of Western Ontario. The credit basically returns to Alan Davenport, who constructed the wind tunnel and satisfied the necessary conditions for proper simulation of the turbulent atmospheric boundary layer. In 1979, Stathopoulos published his doctoral thesis "Turbulent wind action on low-rise buildings", a remarkable publication which created a basic source for codes and standards to formulate the provisions of wind loads. The current wind load provisions of North American building codes and standards are mainly based on Stathopoulos (1979). This section presents numerous studies conducted to investigate wind loads on low-rise building with low-slope or flat roofs.

25

Stathopoulos (1979) studied the wind loads on nine low-rise building models with different sizes and roof slopes under two terrain conditions in the wind tunnel at the University of Western Ontario. Stathopoulos (1979) used the pneumatic-averaging technique (Surry and Stathopoulos, 1978) to evaluate area-averaged wind pressures. This study provided adequate data for the codification of wind loads on low-rise buildings, including the magnitude of pressure coefficients and the size of roof pressure zones. It should be noted that, prior to this study, the size of roof pressure zones was used to be determined as a function of building width only, and Stathopoulos was the first researcher who considered the building height as an important factor that should be taken into account when determining the roof pressure zones.

Stathopoulos and Surry (1983) investigated the scaling effect on wind load measurements on low-rise buildings. The study concluded that a change in building model scale with a factor of 2 would result in a 10% error in the measured data. State-of-the-art papers and reviews of wind loads on low buildings have been published by many researchers, e.g., Stathopoulos (1984), Holmes (1993), Krishna (1995), Kasperski (1996) and Uematsu and Isyumov (1999). Stathopoulos (1984b) presented wind pressure measurement techniques and highlighted the important factors on wind loads and wind tunnel experiments, e.g., geometric scale, building height, terrain exposure…etc.

"There has been some controversy in wind engineering about the magnitude of pressure coefficients measured on flat roof edges and corners" Stathopoulos (1987). Studies showed differences in the magnitude of pressure coefficients on flat roof edges and corners, some studies resulted in high pressure coefficients, e.g. Kind and Wardlaw (1979), and other studies on low pressure coefficients, e.g. Stathopoulos et al (1981). Researchers suggested two explanations for these discrepancies: the first is that each study was conducted under different simulation conditions and the other explanation is the different location of pressure taps in the roof of the model.

The latter explanation was investigated by Stathopoulos (1987). The study used a distinctive flat roof model with a length scale of 1:400 equipped with 224 pressure taps distributed extensively on corner and edge zones in four rows. The first row of pressure taps, unlike the location of taps in the conventional models, was very near to the leading edge (0.54 mm). The model was tested at

the wind tunnel of Concordia University in a simulated open country exposure with power law exponent of 0.15. Stathopoulos (1987) concluded that the location of pressure taps with respect to the leading edge is very important, and pressure coefficients measured for oblique wind direction on edge and corner zones are higher in the order of 2 and 3 times than those evaluated using models equipped with pressure taps in conventional location.

Cochran and Cermak (1992) conducted wind tunnel experiments on two models of Texas Tech University (TTU) experimental building in the wind tunnel of Colorado State University. The TTU experimental building is a gabled roof low-rise building with a small roof slope of 1:60, the dimensions of the building are 9.8 m x 13.7 m x 4 m. The geometric scales used to construct the models were 1:50 and 1:100 and the resulted data were compared with full-scale measurements of TTU experimental building. The results of this study showed that mean pressure coefficients measured on both models agree well with the full-scale data, however, discrepancies arise when the peak suction values are compared with the full-scale data. In addition, Cochran and Cermak (1992) noticed a reduction in peak suction pressures when the larger model (model of 1:50 length scale) is considered. This was due to the lower turbulence intensity at the eave height of the larger model.

Lin et al (1995) conducted wind tunnel experiments on five flat and nearly flat roof models, three of which having three different heights (4, 8, 12 m) and the same plan dimensions (40 m X 40 m), while the other two were models of the TTU experimental building, one of them was a flat roof model, and the other was constructed with 1:60 roof slope. All the models were fabricated at a length scale of 1:50.

Results of Lin et al (1995) showed a good agreement with full-scale data in the mean values of pressure coefficients, however, differences appear when comparing peak pressure coefficients with respective full-scale data. The authors of this study referred these differences to the size of taps, turbulence level, scaling effects, and geometrical details. Generally, as shown in Figure 2-6, data of Lin et al (1995) exhibit better agreement than those of Cochran and Cermak (1992) with the full-scale data of TTU experimental building.

In the evaluation of the most critical wind loads, Lin et al (1995) found that the critical wind direction is 30° (± 5°), considering 0° as the wind direction perpendicular to the leading edge, and by symmetry 60° (± 5°). Furthermore, Lin et al (1995) set no limitation for wind load on the corner of flat roofs. However, the study concluded that the suction pressures are very high on the corner and area average suction pressure decreases as the considered tributary area increases.

Lin and Surry (1998) studied the distribution of wind load on flat roofs of low-rise buildings. The study concluded that the size of roof pressure zones is independent of the plan dimensions of the building, and the size of pressure zones should be related to the height of the building (H). Also, pressure coefficients on the corner zone should be referred to tributary area normalized with respect to H^2. Furthermore, area-averaged pressure coefficients on the corner zone decrease to half beyond a tributary area of 0.1H x 0.1H.

Extensive experiments were carried out in the wind tunnel of the University of Western Ontario to enrich the aerodynamic database of the National Institute of Standards and Technology (NIST). The UWO contribution to the NIST aerodynamic database for wind loads on low buildings was published in three parts: part 1, Ho et al (2005), presents the aerodynamics data, part 2, Pierre et al (2005), includes comparisons with wind provisions in codes and standards, and part 3, Oh et al (2007), provides a detailed study about internal pressures.
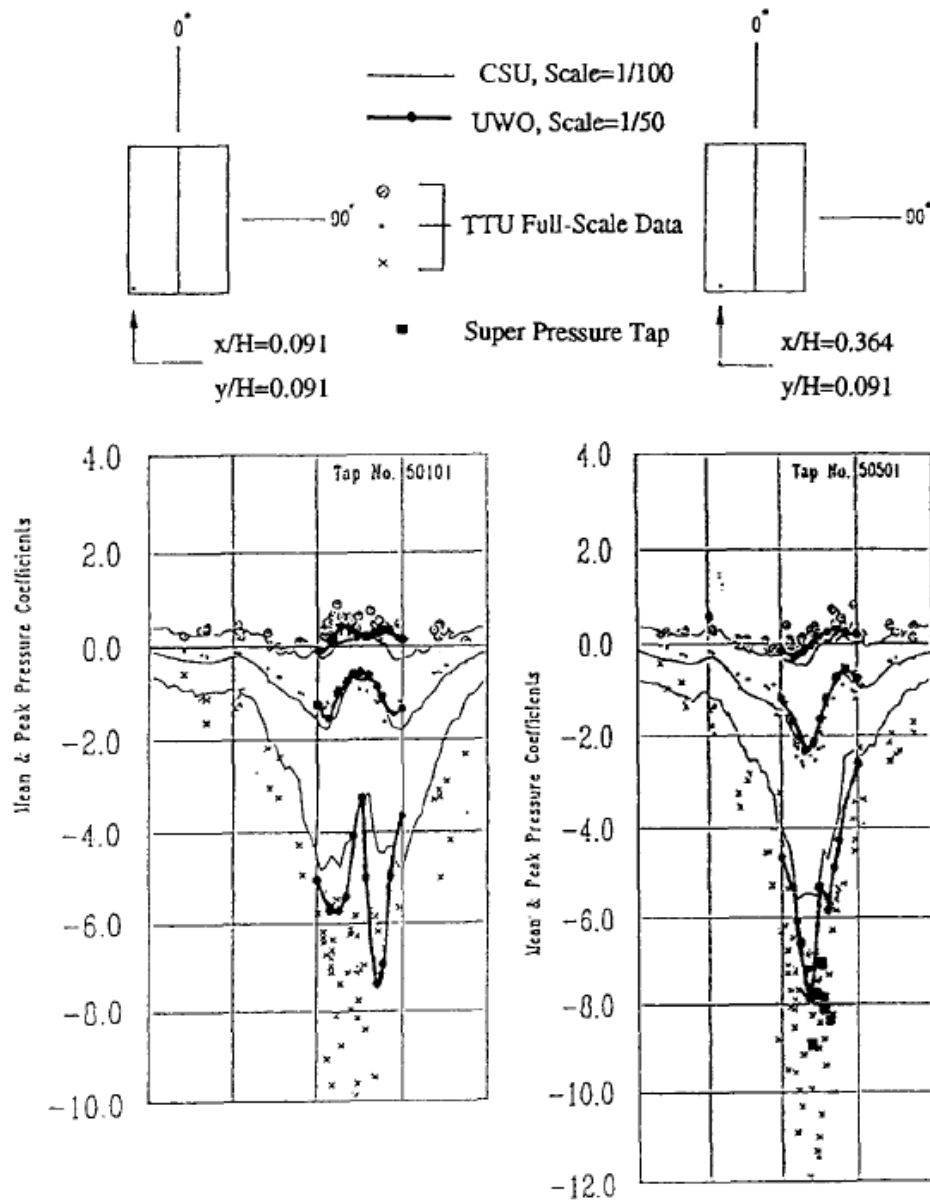
Figure 2-6: Comparison between experimental results of Cochran and Cermak (1992) CSU and Lin et al (1995) UWO with full-scale data of TTU experimental building.

Alrawashdeh and Stathopoulos (2015) was the first study that examined wind loads on buildings with large configurations. The study investigated the effect of wind on flat roof edges and corners of low-rise buildings with large plan dimensions. Nine building models were tested at the wind tunnel of Concordia University in a simulated open country exposure. Each model was constructed

at a length scale of 1:400 with a square flat roof, and the corresponding full-scale plan dimensions of the models were 60 m, 120 m and 180 m. Also, three heights were considered: 5 m, 7.5 m, and 10 m. The experimental results of this study were compared with the American Society of Civil Engineers Standard (ASCE 7-10), the National Building Code of Canada (NBCC 2010), the European Standard (EN 1994-1-4, 2005), and the Australian/New Zealand Standard (AS/NZS 1170.2, 2011).

Alrawashdeh and Stathopoulos (2015) focused on the size of edge and corner zones of roofs of low-rise buildings with large plan dimensions. The study concluded that the size of corner and edge zones for large low-rise buildings of height less than 8 m should not be governed by the condition of 4% of the least horizontal plan dimension (as recommended By ASCE 7-10 and NBCC 2010) but it should be limited to 80% of the building height. The use of the 4% condition of the least horizontal plan dimension may lead to conservative and uneconomic design. Also, the study concluded that the external pressure coefficients in ASCE 7-10 and NBCC 2010 are adequate to be used in the design of large roofs of low-rise buildings.

Kopp and Morrison (2018) examined component and cladding wind pressures on low-slope roofs of low-rise buildings. The study focused on the spatial distribution of wind pressures and the magnitude of pressure coefficients on roofs. The study investigated the wind loads on many building models with gabled roofs in the boundary layer wind tunnel II at the University of Western Ontario under simulated open country terrain exposure and suburban terrain exposure, roof slopes of all models were less or equal to 1:12. Experimental results acquired by Ho et al. (2005) were used in the study of Kopp and Morrison (2018).

The study of Kopp and Morrison (2018) concluded that the components and cladding external pressure coefficients recommended by ASCE 7-10 for low-rise buildings with low-slope roofs are lower than the enveloped area-averaged pressure coefficients obtained by their wind tunnel experiments. In addition, the study showed that the size of pressure zones depends on the building height only, unlike ASCE 7-10 provisions in which the size of pressure zones is defined as a function of height and least plan dimension of the building and recommended an L-shaped corner

zone instead of the square corner zone in ASCE 7-10. Furthermore, in regard of the effect of terrain exposure, it was stated "Both the magnitude of the coefficients, and the spatial distribution can be compared and careful examination indicates that both the magnitude and distribution of the coefficients are similar, noting slight variations in the coefficients because of the turbulence levels and the stochastic nature of peak pressures".

Kopp and Morrison (2018) results were adopted by ASCE 7 by increasing the magnitude of components and cladding external pressure coefficients of low-rise buildings with low-slope roofs, as well as, by modifying the size and the shape of pressure zones for the same type of buildings in ASCE 7-16.

Chapter 3

The North American Wind Codes and Standards

"Wind loading provisions included in the Commentaries of the National Building Code of Canada (NBCC 1995, 2005, 2010) are indeed pioneering whereas the American National Standard ASCE 7-10 (2010) is now considered one of the best in the world, since it incorporates the major research findings in the area of wind building interaction" (Tamura and Kareem, 2013).

This chapter introduces the wind provisions in the North American codes for the roofs of low-rise and mid-rise buildings. It explains the difference between low-rise and mid-rise buildings, it describes the roof zonal systems of ASCE 7-10, ASCE 7-16 and NBCC 2015; and it provides a description of the methodology adopted by the codes to calculate the wind design pressures.

3.1 Low-rise and mid-rise buildings

Height of buildings is a significant factor in the determination of the developed wind-induced pressures on the roof of the building, and it is well known that the taller the building the higher the wind loads acting on its roof. In the North American codes, buildings can be classified in the low-rise category or mid-rise category according to the mean roof height of the building. Based on ASCE 7-10 and ASCE 7-16, a building is addressed as a low-rise building if the building height is less or equal 18 m (60 ft), whereas height limit that separates the low-rise and mid-rise categories in NBCC 2015 is 20 m (65.6 ft). Buildings of heights greater than the mentioned limits are treated as mid-rise buildings. In fact, there is no clear upper limit for mid-rise buildings in the North American codes, however, NBCC 2015 considers buildings with 20 m < H < 60 m as mid-rise buildings for the design of main structural systems, (NBCC 2015 commentary).

Wind provisions that govern the two categories are different; higher wind loads are assigned for mid-rise buildings, as well as, the areas specified for high wind pressures on the roof corners and edges are larger.

3.2 Roof zonal systems of low-slope roof buildings

Wind loads specified by the North American codes for low-slope roofs are provided for three or four pressure zones. Pressure zones divide the building roof into areas according to the variation of wind loads on the roof; the highest wind loads occur in the roof corner on an area known as the corner zone, and high wind loads occur on areas near the roof edges, the edge zones; however, wind loads on edge zones are normally lower than those developed on the corner zone. Low wind loads occur on the middle area of the roof which is called interior zone. Figure 3-1 presents roof zonal systems of the North American Codes for low-slope roofs of low-rise and mid-rise buildings.

For low-rise buildings with small roof slope, ASCE 7-10 and NBCC 2015 provide similar roof zonal systems, see Figure 3-1.a, where the roof is divided into three zones: square corner zone, edge zone and interior zone. The size of corner and edge zones, z, which is also known as the end-zone width, depends on building height and plan dimensions, such that "z is the lesser of 10% of the least horizontal dimension and 40% of height, but not less than 4% of the least horizontal dimension or 1 m" (NBCC 2015). The low-slope roof zonal system of the NBCC 2015 and ASCE 7-10 was basically suggested by Stathopoulos (1979) assuming that the end-zone width, z, is the distance at which the wind pressures drops to 70% of the worst value.

On the other hand, the roof zonal system of ASCE 7-16 for low-slope roofs of low-rise buildings is independent of the plan dimensions, and the size of pressure zones is solely dependent on the building height, as shown in Figure 3-1.b. Also, there are four pressure zones: L-shaped corner zone (zone 3), edge zone (zone 2) and two interior zones (zone 1 and zone 1'). This roof zonal system has been adopted by ASCE 7 after the work of Kopp and Morrison (2018). The size of the long side of zone 3 is 60% of the building height and the short side is 20% of the building height as well.

The roof zonal system of mid-rise buildings in NBCC 2015, ASCE 7-10 and ASCE 7-16 is presented in Figure 3-1.c. ASCE 7-10 and ASCE 7-16 provide similar roof zonal system for mid-rise buildings which exclusively depends on the least horizontal dimension, where "a = 10% of the least horizontal dimension, but not less than 3 ft (0.9 m)" ASCE 7-16. On the other hand, the distance, a, in NBCC 2015 is defined as 10% of the larger horizontal dimension.
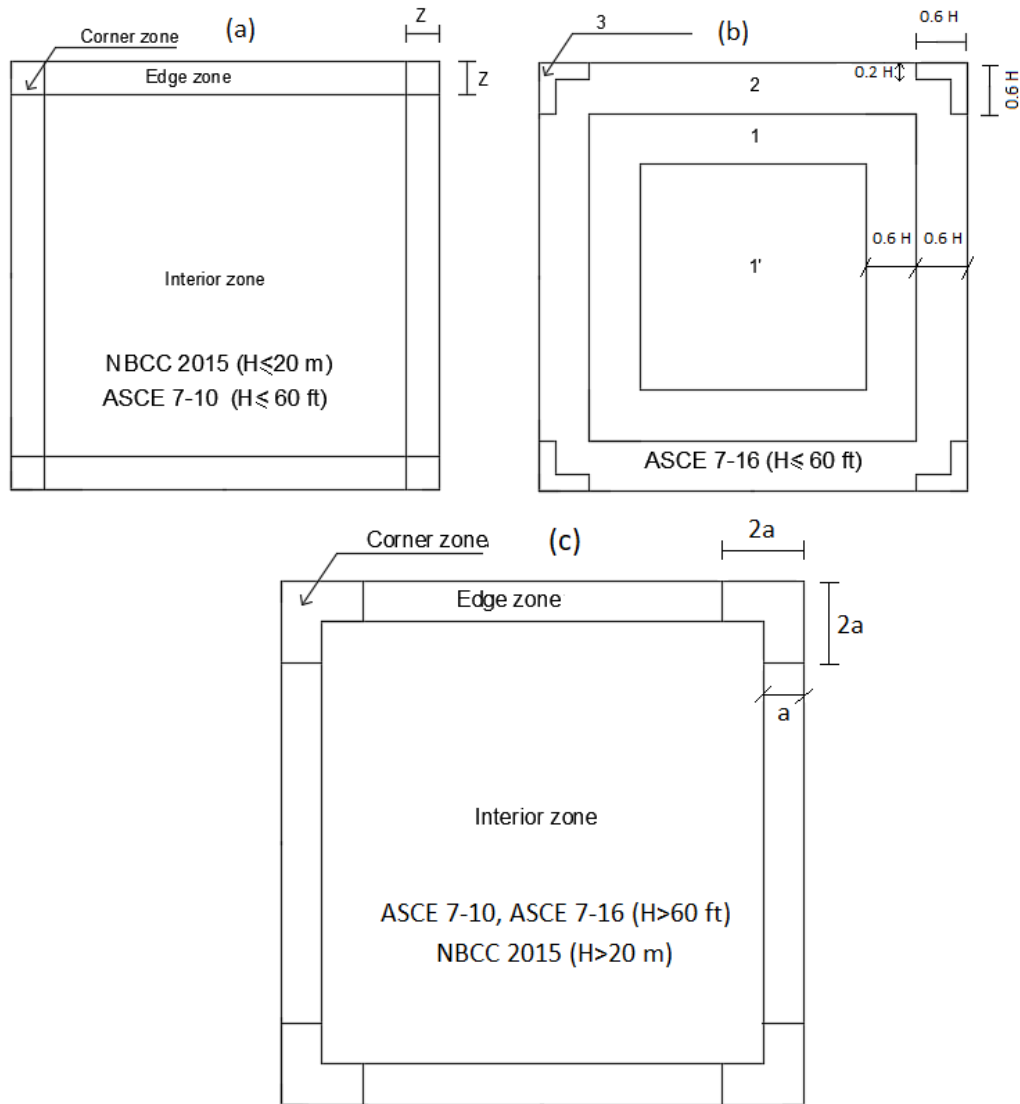
Figure 3-1: Roof zonal systems for low-slope roofs of low-rise and mid-rise buildings in the North American codes: (a) low-rise building in NBCC 2015 and ASCE 7-10, (b) low-rise building in ASCE 7-16 and (c) mid-rise building in the three codes.

34

3.3 Design pressure calculation

Design pressures are calculated in the North American codes based on many parameters. The first parameter is the peak pressure coefficients assigned for the building component in concern, such as a cladding panel at the roof corner, which is given as a function of the tributary area in the wind provisions of the codes.

The second one is the dynamic pressure provided for the region at which the building is located in, which depends and meteorological records and statistics. In addition, other parameters contribute to the calculation of design pressures, including directionality factor, topographic factor, ground elevation factor, and exposure factor.

Based on ASCE 7-10, ASCE 7-16 and NBCC 2015 and neglecting the internal pressures; design wind pressures are calculated according to Equations (3-1), (3-2) and (3-3), respectively.

$$P = \frac{1}{2}\rho V^2 K_z K_{zt} K_d G C_P \qquad (3\text{-}1)$$

$$P = \frac{1}{2}\rho V^2 K_z K_{zt} K_d K_e G C_P \qquad (3\text{-}2)$$

$$P = q I_w C_e C_t C_P C_g \qquad (3\text{-}3)$$

Where:

ρ: Air density

V : Basic wind velocity

K_z and C_e: Exposure factors

K_{zt} and C_t: Topographic factors

K_d: Directionality factor

K_e: Ground elevation factor

$q = \frac{1}{2}\rho V^2$: Velocity pressure

G and C_g: Gust factors

C_P: Mean pressure coefficient

GC_P and $C_P C_g$ refer to peak pressure coefficients in the North American codes, and they are provided as one unit for design components and cladding.

Each of the previously mentioned factors has been included in the design pressure equations to yield safe and economic values of design pressures. Peak pressure coefficients, $C_P C_g$, of the North American codes were enveloped among all wind directions; in other words, the peak pressure coefficients of the codes represent the most critical load values developed when the wind blows from the most critical wind direction. However, the odds of having the most critical wind speed striking from the most critical wind direction are near null, and this raises the necessity of the directionality reduction factor, K_d. The directionality factor appears in the equation of design pressure of ASCE 7, and it has a value of 0.85 for the design of building components and cladding. On the other hand, peak pressure coefficients of NBCC have been already attenuated to account for the effect of directionality, and that is why the directionality factor doesn't appear in the design pressure equation of NBCC 2015.

In addition, peak pressure coefficients of the North American codes were calculated for a 30 ft height building (10 m height building in NBCC 2015) in open country exposure. The exposure factors, K_z and C_e, account for the variation of wind loads with the building height, as well as, the terrain exposure. Exposure factors are higher for the higher buildings since mean wind loads

increase with building height and they are indeed lower for rougher terrains, since the wind speed is reduced as the terrain roughness increases.

Furthermore, topographic factors, K_{zt} and C_t, are used to adjust for the increment of wind speed if hills, ridges or escarpments are near the building. Finally, ground elevation factor, K_e, is a new factor which has been added in ASCE 7-16 to account for the change of air density, although it is allowed to consider $K_e = 1$ for all elevations. More information about wind load factors and coefficients in codes is available in Davenport (1983) and Stathopoulos (2003).

3.4 Component and cladding pressure coefficients

Cladding and component peak pressure coefficients are presented in the North American codes as a function of tributary area. Values provided in ASCE 7-10 and ASCE 7-16 are based on velocity averaging time of 3s, whereas peaks provided in NBCC 2015 are based on 1 hr velocity averaging time. Appendix A presents all the curves of components and cladding peak pressure coefficients in the North American codes for roof design.

Figures 3-2 and 3-3 present cladding and component peak pressure coefficients of NBCC 2015, ASCE 7-10 and ASCE 7-16 for low-slope roofs of low-rise and mid-rise buildings, respectively. Peaks of ASCE 7-10 and ASCE 7-16 were modified to be comparable with NBCC 2015 and the experimental results of the present study by using mean hourly velocity pressure and considering the directionality, topographic and ground elevation factors.

According to ASCE 7-10 and ASCE 7-16, directionality factor, K_d , is equal to 0.85 for the design of cladding and components of buildings, whereas topographic factor, K_{zt} , and ground elevation factor, K_e, are equal to 1. Furthermore, and based on Durst curve, the ratio of wind speed averaged over 3 seconds to the wind speed averaged over 1 hr is equal to 1.525.

For example, the maximum external peak pressure coefficients on zone 3 of ASCE 7-16 is equal to -3.2; then, this coefficient should be multiplied by the directionality factor, topographic factor,

ground elevation factor (for ASCE 7-16) and the square of the wind velocity conversion factor as follows:

$$CpCg_{modified} = (1.525)^2 K_d K_{zt} CpCg_{ASCE\ 7} \qquad (3\text{-}4)$$

$$CpCg_{modified} = (1.525)^2 * 0.85 * 1 * (-3.2) = -6.3 \qquad (3\text{-}5)$$

It should be noted that wind provisions provided for mid-rise buildings in ASCE 7-10 and ASCE 7-16 are identical; they both provide the same peak pressure coefficients and the same zonal systems.

The building of 20 m height is classified as a low-rise building according to NBCC 2015 (H ≤ 20 m). On the other hand, based on ASCE 7-10 and ASCE 7-16, the 20 m (65 ft) height building is a building with intermediate-height. However, the results of the present study, as it will be demonstrated in the following chapters, imply that the provisions of NBCC 2015 for low-rise buildings are inadequate to provide a safe design for the 20 m height building, thus it should be treated as an intermediate-height building.

In fact, NBCC 2015 does not provide graphs for peak pressure coefficients versus tributary area for mid-rise buildings, and it presents wind loads in terms of mean pressure coefficients in each pressure zone. Figure 3-4 shows mean pressure coefficients and pressure zones of NBCC 2015 for buildings with heights greater than 20 m. For the design of cladding and components, the gust factor, Cg, in NBCC 2015 is equal to 2.5.
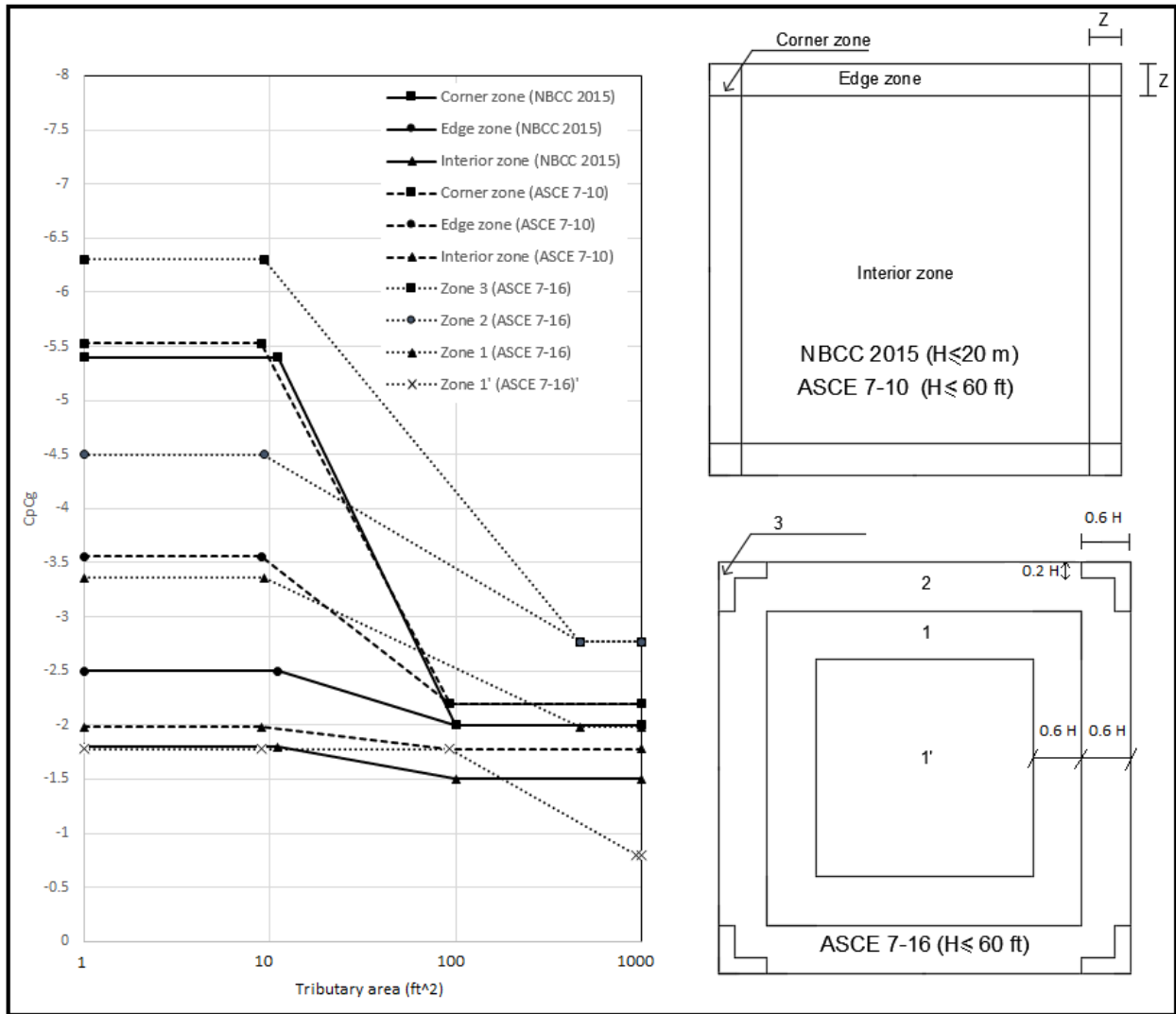
Figure 3-2: External peak pressure coefficients (NBCC format) of the North American codes and standards for low-slope roofs of low-rise buildings (H ≤ 18 m).
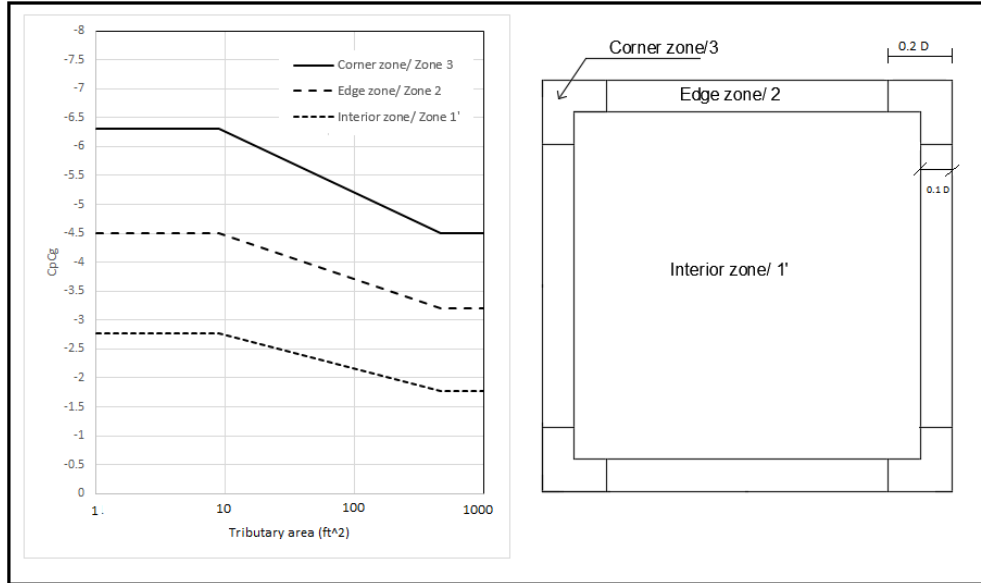
Figure 3-3: External peak pressure coefficients (NBCC format) of the ASCE 7-10 and ASCE 7-16 for roofs of mid-rise buildings.
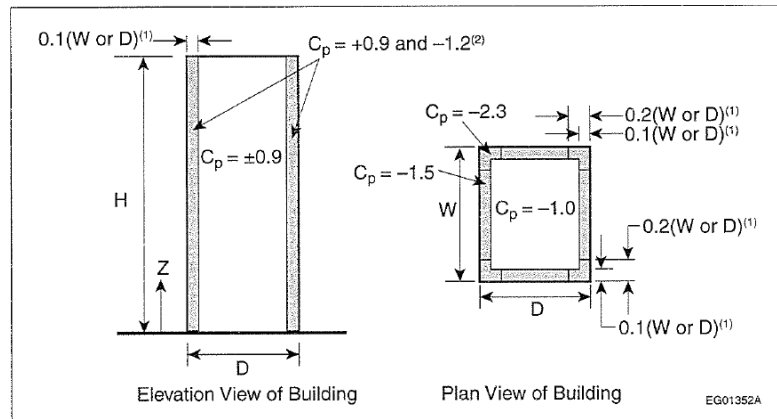
(1) The larger of W or D is to be used.
(2) Where vertical ribs deeper than 1 m are present on the walls, the dimensions 0.1D and 0.1W must be changed to 0.2D and 0.2W and the negative value of C_p must be changed from −1.2 to −1.4.

Figure 3-4: Values of Cp in NBCC 2015 for rectangular buildings of height greater than 20 m on roof and walls for the design of components and cladding and secondary structural supports of cladding. (Figure A-4.1.7.5. (4) in NBCC 2015).

40

Chapter 4

Experimental methodology

This chapter describes the experimental setup of the present study. a description of the wind tunnel of Concordia University is presented first, then, the terrain exposure simulation and building models are introduced, finally, the pressure measurement system is explained.

4.1   The boundary layer wind tunnel of Concordia University

The wind tunnel of Concordia University is an open return circuit atmospheric boundary layer wind tunnel. The tunnel is 12 m long which is adequate to acquire a properly simulated atmospheric boundary layer, and it has a width of 1.8 m and an adjustable height up to 1.8 m. The tunnel is equipped with a double inlet centrifugal blower to generate wind with a maximum velocity of 14 m/s at the testing section. To achieve the desired boundary layer at working section, a metallic screen and four flow straighteners are fixed just after the blower, and a small slope is employed in the transition section, from the blower outlet to the testing area.

The need of testing at different wind directions is inevitable. Therefore, the testing section is equipped with a 4-ft diameter turntable, the turntable can be controlled manually or electronically. A rectangular slot is perforated at the middle of the turntable for the sake of model installation and fixing, as well as, connecting the model with the pressure measurement system.

The wind tunnel is visible from one side through plexiglass windows, and it is visible from both sides at the test section in order to have the tested items seen all the time during the experiments. The tunnel floor is basically furnished by a thick carpet to simulate terrain type of an open country exposure; other roughness elements with different configurations may be utilized for the simulation of other exposures, such as the suburban exposure.

4.2 Terrain exposure simulation and flow characteristics

Two terrain exposures were simulated in the wind tunnel: open country exposure (exposure C) and suburban exposure (exposure B). Figure 4-1 shows the simulation of the two exposures in the wind tunnel. A thick carpet was used to simulate exposure C since it represents an unobstructed exposure and provides sufficient roughness through the carpet small polyester fibers for the simulation of open country exposure. On the other hand, roughness elements, small foam cubes and eggboxes, were placed on the floor of the wind tunnel for the simulation of exposure B. The foam cubes and eggboxes simulate different sizes, shapes and the equivalent roughness of full-scale buildings and structures that are normally located in suburban exposure.

The wind speed was measured using a 4-hole cobra probe fixed at the testing section, which can be operated electronically through a motor. The cobra probe can be moved in all directions, up and down, left and right, and back and forth; such that the wind speed can be measured at any point within the testing section. In addition to wind speed, the cobra probe is also accommodated to measure the turbulence intensity and wind spectra.

The mean wind speed and turbulence intensity were measured at the center of the turntable using the cobra probe for different heights, from zero to 100 cm, to trace the vertical changes in flow characteristics in the wind tunnel for exposure C and exposure B. Figure 4-2 presents the variation of mean wind speed and turbulence intensity with height, the height Z is normalized by the gradient height, Z/Z_g, for both exposures. The mean wind speed at any height, $\bar{V}_Z$, is presented with respect to the mean gradient speed, $\bar{V}_g$.

The power-law exponent was 0.14 for Exposure C and 0.20 for exposure B, which indicates that the wind speed in exposure B increases at a lower rate than it does in exposure C. Gradient speed was recorded at a gradient height of 55 cm from the wind tunnel floor in exposure C, whereas the gradient height was 88 cm for exposure B. This is due to the higher roughness in exposure B where the wind takes a longer vertical distance to readjust to the unobstructed wind speed. Turbulence intensity, I_u, was greater in the suburban exposure compared to the open country exposure. It is

to be noticed that comparable values of turbulence intensities were recorded above the gradient height.
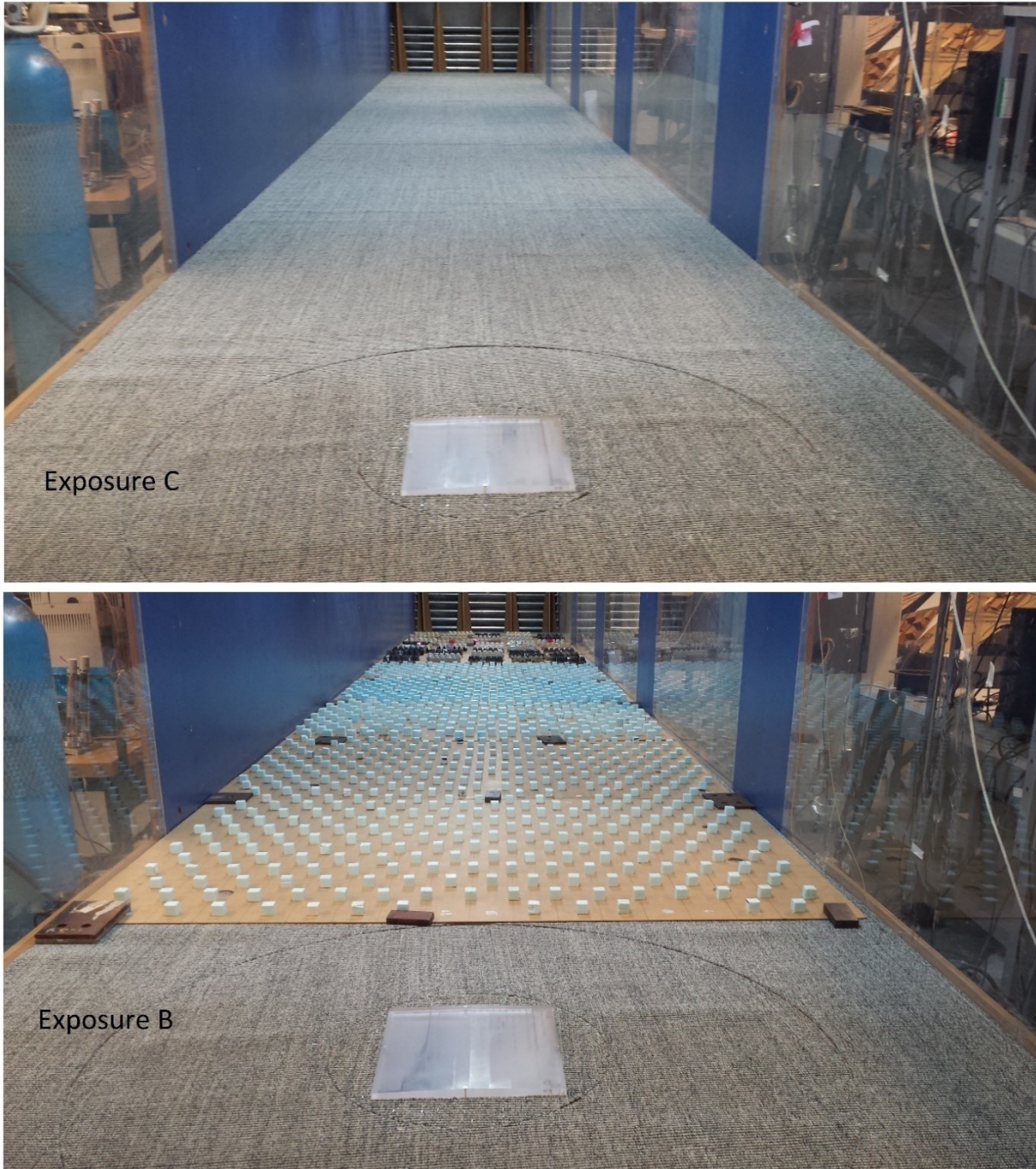
Figure 4-1: Simulation of exposure C and exposure B at the wind tunnel of Concordia University.
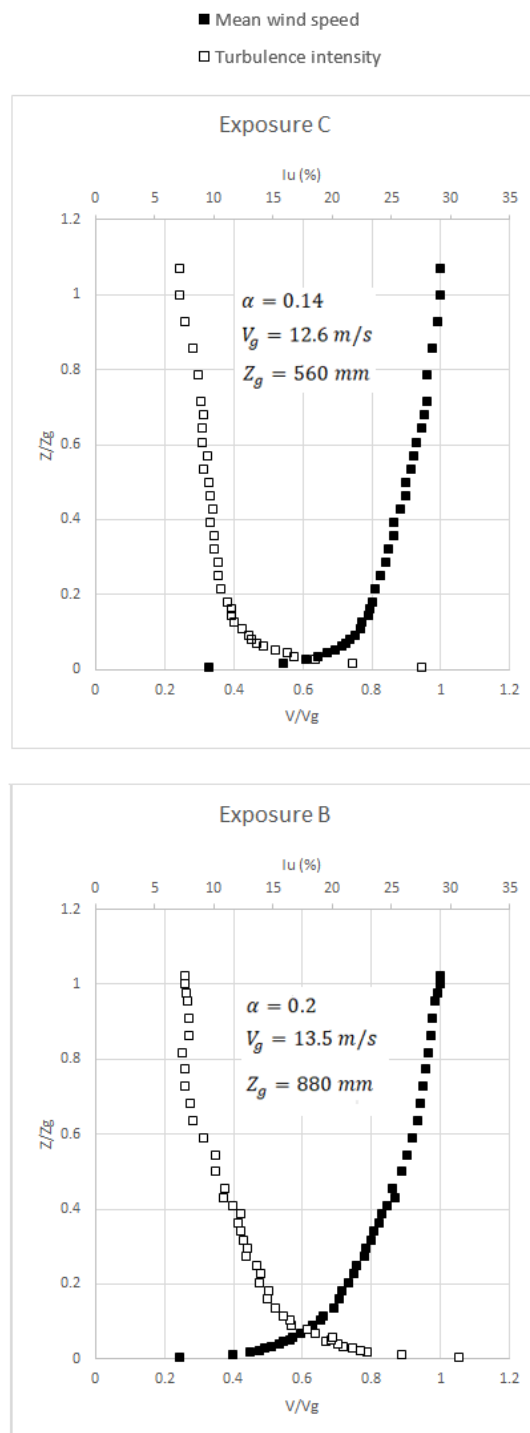
Figure 4-2: Vertical variation of mean wind speed and longitudinal turbulence intensity for exposure C and exposure B.

Figure 4-3 presents the power spectral density of longitudinal turbulence component calculated at one-sixth the gradient height for open country and suburban exposures in the wind tunnel, as well as, the power spectra evaluated based on Von Karman's model and Davenport's model of turbulence in open country exposure at one-sixth the gradient height.

Experimental spectra are close to those plotted using the turbulence models of Von Karman and Davenport which are presented by the continuous and the dashed lines, respectively. Although the wind energy is greater in exposure C than in exposure B, the plotted data for exposure B is lower. The reason is that the measured power spectral density was normalized by the standard deviation of the wind speed which is much higher in exposure B than in exposure C due to the higher turbulence.
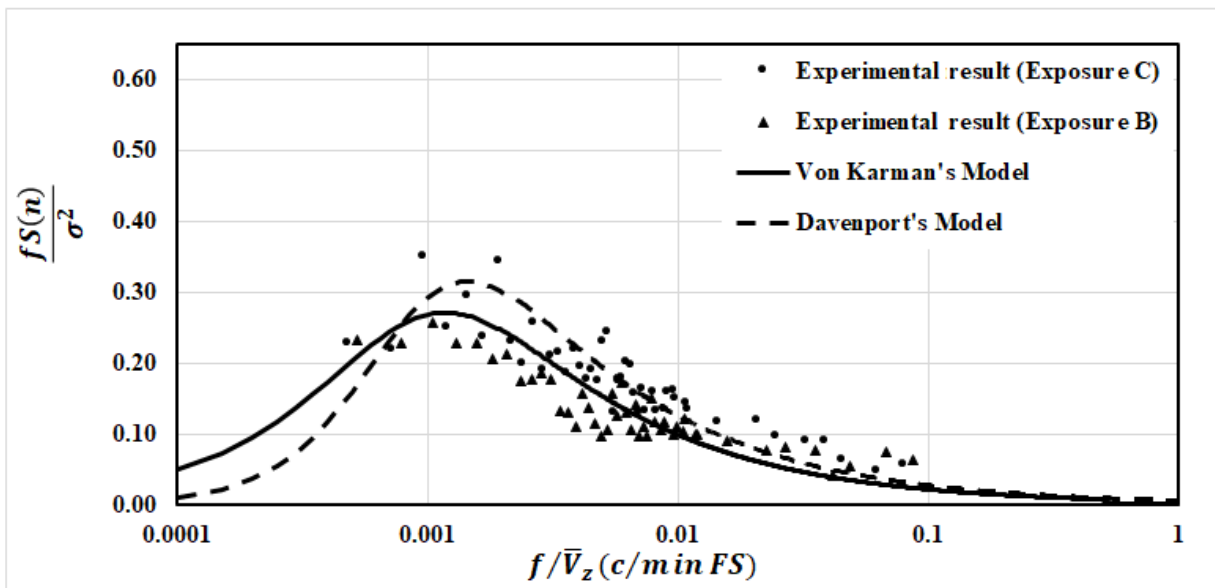
Figure 4-3: Power spectral density of longitudinal turbulence component evaluated at one-sixth the gradient height.

4.3 Building models

Three nearly flat roof building models of similar full-scale plan dimensions of 118 m x 118 m and roof slope of 1.4° (2.5%) were constructed at a geometric scale of 1:400. The model was made from a 10 mm thickness Plexiglass, the roof and the walls were combined using metallic screws to form the basic building model of the present study. The basic model, then, was tested in the wind tunnel for three heights: 5 m (16 ft), 10 m (32 ft) and 20 m (64 ft); in both exposures by sliding the model up and down in a perfectly sized slot at the center of the turntable.

Figure 4-4 shows the three building models installed in the wind tunnel at the center of the turntable for open country exposure and suburban exposure. As shown, the floor of the wind tunnel was furnished by a carpet in exposure C simulation, and it was covered by roughness elements for the simulation of exposure B. Furthermore, the heights of the building models in the wind tunnel scale are 12.2 mm, 24.4 mm and 48.8 mm corresponding to the full-scale heights of 5 m, 10 m and 20 m, respectively.

Figure 4-5 shows roof dimensions with pressure taps layout, and Figure 4-6 presents a detailed pressure tap assembly in the bottom-left quarter of the roof. The roof was equipped with 188 pressure taps in the bottom-left quarter with a high density in the roof corner and edges and additional 6 pressure taps in the top-left corner. The first pressure taps line in both X and Y directions is 1 m from the roof edge, and the distribution of pressure taps is the same along X and Y directions, therefore, the location of each pressure tap is presented in the vertical direction only.

The results of this study are to be compared with full-scale measurements of the experimental building of Duro-Last Roofing, Inc. in Iowa, the black pressure taps in the bottom-left quarter in Figure 4-5 and the 6 pressure taps in the top-left corner represent the full-scale pressure tubes equipped in the roof of Duro-Last roofing experimental building.

Figure 4-4: Installation of building models in the wind tunnel for both exposures.
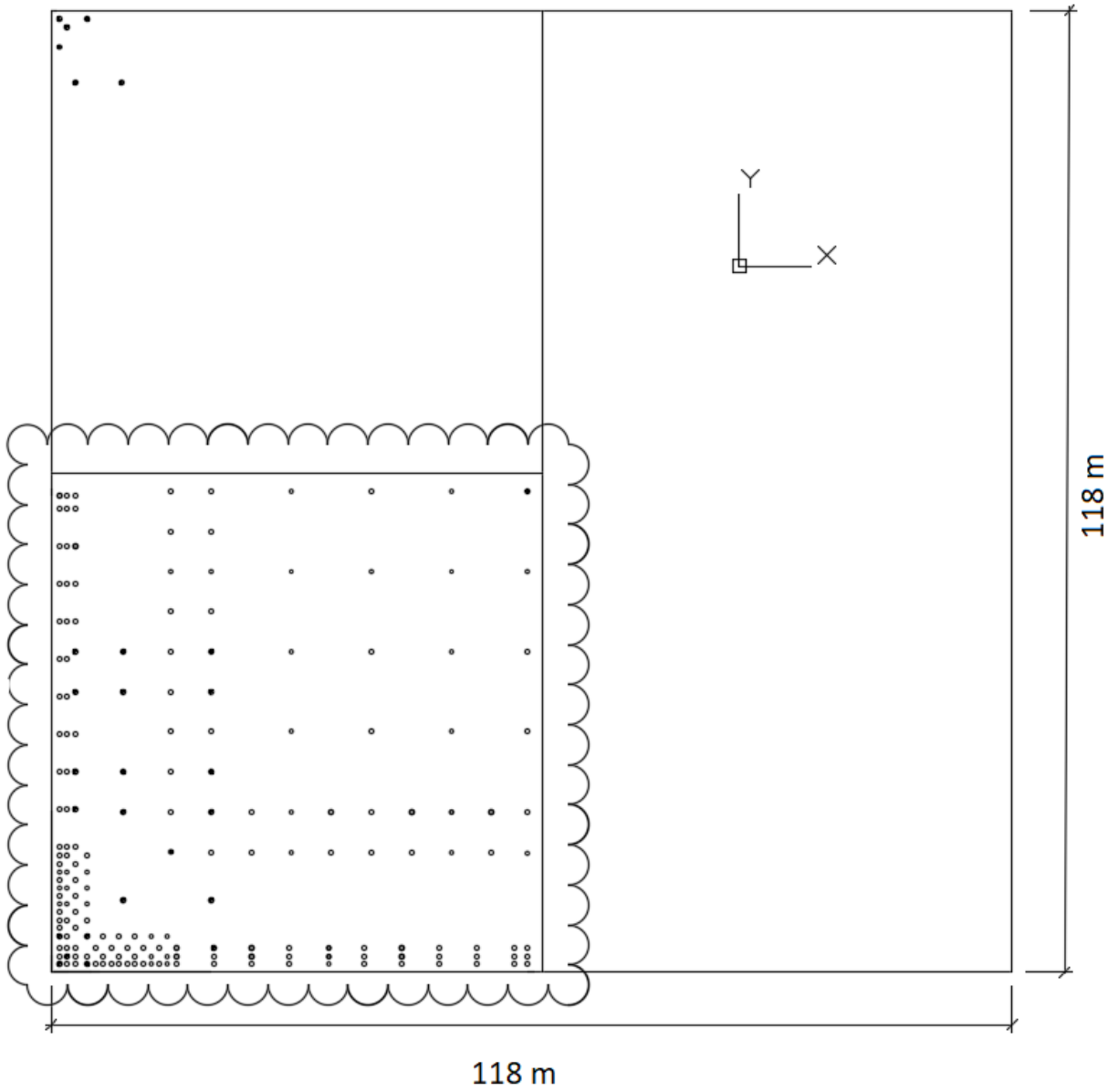
Figure 4-5: Roof plan dimensions with pressure tap layout.
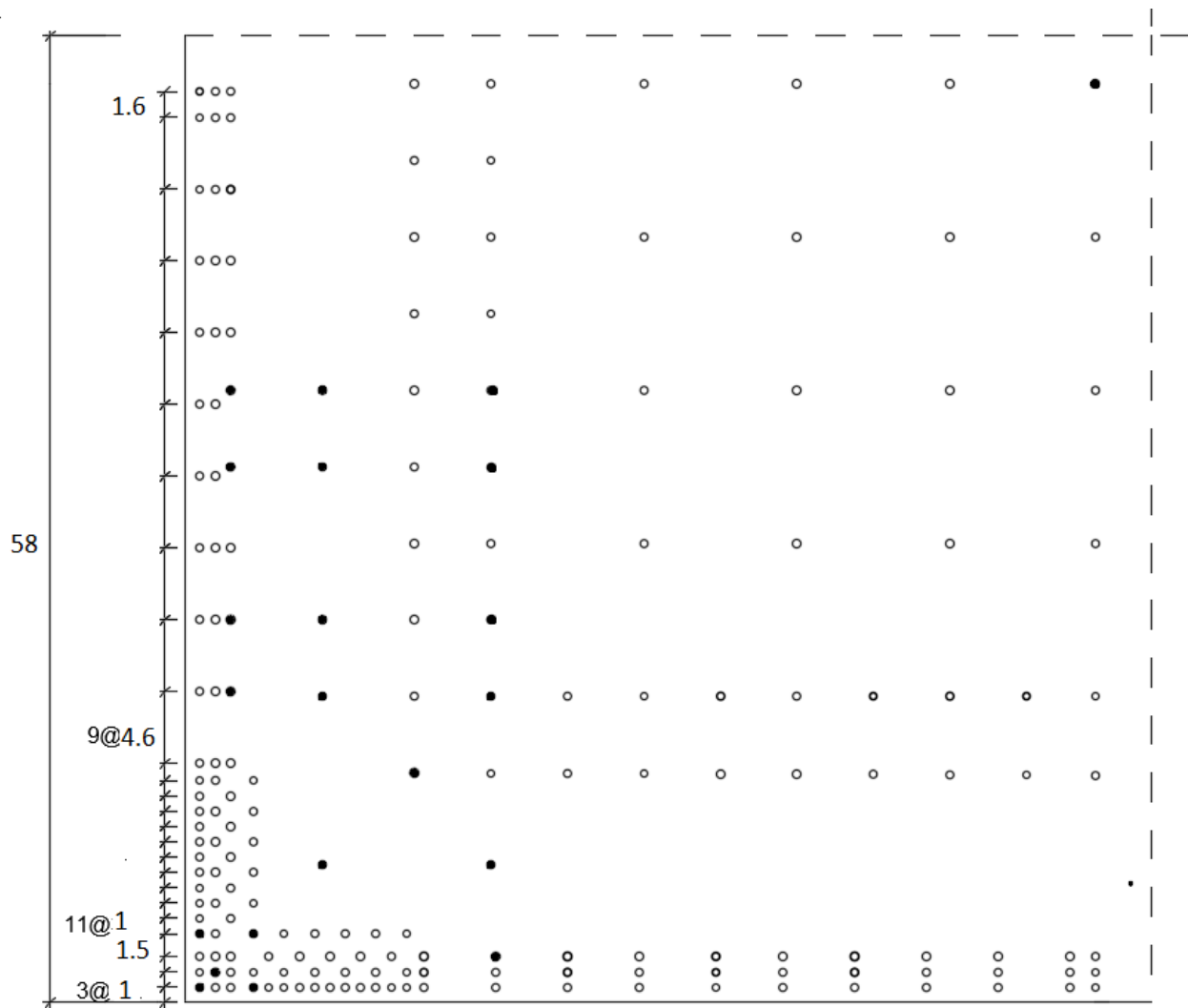
Figure 4-6: Detailed pressure tap assembly in the bottom-left quarter of the roof (dimensions in meter).

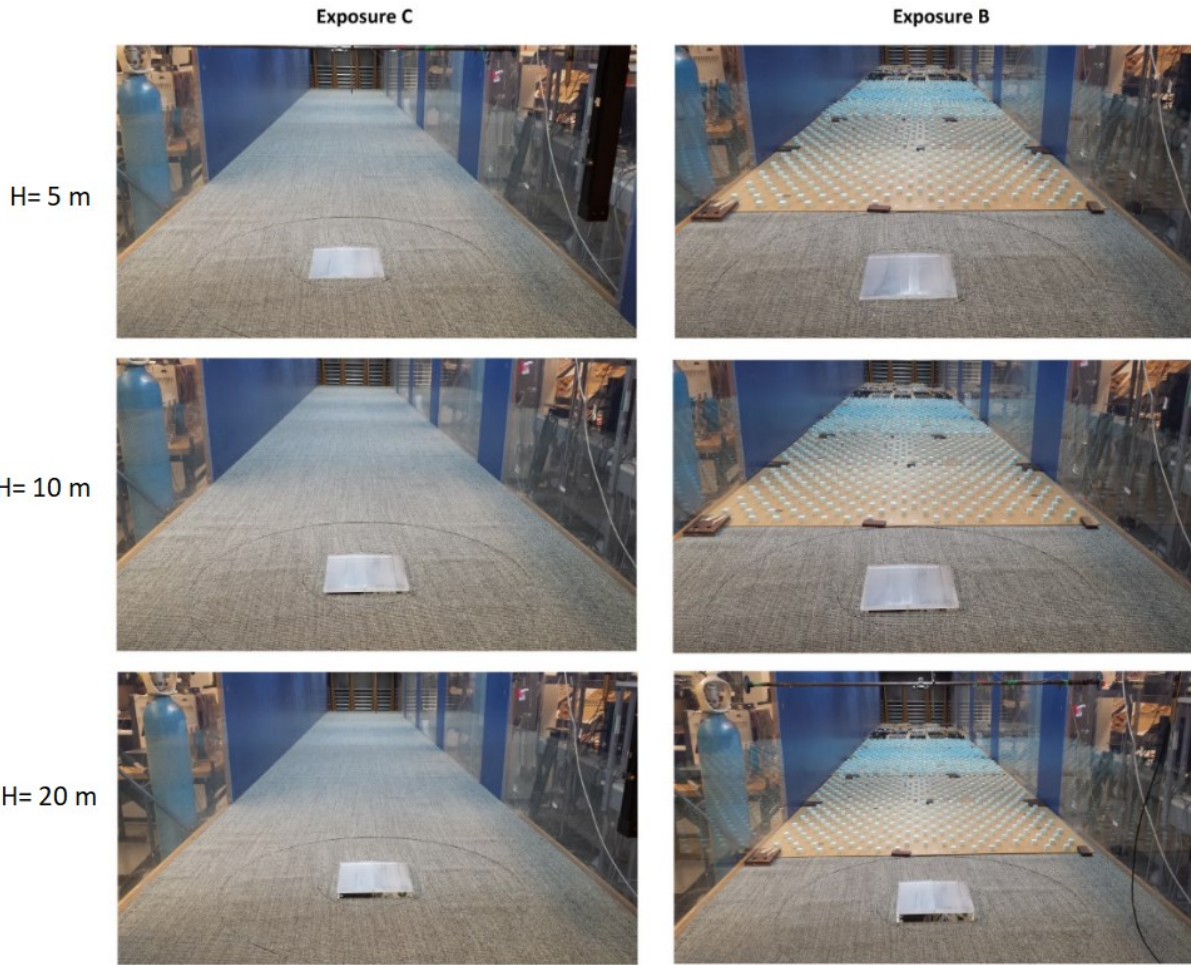## 4.4 Pressure measurements

Pressure measurements were carried out in the wind tunnel using pressure measurement system produced by Scanivalve Corporation. The system consists of four pressure scanners (ZOC33/64 Px), Digital Service Module (DSM 3400), tiny plastic tubes with an inner diameter of 1.37 mm, brass pipes (pressure taps) with an inner diameter of 0.8 mm, pitot tube to measure the wind dynamic pressure, and a desktop computer.

The pressure taps and the pitot tube were connected to the pressure scanners through the tiny plastic tubes, each pressure scanner has a capacity of 64 pressure taps, for this reason, the first pressure scanner was connected to 63 pressure taps and the pitot tube, the second and the third pressure scanners were connected to 128 pressure taps, 64 taps for each of them, and the remaining 3 pressure taps were connected to the fourth pressure scanner. Four slots are available in the DSM to hookup the pressure scanners; finally, the DSM is linked with a computer.

The pressure scanners read the pressure signals on the roof from all pressure taps and pitot tube and send them to the DSM which in turn converts the pressure signals into readable data on the computer monitor.

Results in this study are presented using pressure coefficients, i.e. velocity-independent dimensionless parameter – see section 2.7.1. The pressure coefficient can be defined as the wind-induced pressure, the difference between wind pressure and atmospheric pressure, normalized by the mean hourly averaged dynamic pressure at the eave height.

The pressure measurements on the roof of each model were performed for 7 wind directions: 0°, 15°, 30°, 45°, 60°, 75° and 90° and for two terrain exposures: exposure C and exposure B. The instantaneous pressures were measured at a frequency of 300 Hz for 27.3 seconds, which provides a time history of 8200 pressure readings for each pressure tap. Mean pressure coefficient (C_P) is the average value of 8200 readings, while peak pressure coefficient ($C_P C_g$) is the average of the maximum 10 peaks among the data in the time history.

Finally, instantaneous area- averaged pressure coefficients $C_{P,A}(t)$ were measured on several areas in corner, edge and interior zones based on the following formula:

$$C_{P,A}(t) = \frac{\sum_{i=1}^{N} C_{Pi}(t)A_i}{\sum_{i=1}^{N} A_i}$$

(4-1)

where A_i is the tributary area of the ith pressure tap, N is the number of pressure taps in the considered area, and $C_{Pi}(t)$ is instantaneous pressure coefficient of ith pressure tap at instant t.

Chapter 5

Results and discussion

In this chapter, the experimental findings are presented in terms of contours of most critical pressure coefficients over the roof, extreme local pressure coefficients for each wind direction, and area-averaged peak pressure coefficients. In addition, comparisons of the experimental results with previous studies and full-scale data are included.

5.1   Contours of the most critical pressure coefficients

The building models have been tested for 7 wind directions: 0°, 15°, 30°, 45°, 60°, 75° and 90° to obtain the most critical wind pressures on the roof of the building. Figures 5-1 through 5-12 show contours of most critical mean and peak pressure coefficients among all wind directions for three heights, 5, 10 and 20 m and for two exposures.

The contours show wind pressure coefficients within the bottom-left quarter of the roof, which is the area equipped with pressure taps. All contours were created by the mapping software "surfer 15", contour intervals are 0.2 for mean pressure coefficients, Cp, and 0.5 for peak pressure coefficients, CpCg. Contours of mean and peak pressure coefficients for each wind direction are presented in appendix B, appendix C, and appendix D.

As shown in the figures, and except for building of 5 m height, pressure coefficients decrease from the highest value on the roof corner to relatively smaller pressure coefficients along both windward edges until the middle of the windward edge, beyond this middle point, pressure coefficient values increase to reach the highest value on the other corner of the roof. However, for the building of 5 m height, wind loads developed on corner and edge zones are comparable. This may be ascribed to the very high turbulence at the roof level of the 5 m height building.

52

Pressure coefficients decrease from the windward edge toward the interior zone along a line normal to the windward edges. This is so, because of the flow separation that happens at the windward edges and causes high wind pressures on corner and edge zones compared to those on the interior zone.

Height is a significant factor that affects the value of pressure coefficients, as well as, the area at which the maximum pressure coefficients extend on the roof. Clearly, the taller the building the higher the pressure coefficients and the larger the area that receives high wind pressures. This is because of the higher wind velocity at the roof level of the higher buildings.

Terrain exposure affects the wind velocity and the turbulence level in the atmospheric boundary layer, especially near the ground surface where the influence of ground roughness is very high. Turbulence level in exposure C is lower than in exposure B, while wind velocity is higher in exposure C. As shown in the figures, experimental results imply that the spatial distribution of mean and peak pressure coefficients over the roof is similar in both exposure C and Exposure B. Also, the values of mean pressure coefficients are comparable; however, the values of peak pressure coefficients measured on building roofs in exposure B are higher than those in exposure C.

Figure 5-1: Values of most critical mean pressure coefficients (Cp) for all wind directions (H=5 m, Exposure C).

Figure 5-2: Values of most critical peak pressure coefficients (CpCg) for all wind directions (H=5 m, Exposure C).

Figure 5-3: Values of most critical mean pressure coefficients (Cp) for all wind directions (H=10 m, Exposure C).

Figure 5-4: Values of most critical peak pressure coefficients (CpCg) for all wind directions (H=10 m, Exposure C).

Figure 5-5: Values of most critical mean pressure coefficients (Cp) for all wind directions (H=20 m, Exposure C).

Figure 5-6: Values of most critical peak pressure coefficients (CpCg) for all wind directions (H=20 m., Exposure C).

Figure 5-7: Values of most critical mean pressure coefficients (Cp) for all wind directions (H=5 m, Exposure B).
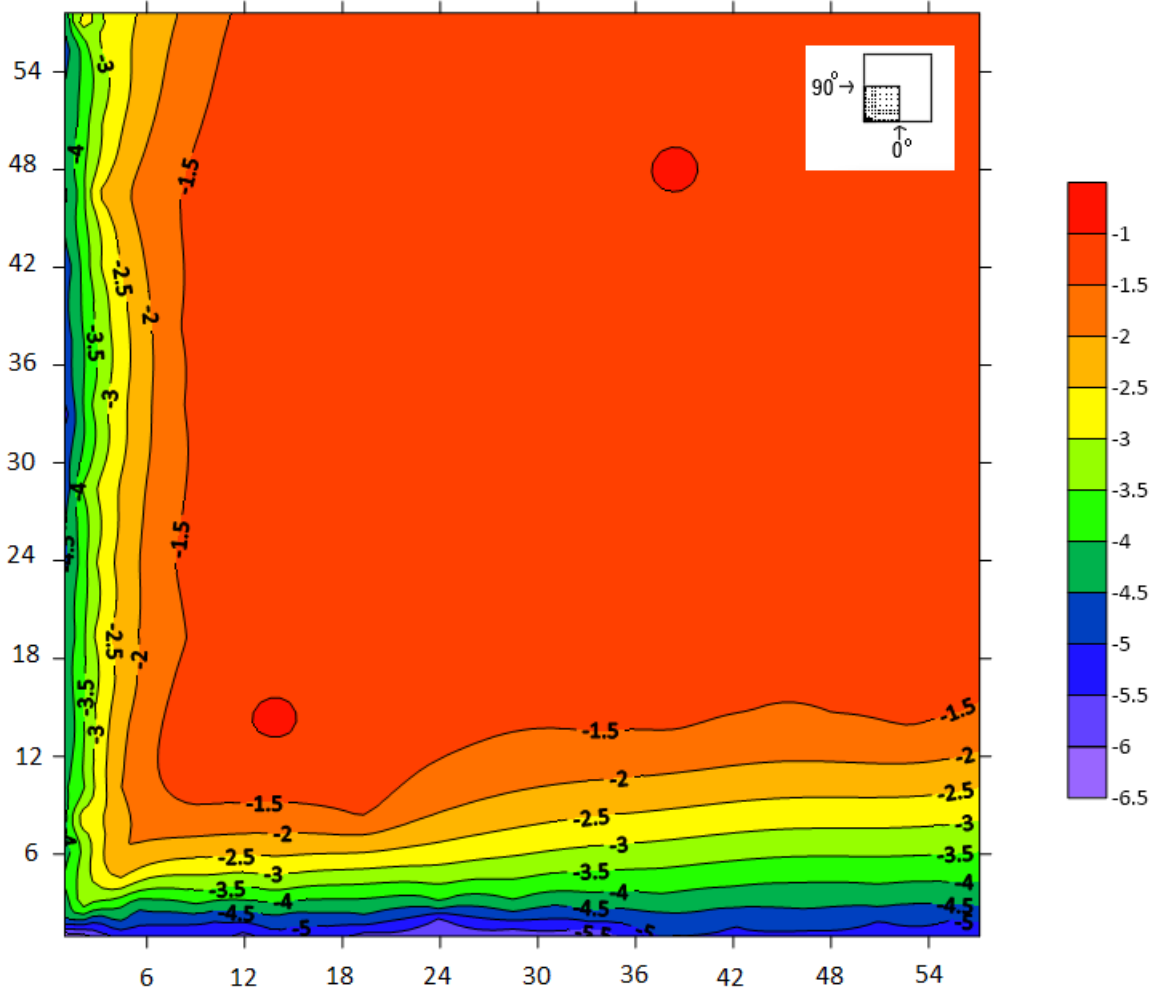
Figure 5-8: Values of most critical peak pressure coefficients (CpCg) for all wind directions (H=5 m, Exposure B).
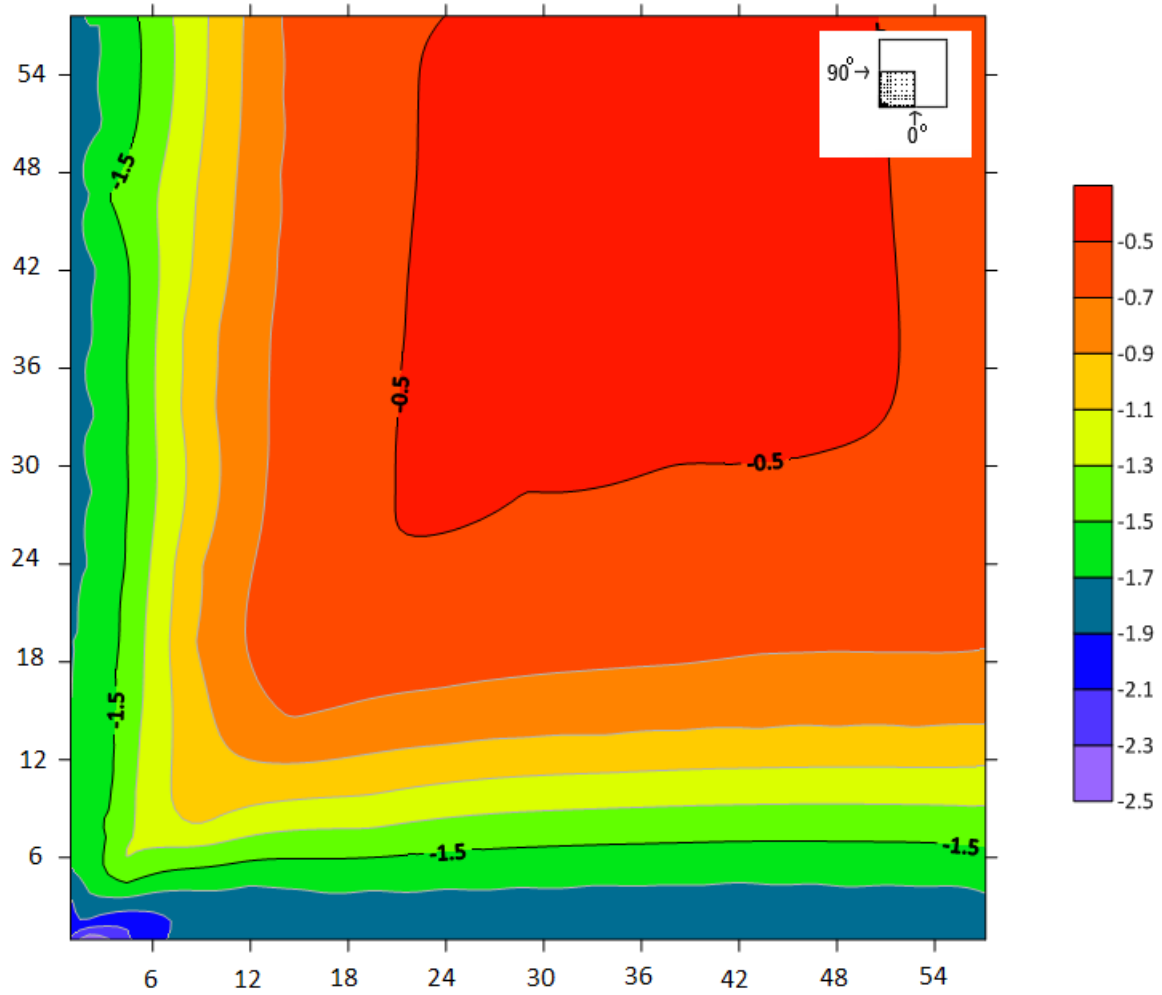
Figure 5-9: Values of most critical mean pressure coefficients (Cp) for all wind directions (H=10 m, Exposure B).
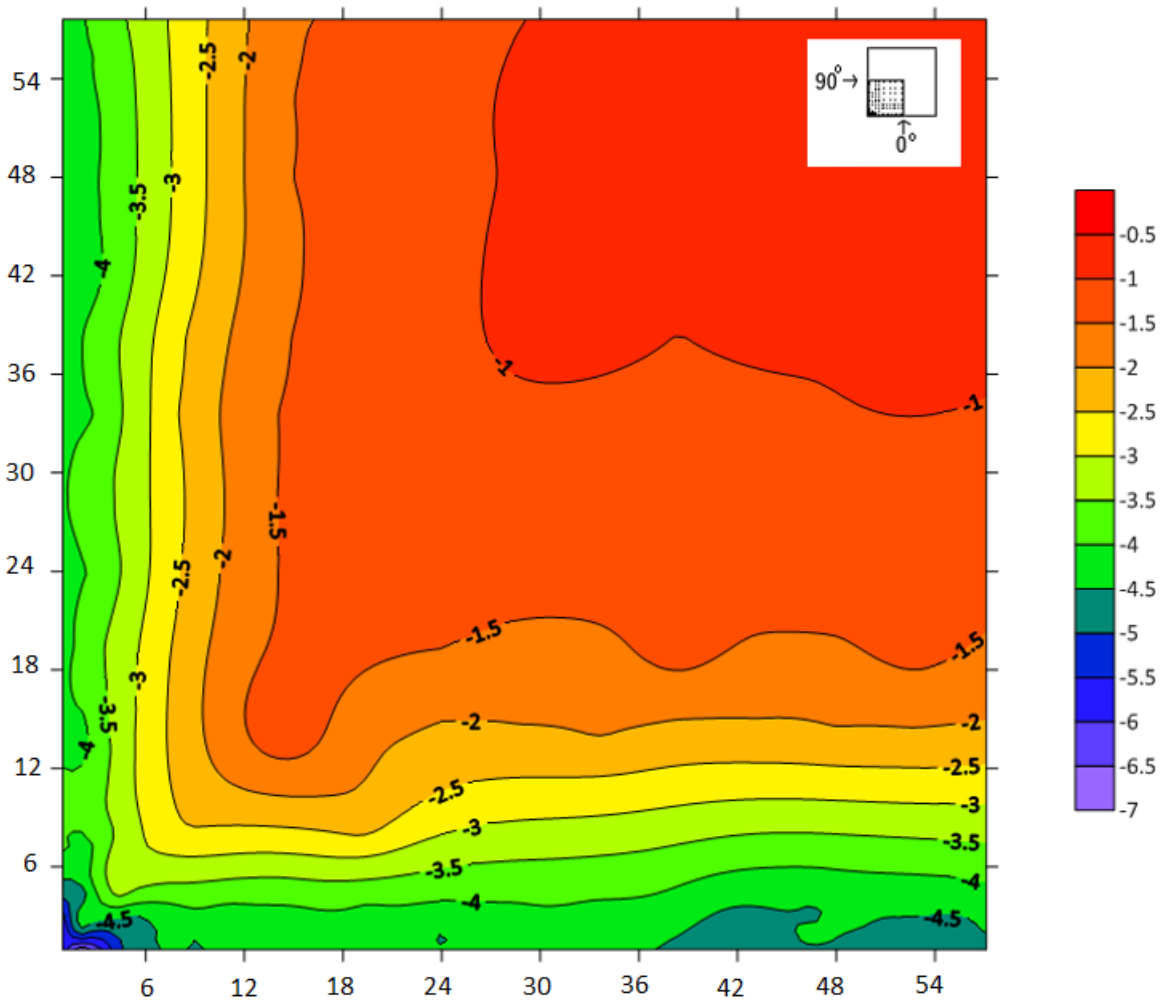
Figure 5-10: Values of most critical peak pressure coefficients (CpCg) for all wind directions (H=10 m, Exposure B).
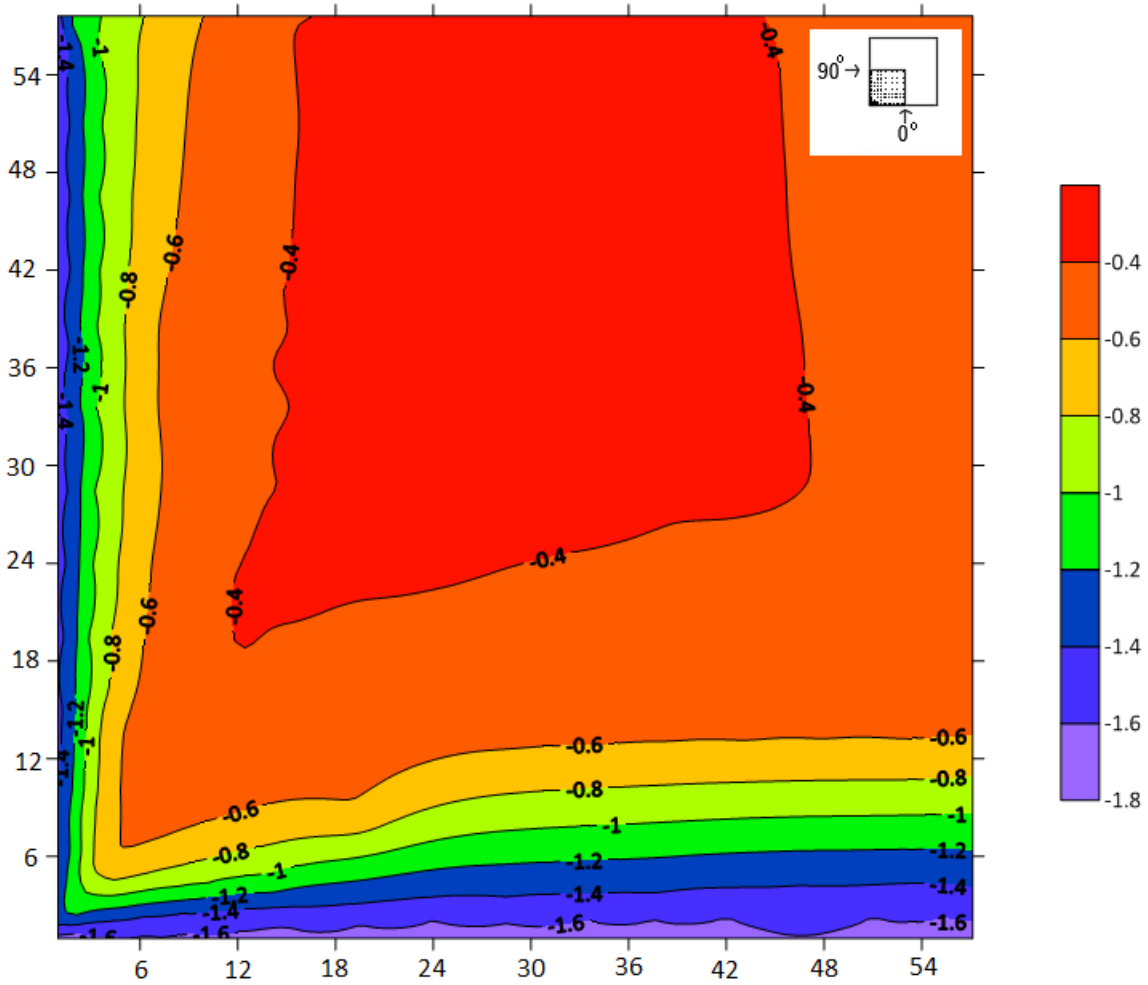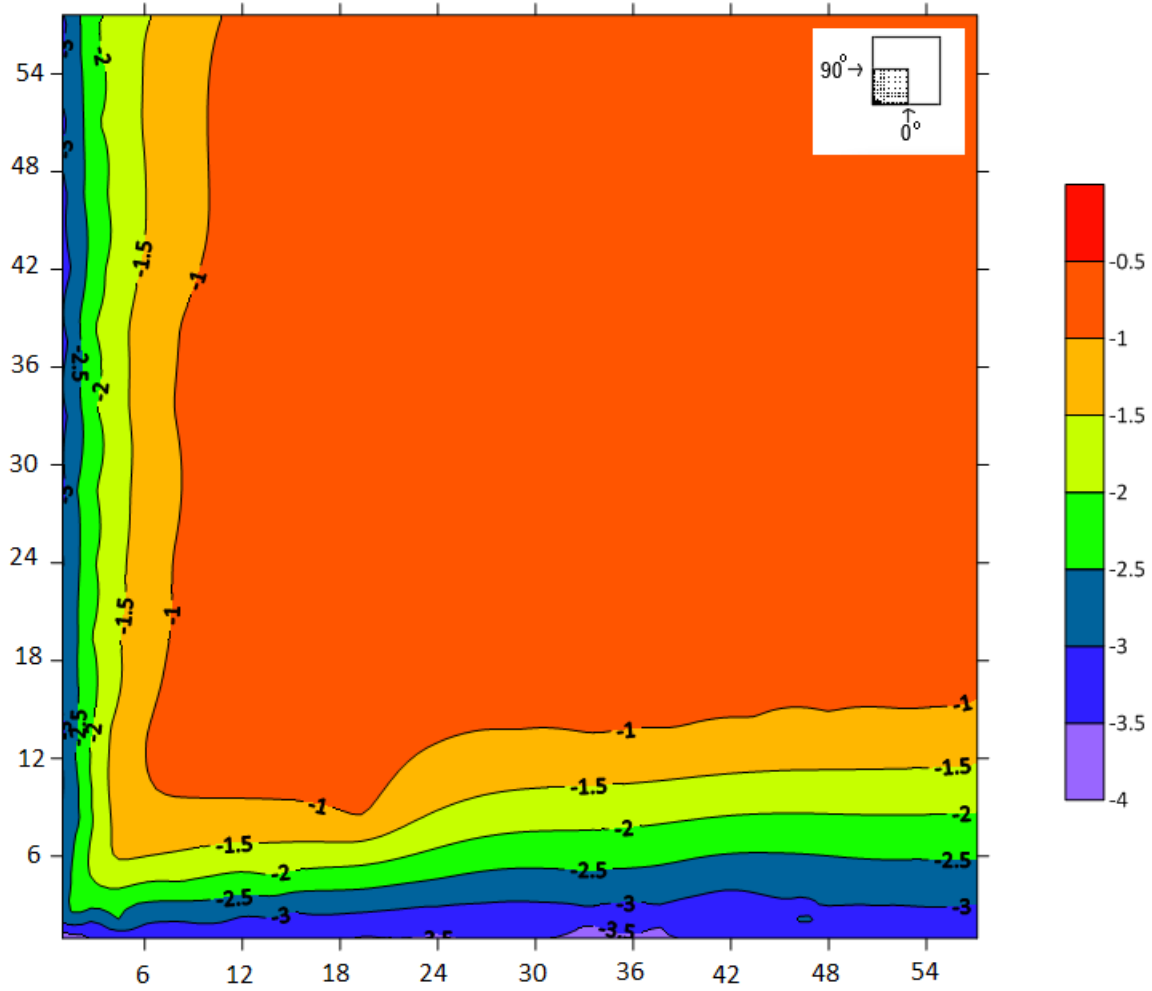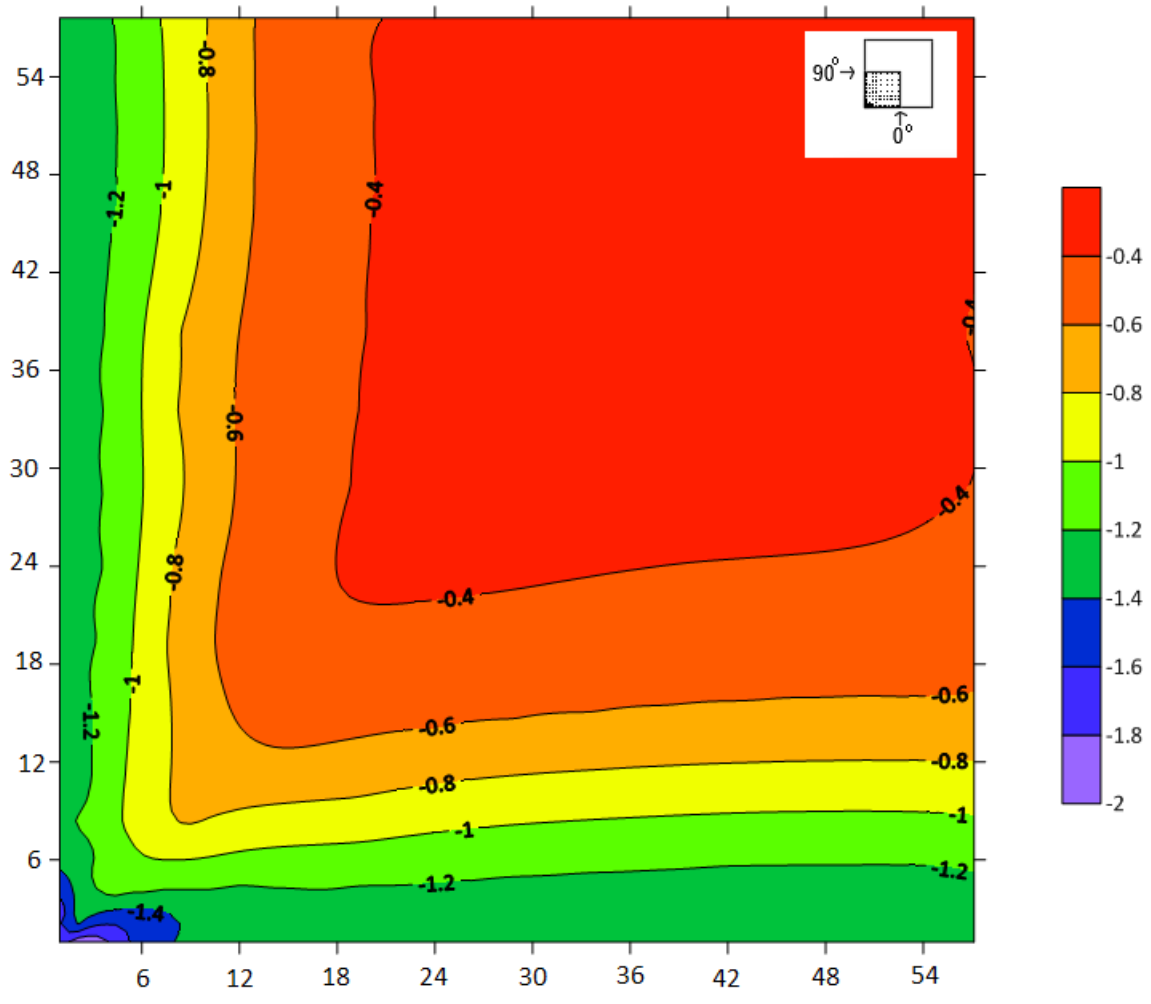
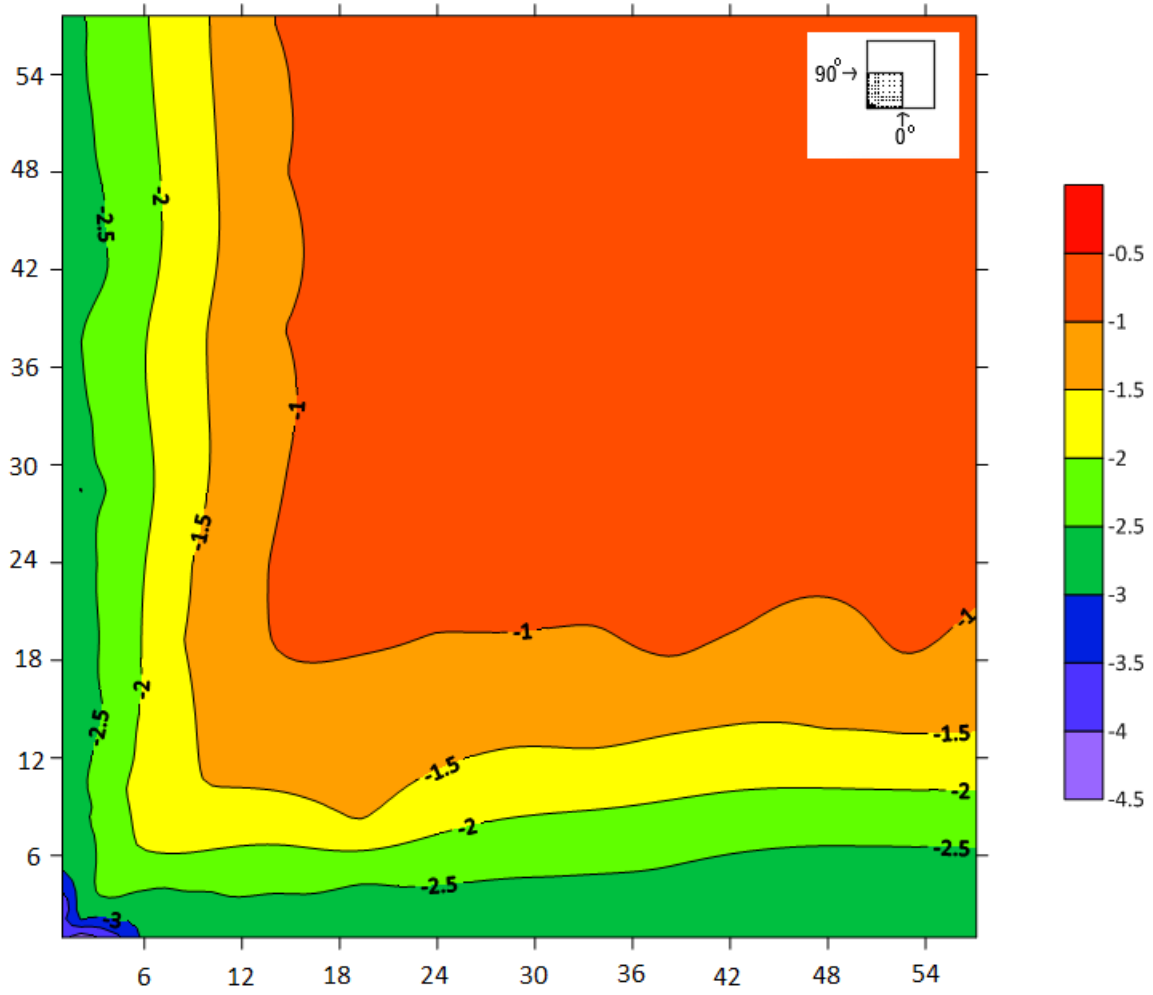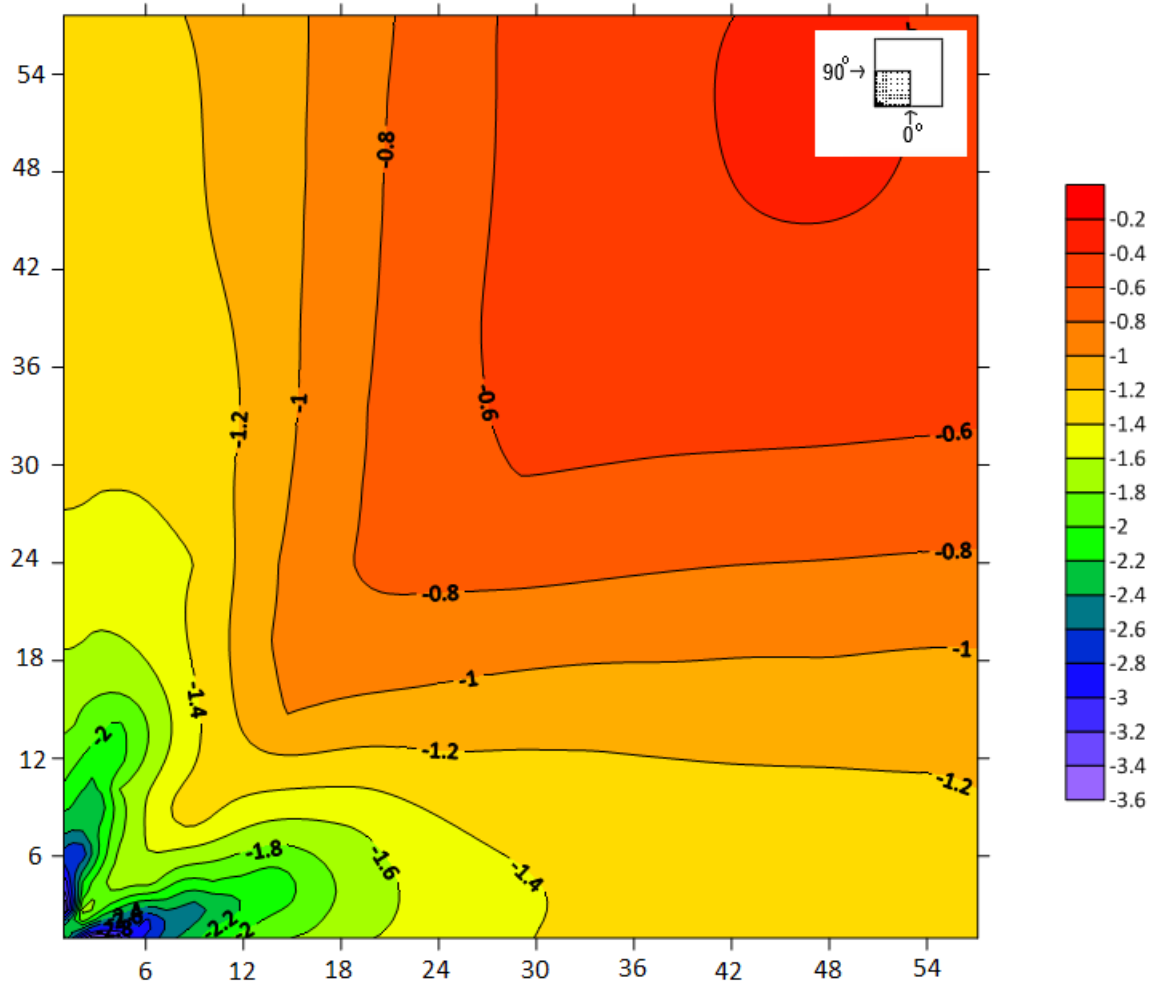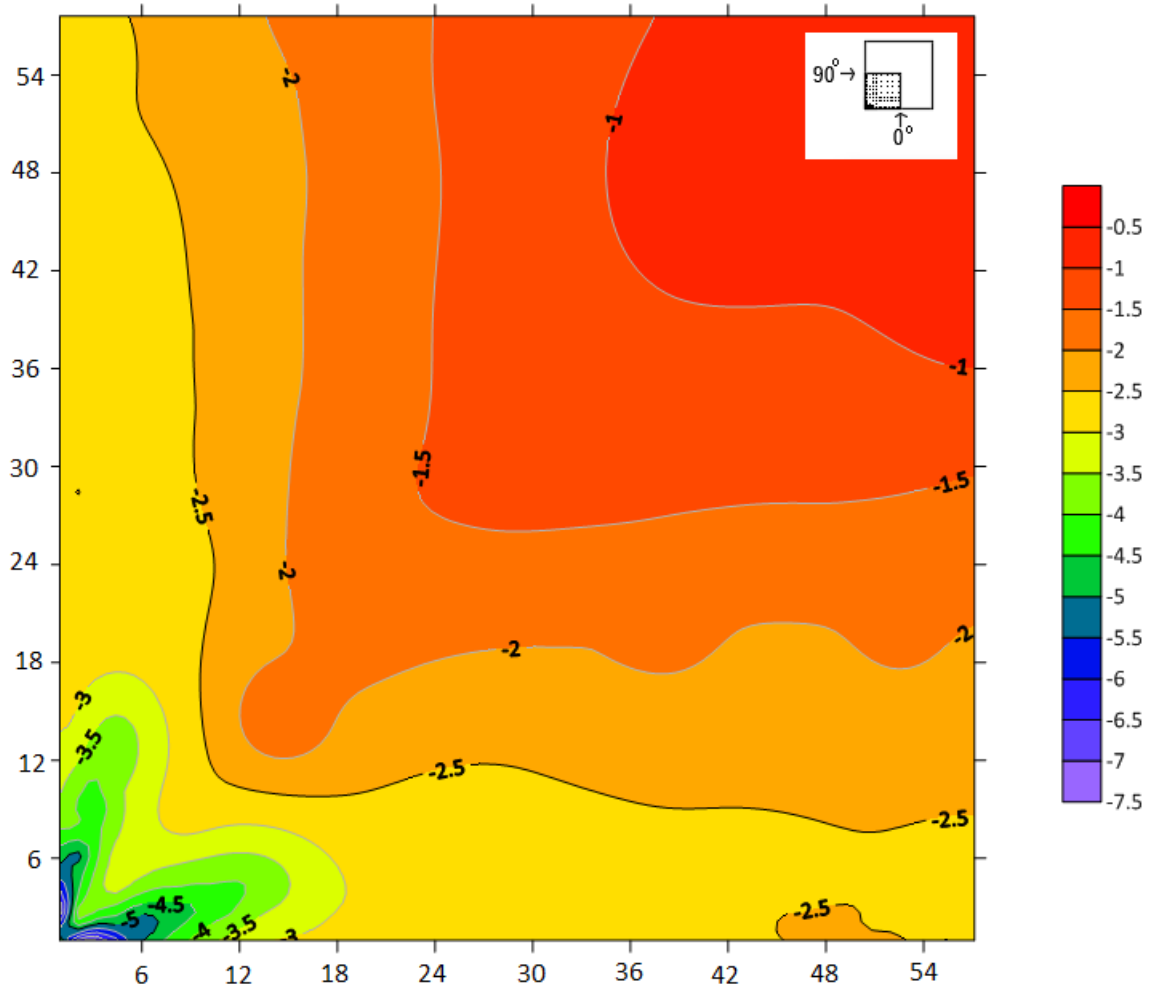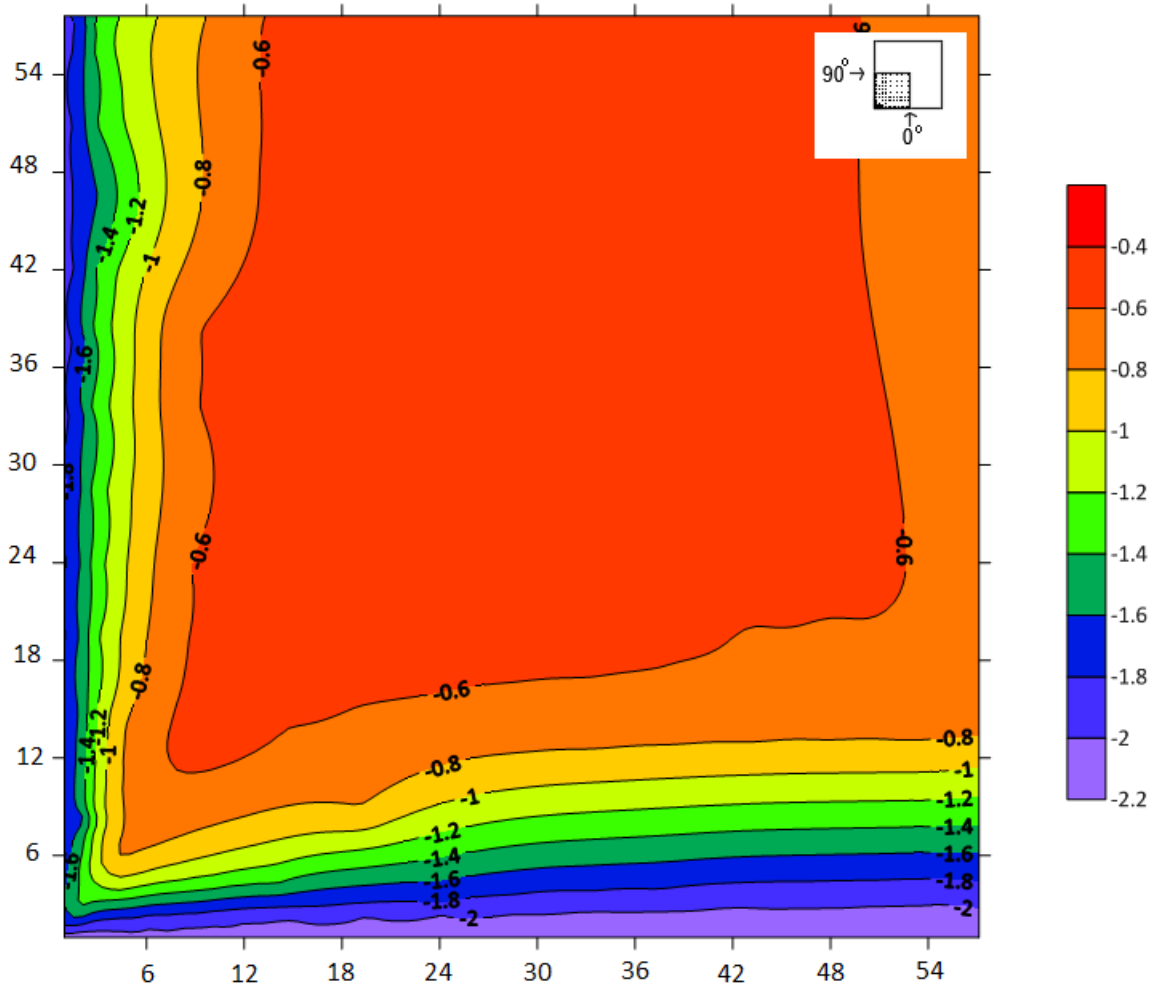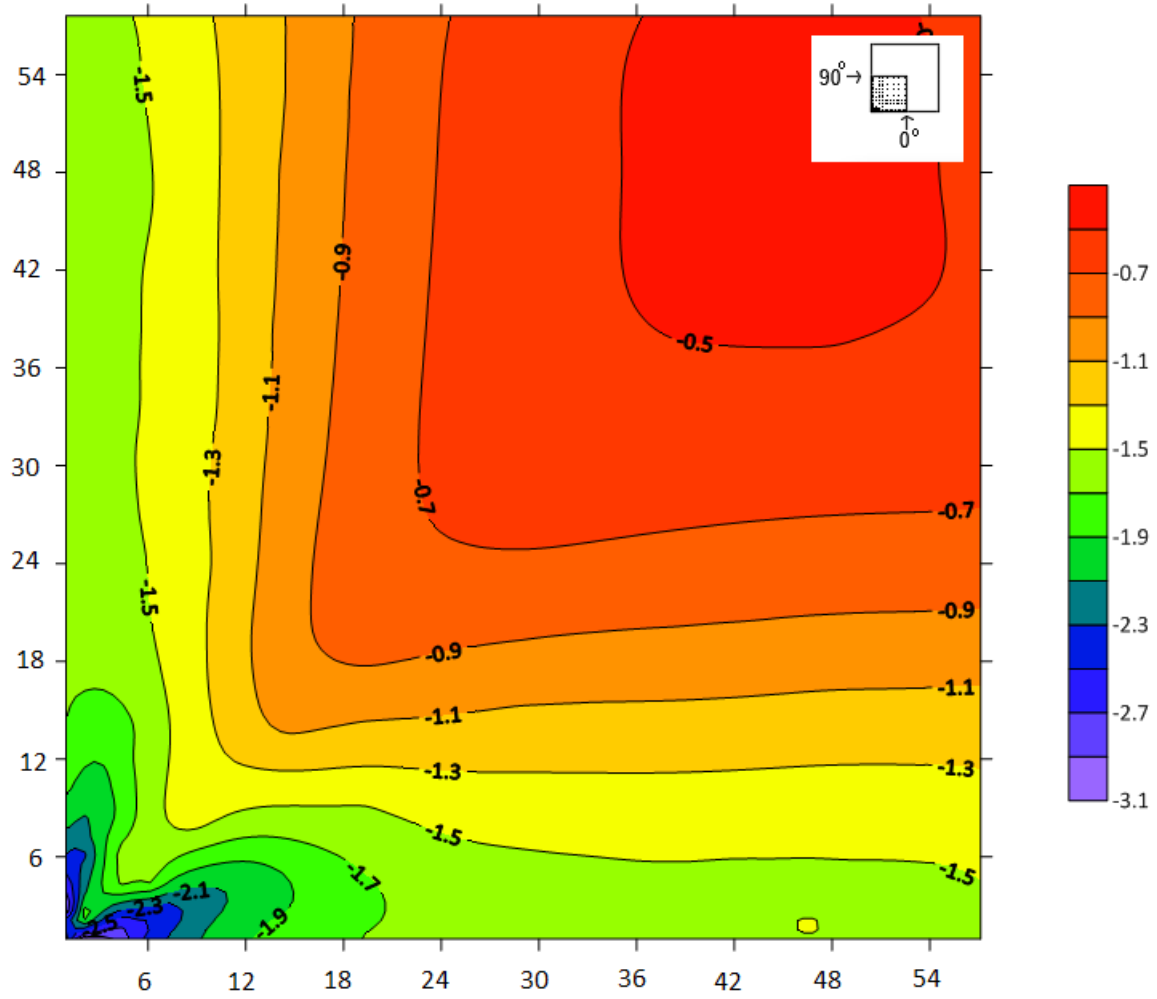Figure 5-11: Values of most critical mean pressure coefficients (Cp) for all wind directions (H=20 m, Exposure B).
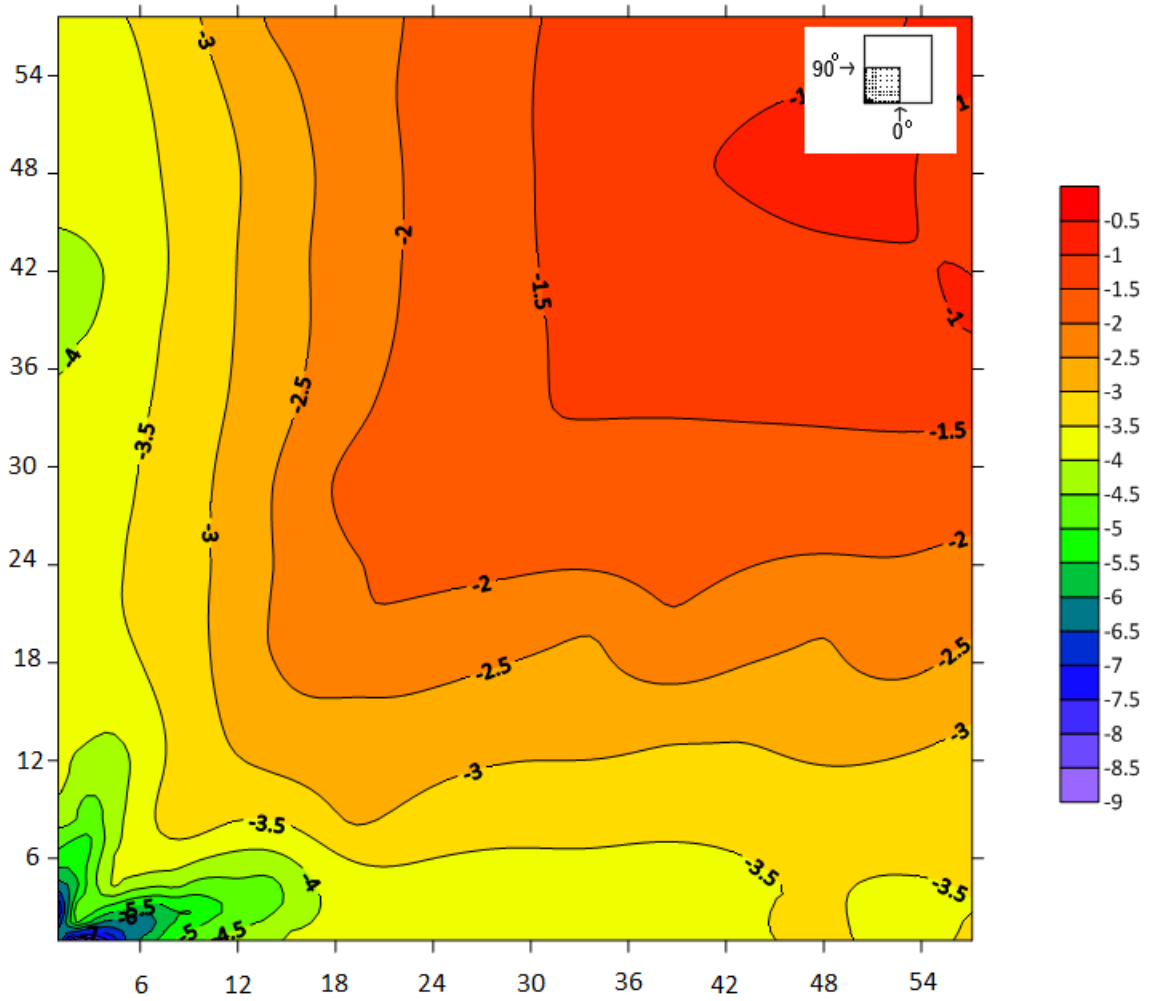
Figure 5-12: Values of most critical peak pressure coefficients (CpCg) for all wind directions (H=20 m, Exposure B).

5.2 Local pressure coefficients and wind directional effects

Extreme local mean and peak pressure coefficients have been evaluated for each wind direction. Since the roof zonal system of ASCE 7-16 is different from the one recommended by both ASCE 7-10 and NBCC 2015, extreme pressure coefficients have been determined and presented in two figures: the first figure is based on the zonal system of ASCE 7-10 and NBCC 2015, while the second figure is based on ASCE 7-16 roof zonal system.

Figure 5-13 presents extreme mean and peak pressure coefficients on the pressure zones of NBCC 2015 and ASCE 7-10 evaluated for each wind direction and for the 3 buildings in exposure C and exposure B. Although technically the building of 20 m height is classified as a low-rise building according to NBCC 2015 (H ≤ 20 m or 65.6 ft), it will be also treated as mid-rise building because the height is at the limit of low-rise building definition. The inadequacy of low-rise building provisions of NBCC 2015 to cover the high wind loads measured on the building roof of 20 m height in the present study, will be discussed in chapter 6.

As mentioned earlier, the taller the building the larger the magnitude of wind pressure acting on its roof, which reflects the increased wind velocity pressure at the roof of the higher building. For instance, peak pressure coefficient, CpCg, on corner zone and at wind azimuth of 30° in exposure C is -7.4 for the building of 20 m (64 ft) height and -4.1 for the building of 10 m (32 ft) height, which results in a large difference of 3.3. On the other hand, the difference in pressure coefficients on the corner zone between the 10 m (32 ft) and 5 m (16 ft) height buildings is low and doesn't exceed 1 at the most critical wind azimuth. This can be justified by realizing that the building of 20 m (64 ft) height belongs to the mid-rise building category, and a larger wind load normally occurs on its roof compared with that on low-rise buildings, i.e. buildings of 10 m (32 ft) and 5 m (16 ft) heights.

Values of peak and mean pressure coefficients on the edge zone of the building of 20 m (64 ft) height are lower than those of the other two low-rise buildings, 10 m (32 ft) and 5 m (16 ft) height buildings. Actually, this does not contrast the conclusion mentioned earlier (i.e. the taller the

building the higher the pressure coefficients), the reason is that the size of the corner zone of the mid-rise building according to the North American codes is very large, such that it extends much along the edge and leaves a small area for the edge zone at the middle area of the roof near the edge where the wind pressure coefficients are low. Further, pressure coefficients measured on the edge zone of the 5 m (16 ft) height building are higher than those of the 10 m (32 ft) height building. The reason is that the wind load distribution on the roof of the 16 ft height building is different, at which the peak pressure coefficients measured on the edge zone are approximately equal to the high peak pressure coefficients developed on the corner zone, this is probably due to the high turbulence level at the height of 5 m (16 ft). On the other hand, wind loads developed on roof of the 10 m (32 ft) height building decrease along the leading edge toward the middle of the roof.

Except for the 5 m (16 ft) height building, most critical pressure coefficients on corner zone were recorded at wind azimuth with a range of 15° to 30° or 60° to 75°. However, the worst wind loads on the roof of the 5 m (16 ft) height building occurs at normal wind directions. It should be noted that values of pressure coefficients for wind directions from 0° to 45° are not equal to those for wind direction from 45° to 90°. This is probably due to the small roof slope (1.4°) and the small margin of experimental error. In addition, there is also some asymmetric wind speed distribution with respect to the centerline of the testing area in the wind tunnel - the error in this regard does not exceed 5% (Stathopoulos, 1984).

Mean pressure coefficients are similar in both terrain exposures, while peak pressure coefficients in suburban exposure are higher which reflects the increased gustiness in the rougher exposure. Generally, mean wind speed at eave height for a building immersed in exposure B is lower than the mean wind speed at eave height of a building in Exposure C; nevertheless, the turbulence is higher at the roof level of the building in suburban exposure. Knowing that the pressure coefficients are normalized by the velocity pressure at eave height, the actual reason for the high pressure coefficients on buildings in suburban exposure is the smaller velocity pressure in exposure B compared to exposure C. It very important to realize that the higher peak pressure coefficients evaluated in exposure B do not reflect higher wind pressures developed on the building. In fact, codes and standards provide lower design pressures for buildings in exposure B compared to those

provided for buildings immersed in exposure C by considering higher exposure factors for wind load estimation on buildings in exposure C. For instance, according to ASCE 7 and for a building of 5 m (16 ft) height, the exposure factor K_Z is 0.883 and 0.7 for exposure C and exposure B, respectively.

Figure 5-14 presents extreme mean and peak pressure coefficients on pressure zones of ASCE 7-16 evaluated for each wind direction and for the 3 buildings in exposure C and exposure B. Although the roof zonal system of ASCE 7-16 is different, the extreme mean and peak pressure coefficients determined on the corner zone (zone 3) and edge zone (zone 2) are identical in both Figure 5-13 and Figure 5-14. However, this does not indicate a similar distribution of wind loads over the different pressure zones recommended by the codes.

As shown in Figure 5-13, ASCE 7-10 and NBCC 2015 suggest one interior zone, and peak and mean pressure coefficients are lower compared to those of corner and edge zones, also, the wind pressure coefficients are higher for the taller building. On the other hand, the new zonal system of ASCE 7-16 divides the interior zone into two zones: zone 1 and zone 1'. Figure 5-14 shows pressure coefficients on zone 1 for two buildings only, namely 10 m (32 ft) and 5 m (16 ft) heights. Clearly, pressure coefficients are higher for the 5 m (16 ft) height building, because the size of the corner zone in ASCE 7-16 depends only on the building height, and it is not limited to the least plan dimension, which makes zone 1 very small for the 5 m (16 ft) height building. Consequently, zone 2 becomes smaller leaving zone 1 to cover a critical area of high wind loads, unlike zone 1 of the 10 m (32 ft) height building, where it covers an area subjected to low wind loads.

In addition, zone 1 is not applicable to the building of 20 m (64 ft) height, since the latter is a building of intermediate height, for which another zonal system of 3 pressure zones is considered, as shown at the top of Figure 5-14 for buildings of height greater than 60 ft. For zone 1', Figure 5-14 shows higher pressure coefficients for the higher building. It should be noted that values of pressure coefficients on zone 1' in Figure 5-14 are similar to those on the interior zone in Figure 5-13; in other words, zone 1' in ASCE 7-16 and interior zone of ASCE 7-10 and NBCC 2015 are approximately the same.
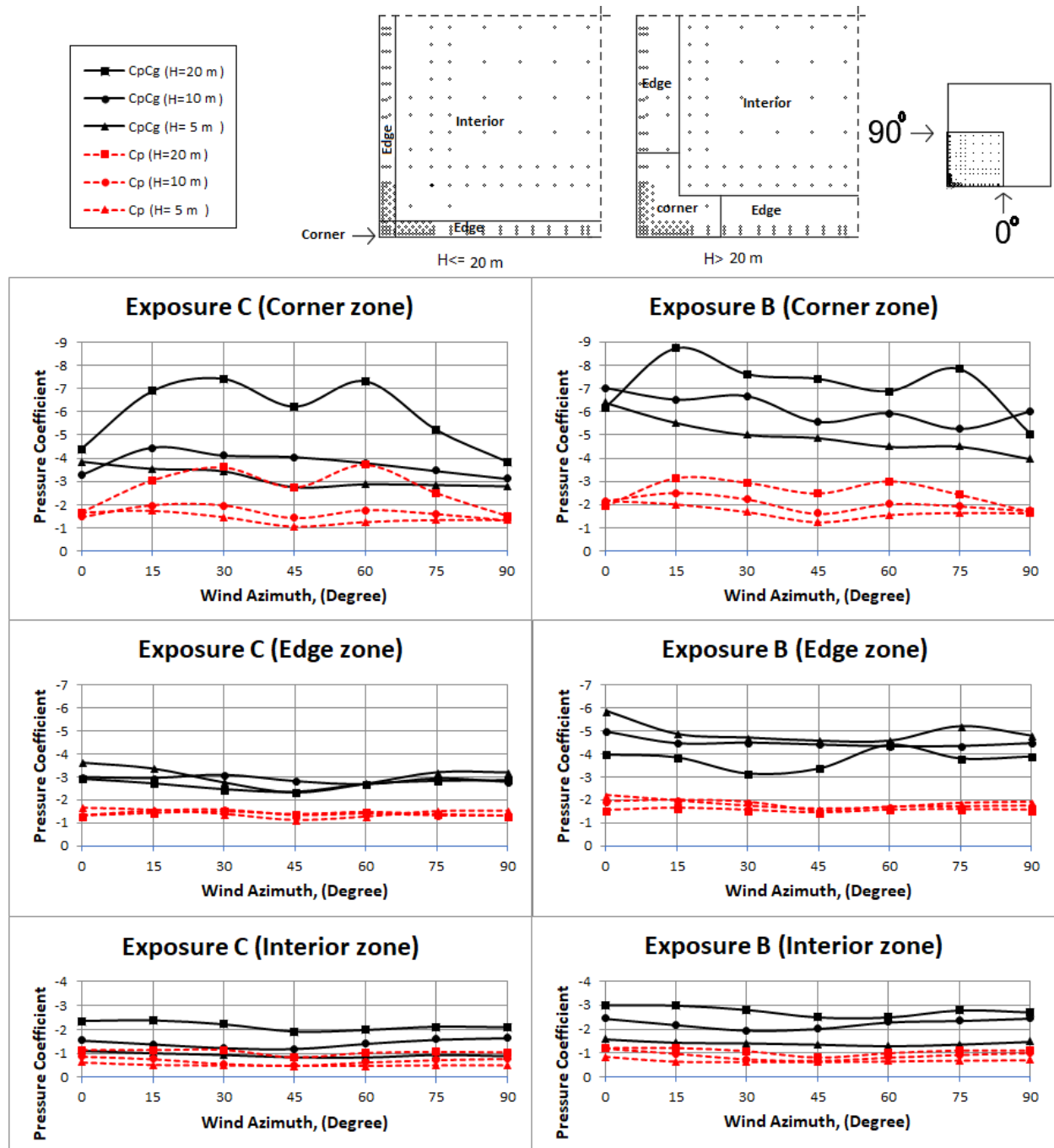
Figure 5-13: Extreme peak and mean pressure coefficients for pressure zones defined by ASCE 7-10 and NBCC 2015 versus wind direction for 3 different heights and two exposures.
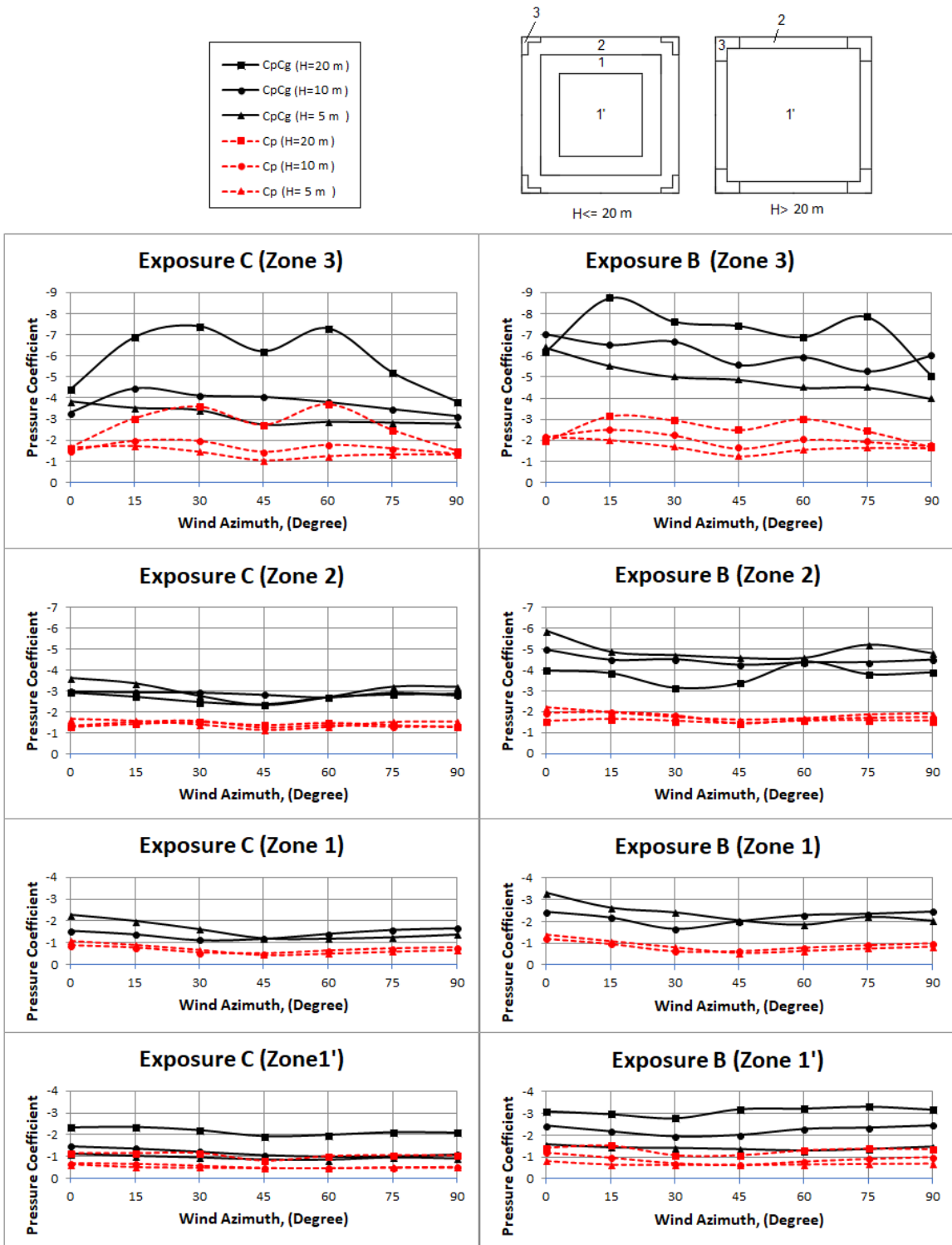
Figure 5-14: Extreme peak and mean pressure coefficients for pressure zones defined by ASCE 7-16 versus wind direction for 3 different heights and two exposures.

5.3 Area averaged peak pressure coefficients

Design of cladding and components against wind loads depends on the area loads rather than the point loads, because wind loads acting on the façade or the roof are resisted by an entire single component, such as an aluminum cladding panel or a roof tile. This raises the need of evaluating area wind loads in order to obtain accurate wind loading for the design of components and cladding with different areas. This is the reason that wind loads are presented in wind codes and standards as a function of the tributary area. Due to the area-averaging effect, area-averaged peak pressure coefficients on small areas are greater in magnitude than those on large areas.

The tributary areas represent the areas associated with each pressure tap and combination of two or more pressure taps. It should be noted that area-averaged peak pressure coefficients in this thesis are presented in the NBCC format. Figure 5-15 presents enveloped area-averaged peak pressure coefficients versus tributary area on the pressure zones of NBCC 2015 and ASCE 7-10 for buildings of 5 m (16 ft) and 10 m (32 ft) heights in exposure C. Values of area-averaged peak pressure coefficients decrease as the tributary area increase in the corner zone, while the reduction in the values of area-averaged coefficients with the tributary is small in the edge zone, also, the experimental results show that the reduction of area-averaged wind loads is very small over the tributary areas in the interior zone.

Figure 5-16 shows most critical area-averaged peak pressure coefficients versus tributary area on the pressure zones of ASCE 7-16 for buildings of 5 m (16 ft) and 10 m (32 ft) heights in exposure C. Values of most critical area-averaged peak pressure coefficients on corner and edge zones of ASCE 7-16 are similar to those of NBCC 2015 and ASCE 7-10.

Zone 1 and zone 1' in ASCE 7-16 correspond to the interior zone of ASCE 7-10 and NBCC 2015; however, values of area-averaged peak pressure coefficients of the 5 m (16 ft) height building on zone 1 are higher than those evaluated on the interior zone of ASCE 7-10 and NBCC 2015. This is, as stated earlier, due to the small size of both zone 3 and zone 2, which makes zone 1 go very close to the roof corner in which the wind loads are higher than in the rest of the roof. On the other

hand, the area-averaged peak pressure coefficients developed on the roof of the 10 m (32 ft) height building on Zone 1 and Zone 1' are the same as the area-averaged peaks developed on the interior zone specified by NBCC 2015 and ASCE 7-10. Figure 5-17 shows the most critical area-averaged peak pressure coefficients for the 20 m (64 ft) height building and results exhibit the same trend as in figure 5-15.
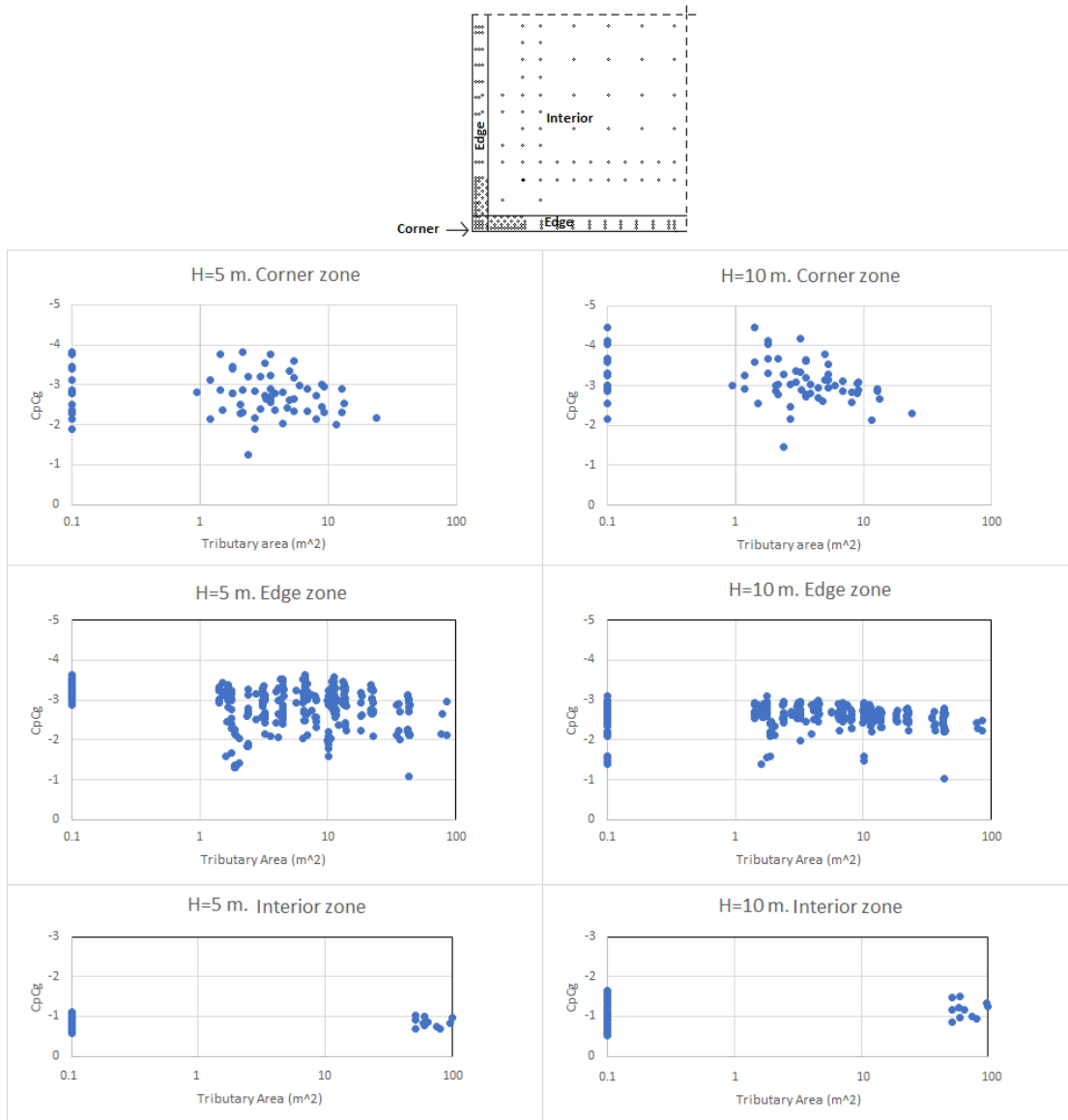
Figure 5-15: Most critical area-averaged peak pressure coefficients for all wind directions on the pressure zones defined by ASCE 7-10 and NBCC 2015 for buildings of 5 m and 10 m heights.
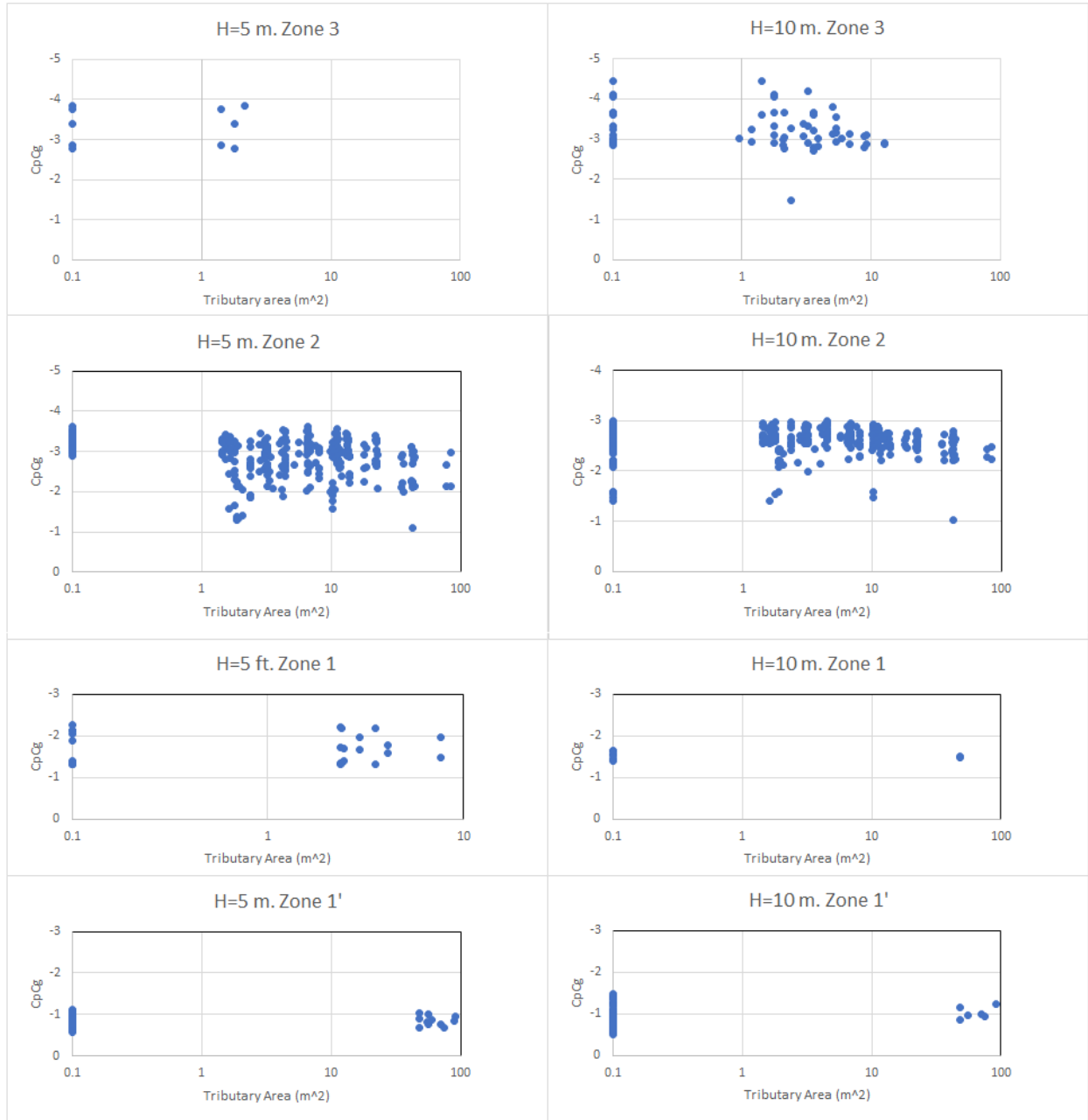
Figure 5-16: Most critical area-averaged peak pressure coefficients for all wind directions on the pressure zones defined by ASCE 7-16 for buildings of 5 m and 10 m heights.
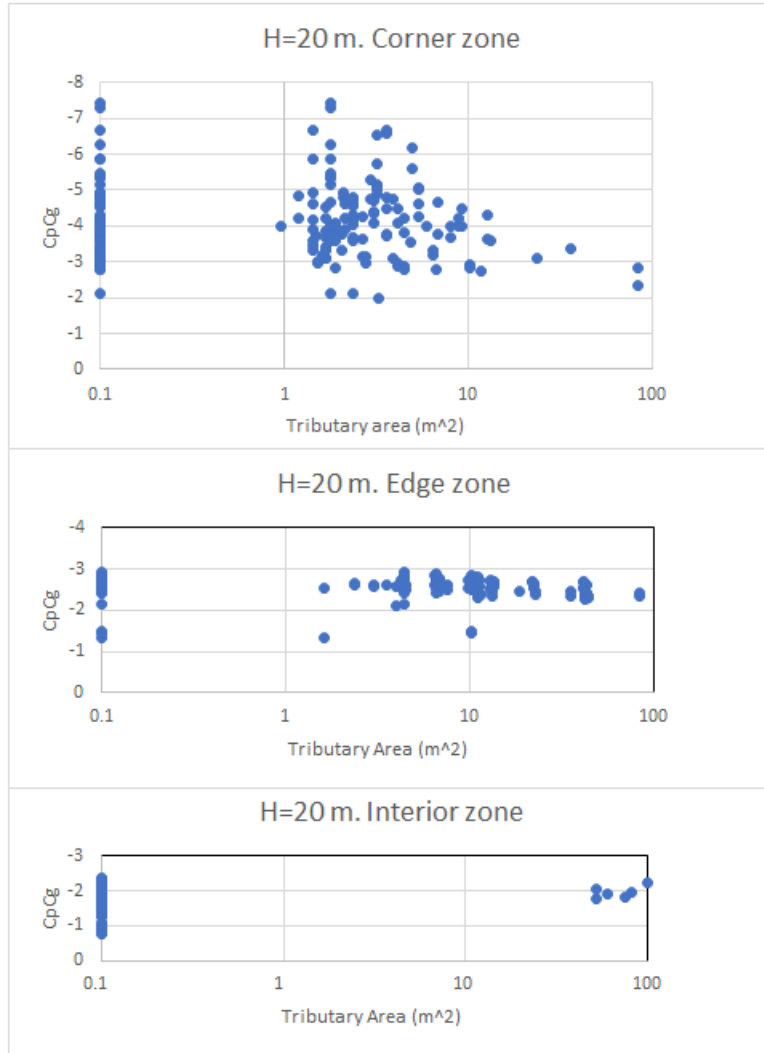
Figure 5-17: Most critical area-averaged peak pressure coefficients for all wind directions on pressure zones defined by NBCC 2015, ASCE 7-10 and ASCE 7-16 for building of 20 m height.

5.4 Comparison with previous studies

For validation purposes, the results of the present study of the 10 m (32 ft) height building were compared with three previous studies: Alrawashdeh and Stathopoulos (2015), Stathopoulos (1987) and Ho et al (2015).

5.4.1 Alrawashdeh and Stathopoulos (2015)

Nine building models of square flat roofs were tested in a simulated open country exposure in the study of Alrawashdeh and Stathopoulos (2015) at the wind tunnel of Concordia University to investigate the wind loads on large roofs. The results of the 10 m height building in the present study have been compared with the results of a building of 10 m height with plan dimensions of 120 m in the study of Alrawashdeh and Stathopoulos (2015). The comparisons are presented in Figure 5-18 and Figure 5-19.

Figure 5-18 shows a comparison of extreme pressure coefficients for the corner and edge zones versus the wind direction. In the corner zone, mean pressure coefficients are in a good agreement with small differences at wind azimuth of 30° and 75° due to the small difference between the two studies (i.e. roof slope, model size).

Peak pressure coefficients are close at wind azimuth of 30° or less but larger discrepancies appear at wind azimuths more than 30°. In the edge zone, pressure coefficients of the present study are greater than those of Alrawashdeh and Stathopoulos (2015). This is probably due to the fact that the model of the present study has plenty of pressure taps in the corner and the edge zones, which makes the tracing of pressure gradient at the transition between the corner zone and the edge zone more accurate and reflects the actual reduction in wind pressures along the leading edge. In other words, the pressure tap assembly in the present model records the wind pressure just before and after the line separated corner and edge zones, which results in relatively high pressure coefficients in the edge zone.

Figure 5-19.a shows the variation of peak and mean pressure coefficients along the centerline of the roof for 0° wind direction. Results of both studies are very close except the peak coefficient value of the pressure tap near the leading edge.

Figure 5-19.b shows the variation of peak and mean pressure coefficients along the line at the concurrent edge (X/B = 0.01) for 45° wind direction. Discrepancies appear in the values of peak pressure coefficients along the entire line and the values of mean pressure coefficients near the leading edge (Y/L < 0.1). This is again attributed to the different number and locations of pressure taps in this area accentuated by the conical vortices developed along the edge when the wind strikes at an azimuth of 45°. However, the values of mean pressure coefficients show a good agreement beyond Y/L = 0.1.
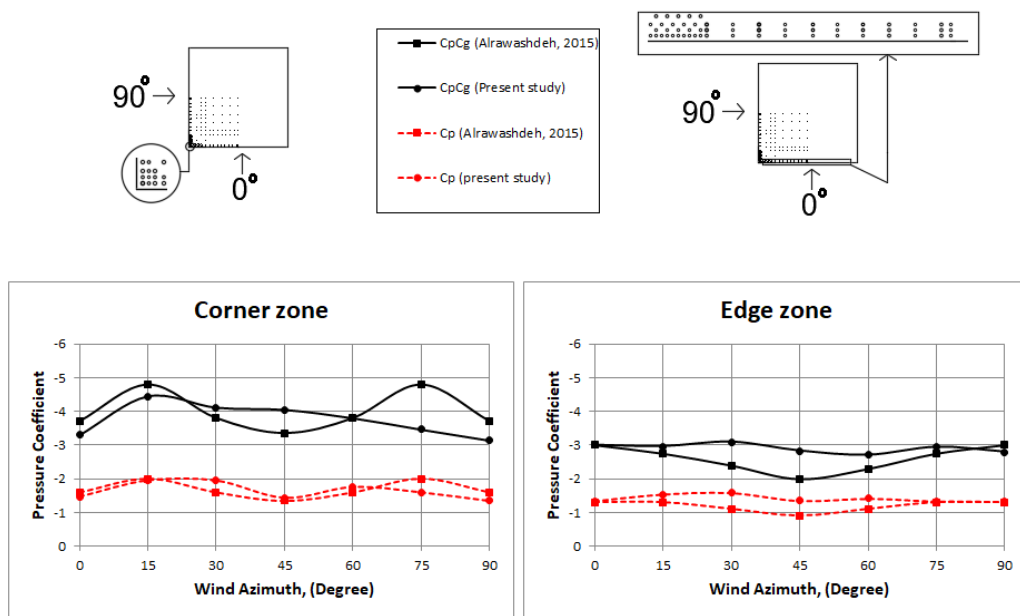
Figure 5-18: Comparison of extreme peak and mean pressure coefficients on the corner and the edge zones between the present study and Alrawashedh and Stathopoulos, 2015.
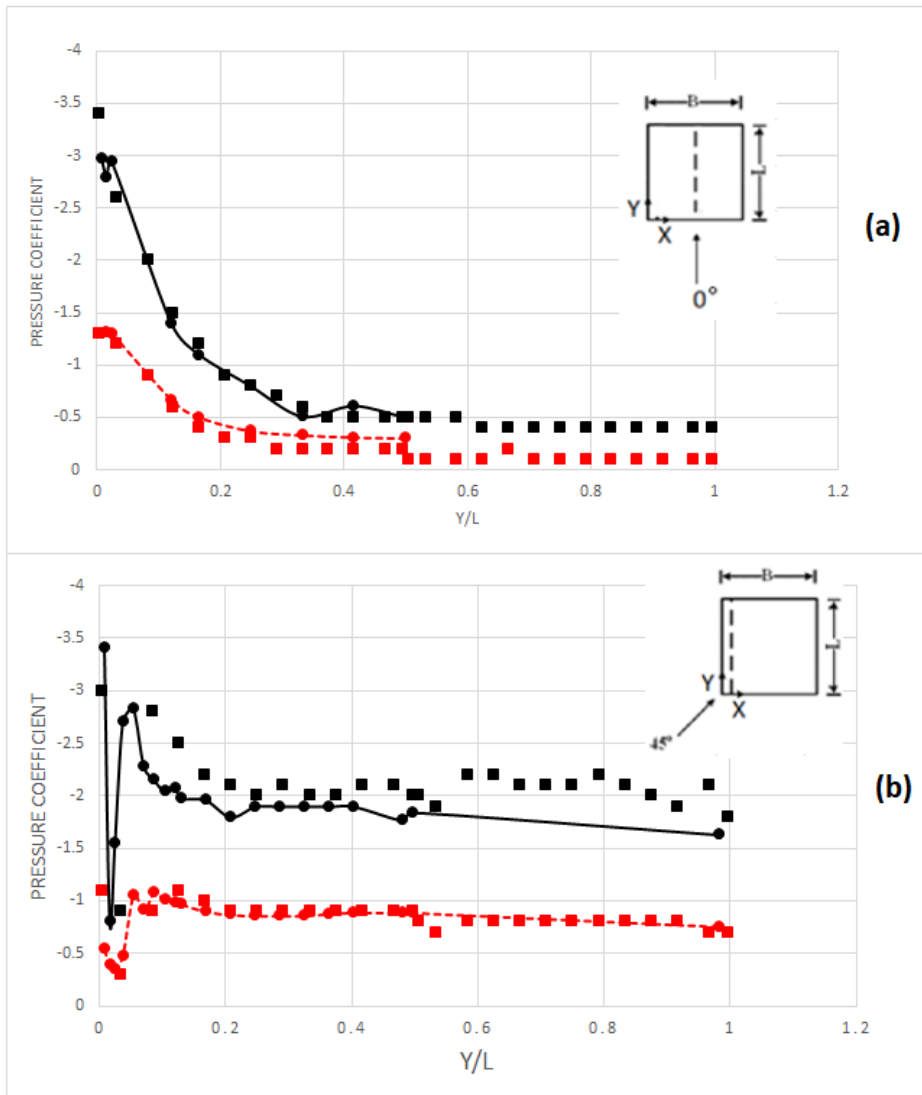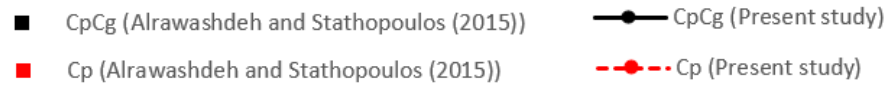
Figure 5-19: Comparison between the present study and Alrawashdeh and Stathopoulos (2015), a) Variation of wind pressure coefficients along the roof centerline for 0° wind direction; b) Variation in wind pressure coefficients along the line at the concurrent edge for 45° wind direction.

5.4.2   Stathopoulos (1987)

Figure 5-20 compares values of extreme pressure coefficients on the corner zone in open country exposure between Stathopoulos (1987) for a building of 10 m height and square plan dimension of 60 m and the present study for the 10 m height building. Values of Cp and CpCg (Stathopoulos, 1987) represent pressure coefficients recorded by the fourth row of pressure taps in the model of Stathopoulos (1987), which lies in the same location of the first row of pressure taps in the model of the present study.

Excellent agreement between the mean and peak pressure coefficients of the two studies with the exception of wind direction of 30° probably because of the differences in pressure tap location on the present model and the model used in the study of Stathopoulos (1987).
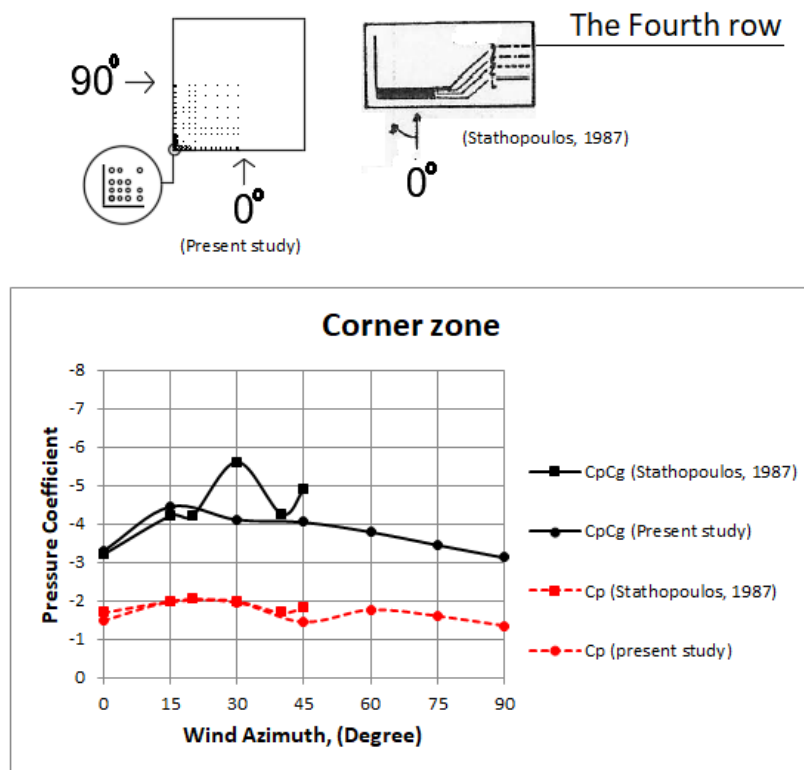
Figure 5-20: Comparison of extreme peak and mean pressure coefficients on the corner zone between the present study and Stathopoulos (1987).

5.4.3 Ho et al (2005)

Ho et al (2005) is a study conducted at the University of Western Ontario for numerous low-rise building models with different plan dimensions, heights and roof slopes. Figure 5-21 presents a comparison of mean pressure coefficients recorded along the roof mid-line for normal wind direction for a building of 10 m height, plan dimensions of 38 m X 25 m, and roof slope of 1:12; and the present study for the 10 m height building in exposure C.

Mean pressure coefficients are plotted over a distance normalized with respect to the building height. Mean pressure coefficients of Ho et al (2005) are very close to those of the present study at a distance near the building edge (i.e. $Y/H < 0.5$) and lower than the mean values of the present study at other points in the interior zone (i.e. $Y/H > 0.5$) with a small difference that does not exceed 0.2. This might be justified because the model of Ho et al. (2005) has a steeper roof slope and different plan dimensions. Peak pressure coefficients for this case were not reported in Ho et al. (2005)
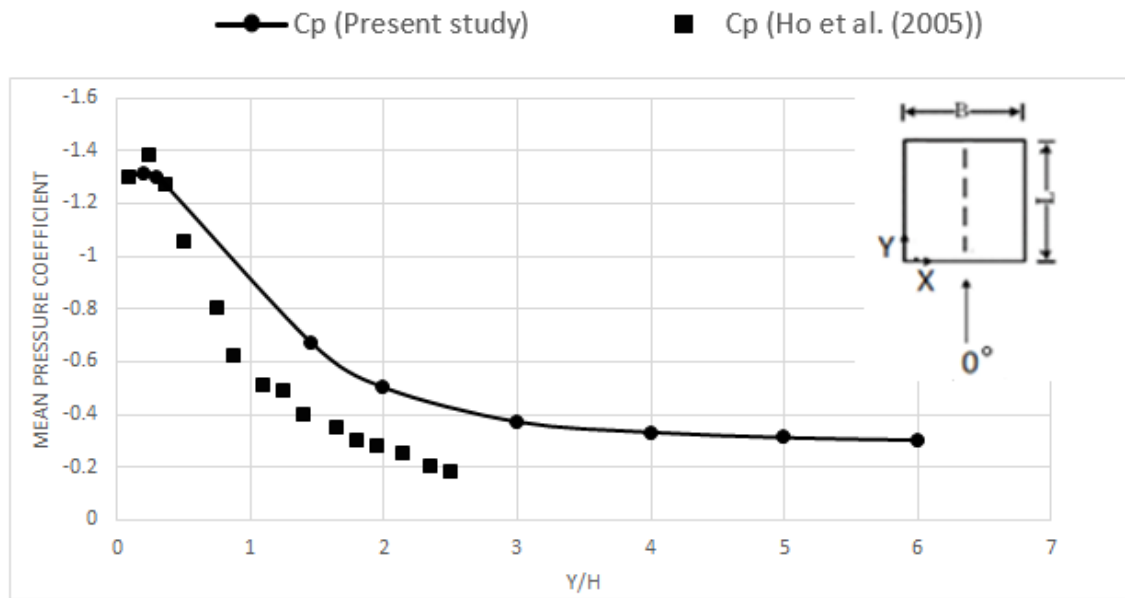
Figure 5-21: Variation of wind pressure coefficients of the present study and Ho et al (2005) along the roof centerline for normal wind direction.

5.5   Comparison with full-scale data

The results of the present study were compared with full-scale pressure measurements on the roof of the experimental building of Duro-Last Roofing Inc. in Iowa site. The field measurements on the experimental building were made in order to investigate the new low-slope roof low-rise building wind load provisions of ASCE 7-16. Figure 5-22 presents the roof plan of the experimental building, as well as, the layout of pressure tubes equipped in the roof.

As shown in Figure 5-22, the experimental building has square plan dimensions of 73 m (240 ft) , eave height of 6 m (20 ft), and 1.4° roof slope. The roof of the experimental building is equipped with 28 pressure tubes, 6 tubes in the top-left roof corner and the rest in the bottom-left quarter. Figure 5-22.a presents a detailed layout of the pressure tubes on the bottom-left quarter of the roof, which is divided into 4 pressure zones: zone 3, zone 2, zone 1, and zone 1', the same pressure zones as in ASCE 7-16.

Two manometers are utilized to measure the wind velocity in the site: one is fixed beside the building at a height of 8 m (26 ft) above the ground, the other is installed above the building at a height of 12 m (38 ft) from the ground level. Moreover, the terrain exposure of the surrounding area near the experimental building can be classified as an open country exposure.

The experimental building was modeled at a length scale of 1:250, and the model was tested in the wind tunnel in a simulated open country exposure. As shown in Figure 4-5 and Figure 4-6 and also clarified earlier, 196 pressure taps were installed in the roof of the model. The black pressure taps in the bottom-left quarter and the 6 pressure taps in the top-left corner represent the full-scale pressure tubes in Duro-Last Roofing Inc. experimental building.
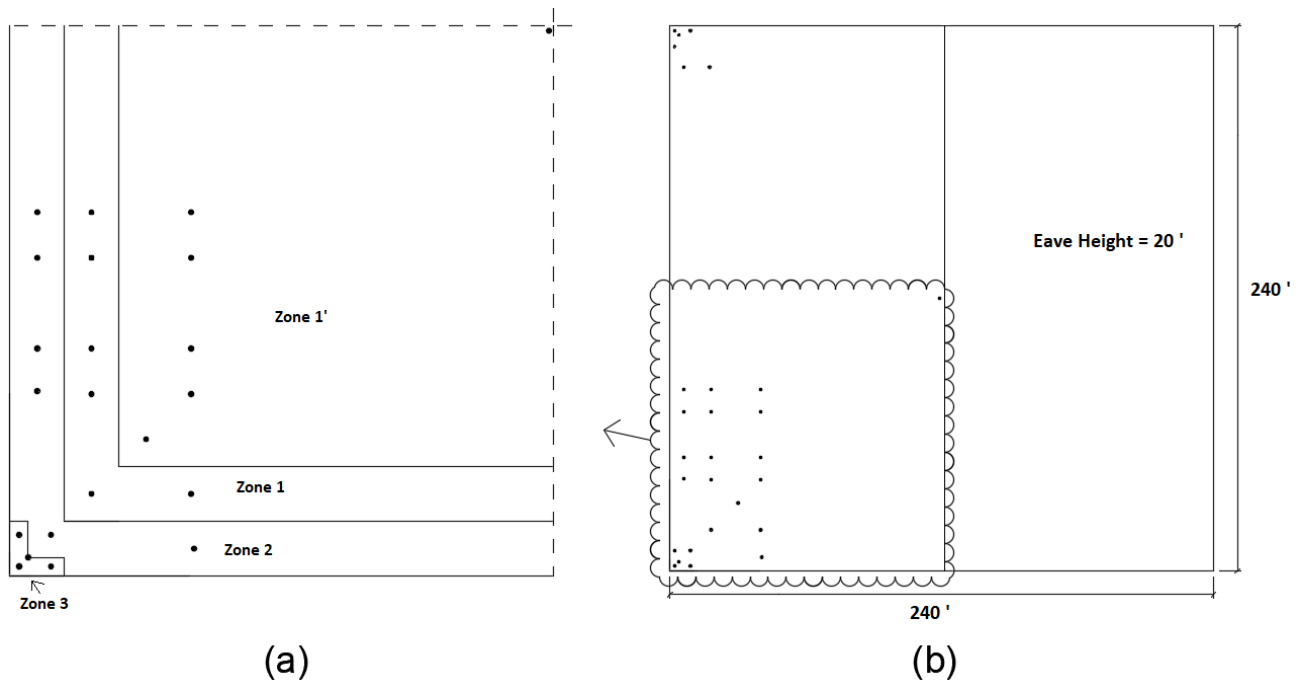
Figure 5-22: The experimental building of Duro-Last Roofing Inc. (a) Detailed pressure tap assembly, (b) Roof plan dimensions with pressure tap layout.

The full-scale peak pressure coefficients were calculated based on pressure measurements recorded at wind speed higher than 16 m/s (35 mph). Figure 5-23 presents the full-scale maximum, average and minimum peak pressure coefficients versus wind direction, as well as, the wind tunnel results based on the records obtained from the pressure taps corresponding to the full-scale pressure tubes. The full-scale peak pressure coefficients are presented for 3 wind directions: 0°, 90° and 135°. All peak pressure coefficients are presented in the format of ASCE 7, which is based on a velocity averaging time of 3 seconds.

The results of the present study are in good agreement with the average full-scale peak pressure coefficients in zone 3 and zone 1 except at wind direction of 135° in zone 1, at which the peak pressure coefficient of the present study coincides with the minimum full-scale peak. In zone 1', however, the peak pressure coefficients of the present study are a bit higher or lower than the minimum peak pressure coefficients of the full-scale results.

81

Figure 5-24 shows the enveloped peak pressure coefficients of the full-scale data and the experimental results for three wind directions, namely, 0°, 90° and 135° in the pressure zones defined in ASCE 7-16. The enveloped wind tunnel peaks show a perfect agreement with the enveloped average full-scale peak pressure coefficient in zone 3, zone 2 and zone 1; while it is closer to the minimum enveloped full-scale peak in zone 1'.
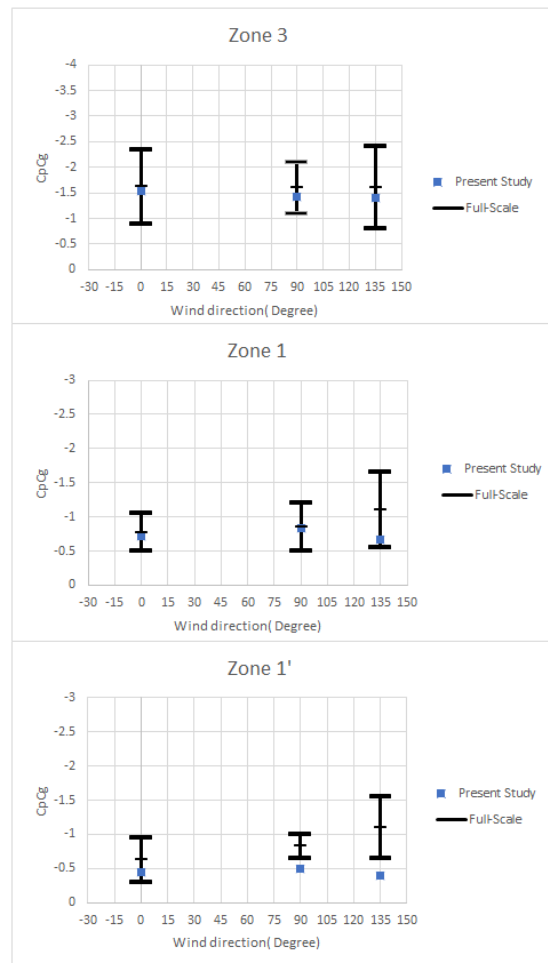
Figure 5-23: Comparison of peak pressure coefficients versus wind direction for zone 3, zone 1, and zone 1' between the results of the present study and the full-scale data measured on the experimental building of Duro-Last Roofing, Inc. in Iowa site.
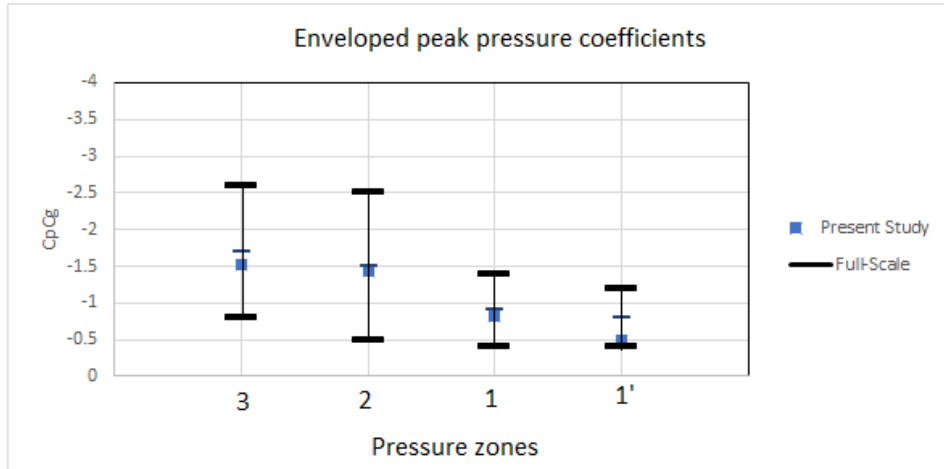
Figure 5-24: Comparison of the enveloped peak pressure coefficients between the full-scale data and the present study in ASCE 7 roof pressure zones.

Chapter 6

Comparison of the present study

with the North American Codes and Standards

The experimental findings of the present study were compared with the wind provisions of the North American codes and standards to investigate their applicability to provide an adequate design for buildings of large horizontal dimensions. The comparison was implemented in two regards: peak pressure coefficients on the roof pressure zones and roof zonal systems.

6.1 Peak pressure coefficients

Local and area-averaged peak pressure coefficients of the present study were compared with the corresponding peaks provided by the North American codes and standards to examine the suitability of wind loads specified by the codes to provide safe and economical design for large roofs.

Since the present study examines the wind loads on building roofs for three heights, the peaks provided by the codes should be modified to be comparable to the results of each building by considering the exposure factor. For instance, the external peak pressure coefficients for zone 3 in ASCE 7-16 is equal to -6.3, see Figure 3-3, and the exposure factor, K_z, of the building of 20 m (64 ft) height is equal to 1.16, then, the final value of peak pressure coefficient, CpCg, specified in ASCE 7-16 for the 64 ft height building becomes -7.3.

Table 6-1 summarises the exposure factors for the three buildings according to NBCC 2015, ASCE 7-10 and ASCE 7-16 in exposure C.

Table 6-1: Exposure factors for the three buildings in the present study in exposure C.

Building height (m)	(C_e), NBCC 2015	(K_z), ASCE 7-10/16
5	0.9	0.88
10	1.01	1.01
20	1.15	1.16

6.1.1   Local pressure coefficients

As mentioned before, external peak pressure coefficients recommended by NBCC and ASCE 7 are provided as area-averaged peak pressure coefficients, such that the maximum (in an absolute sense) external peak pressure coefficients are assigned for the minimum tributary areas (less than $1\ m^2$), and then, the external pressure coefficients attenuate to reach the minimum value for larger tributary areas. In this section, the most critical local pressure coefficients of the present study will be compared with the codes external peak pressure coefficients corresponding to the minimum tributary area (i.e. $1\ m^2$) in each pressure zone.

Figure 6-1 shows comparisons between the most critical peak pressure coefficients, CpCg, among all wind directions for the three buildings in the present study and the peaks recommended by the codes. Peak pressure coefficients of the 5 m (16 ft) height building are lower than values of external pressure coefficients specified by NBCC 2015 and ASCE 7-10 in the corner and the interior zones. However, in the edge zone, values of peak pressure coefficients of NBCC 2015 and ASCE 7-10 are exceeded by the experimental peak. It seems that the high turbulence at the roof level of the 5

85

m (16 ft) height building extends the high peaks into the edge zone. Peak pressure coefficients of the new edition of the American standard, ASCE 7-16, are higher than the experimental results in all pressure zones with a difference reaching 1.7 in the corner zone. This results in an overestimation of the design loads on large roofs and leads to overdesign and extra cost. Although the peak pressure coefficients specified for the corner zone are higher than those for the edge zone in NBCC and ASCE 7, experimental results of the 5 m (16 ft) height building showed that similar peak pressure coefficients were recorded on the corner zone and the edge zone.

For the building of 10 m (32 ft) height, values provided by the three codes are higher than the experimental peaks in all zones, except the peak recommended by NBCC 2015 for the edge zone, which is lower than the experimental findings of the present study. Again, values of external pressure coefficients of ASCE 7-16 are much higher than the experimental results, with a difference of 1.9 in the corner zone.

The bottom graph in Figure 6-1 shows a comparison between the results of the present study for the 20 m (64 ft) height building and the North American codes. Both ASCE 7-16 and ASCE 7-10 provide the same external peak pressure coefficients and pressure zones for buildings of heights more than 60 ft. The experimental most critical peak pressure coefficient evaluated on the corner zone is approximately equal to the peak pressure coefficient of ASCE 7-10 and ASCE 7-16, whereas the peak pressure coefficients of the same codes are higher than the experimental most critical peak coefficients calculated on the edge and the interior zones with a high difference of 2.1 for the edge zone. As mentioned previously, when the building height is less than 20 m (65.6 ft), then it is considered as low-rise building based on NBCC 2015. The 20 m (64 ft) height building is at the limit, and for this reason, values of most critical peak pressure coefficients evaluated on its roof have been compared with the provisions of NBCC 2015 for low-rise buildings and mid-rise buildings. As shown in the figure, values of experimental peak pressure coefficients are significantly higher than those specified for low-rise buildings in NBCC 2015. On the other hand, the peak pressure coefficients of NBCC 2015 for mid-rise buildings are greater than the experimental results, except for the corner zone, where the difference is relatively small. Clearly,

for a building of height close to 20 m, it is recommended to consider the provisions of the mid-rise buildings.

| -3.8 (-4.9) | -3.6 (- 2.25) | -3.6 (- 3.1) | -3.8 (-4.9) |

-1.1 (-1.6) -1.1 (-1.75)

NBCC 2015   ASCE 7-10

ASCE 7-16

-1.1 (-1.6)   H=5 m

-2.3 (-2.9)

-3.6 (- 4)

-3.8 (-5.6)

| -4.5 (-5.5) | -3 (- 2.5) | -3 (- 3.6) | -4.5 (-5.6) |

-1.7 (-1.8)   -1.7 (-2)

NBCC 2015   ASCE 7-10

ASCE 7-16

-1.5 (-1.8)   H=10 m

-1.7 (-3.4)

-3 (- 4.6)

-4.5 (-6.4)

| -7.4 (-6.2) | -4.1 (- 2.9) | -2.9 (- 5.2) | -7.4 (-7.3) |

-2.71 (-2.1)   -2.4(-3.2)

NBCC 2015
(H <= 20 m)

ASCE 7-10
&
ASCE 7-16

NBCC 2015
(H > 20 m)

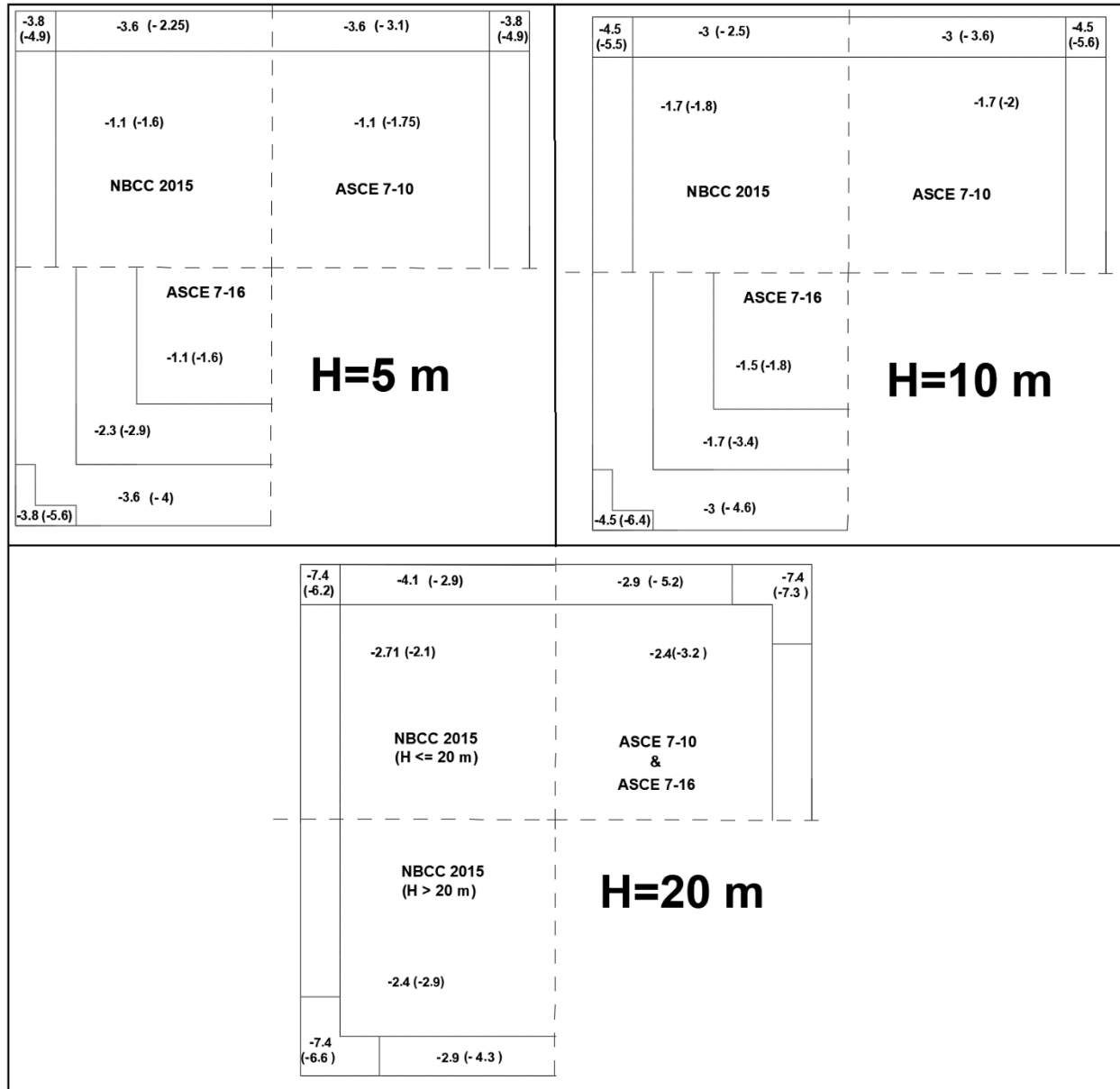H=20 m

-2.4 (-2.9)

-7.4 (-6.6)   -2.9 (- 4.3)

Figure 6-1: Comparison of most critical peak pressure coefficients between the present study for the three buildings in open country exposure and the corresponding recommended peaks of NBCC 2015, ASCE 7-10 and ASCE 7-16. (coefficients between brackets are the recommended codes values).

6.1.2　Area-averaged peak pressure coefficients

Since the wind loads are presented as a function of tributary area, it is very important to compare the experimental area-averaged peaks with those specified by the North American codes and standards in order to assess the suitability of area-averaged peak pressure coefficients of the North American codes to provide safe and economical design for large roofs.

Figure 6-2, 6-3 and 6-4 present comparisons between the area-averaged peak pressure coefficients of the present study and those provided by NBCC 2015, ASCE 7-10 and ASCE 7-16 in exposure C. As shown in Figure 6-2, the experimental area-averaged peaks evaluated on the edge zone of the 5 m (16 ft) height building are higher than those specified by NBCC 2015 and ASCE 7-10, while they are higher than the peak pressure coefficients provided by NBCC 2015 only for the 10 m (32 ft) height building, see Figure 6-3.

The experimental peaks recorded on some areas in the edge zone of the 5 m (16 ft) height building are similar in magnitude to those recorded in the corner zone, and the exact location these areas at which the highest wind loads occur in the edge zone could not be determined. However, the codes recommend lower pressure coefficients for the edge zone, and to ensure a safe design for the components and cladding of the edge zone of this building, the recommended design peak pressure coefficients for the edge zone should be raised to be comparable to those recommended for the corner zone. This indeed will be very expensive for large buildings, but it is the only way to provide safe design for the edge zone. On the other hand, area-averaged peaks of NBCC 2015 and ASCE 7-10 are higher than the experimental results in the corner and the interior zones for the 5 m (16 ft) and 10 m (32 ft) height buildings.

Peaks of ASCE 7-16 are higher than the experimental results with a large difference in all pressure zones except in the corner zone of the 20 m (64 ft) height building, where the ASCE 7-16 peak is a bit lower than the experimental peak. Again, the values of external peak pressure coefficients

provided by ASCE 7-16 for low-slope roofs of low-rise buildings are very conservative and result in a costly design for large roofs.

The experimental results showed that the reduction in the magnitude of the enveloped area wind loads is small in the edge zone as the tributary area increases. However, this is not the scenario presented in the North American codes at which the area-averaged peak pressure coefficients specified for the edge zone drop from -4.5 to -2.75 in ASCE 7-16, -3.5 to -2.25 in ASCE 7-10; and -2.5 to -2 in NBCC 2015, see Figure 3-2.

In the corner zone, area-averaged peak pressure coefficients decrease with tributary area. In addition, the reduction in experimental area-averaged peak pressure coefficients with the tributary area in the interior zone agrees with the curves specified by the codes for the interior zone at which the area-averaged peak pressure coefficients decrease marginally as the tributary area increases.

Moreover, it should be noted that the tributary area which corresponds to the minimum area-averaged peak pressure coefficients has been increased to be $46\ m^2$ ($500\ ft^2$) in ASCE 7-16. This change agrees well with the results of the presents study, at which the minimum area-averaged peak pressure coefficient was found on areas much greater than $9\ m^2$ ($100\ ft^2$). For example, the minimum area-averaged peak pressure coefficient occurs on a tributary area of $24\ m^2$ ($256\ ft^2$) in the corner zone of the 32 ft height building.

Ultimately, the advantage of having the minimum peak assigned for a tributary area of $46\ m^2$ ($500\ ft^2$) in the curve of the area-averaged peak pressure coefficients in the codes is clear by observing the experimental area-averaged peaks on the corner zone in Figure 6-2 and Figure 6-3. The curve of peak pressure coefficients in ASCE 7-10 and NBCC 2015 would cover all the experimental results if the minimum value of peak pressure coefficients would have shifted to the right until it corresponds to a tributary area of $46\ m^2$ ($500\ ft^2$).

Figure 6-2: Comparison of the most critical area-averaged peak pressure coefficients, CpCg, of the present study and the values recommended by the codes (H=5 m, Exposure C).

Figure 6-3: Comparison of the most critical area-averaged peak pressure coefficients, CpCg, of the present study and the values recommended by the codes (H=10 m, Exposure C).
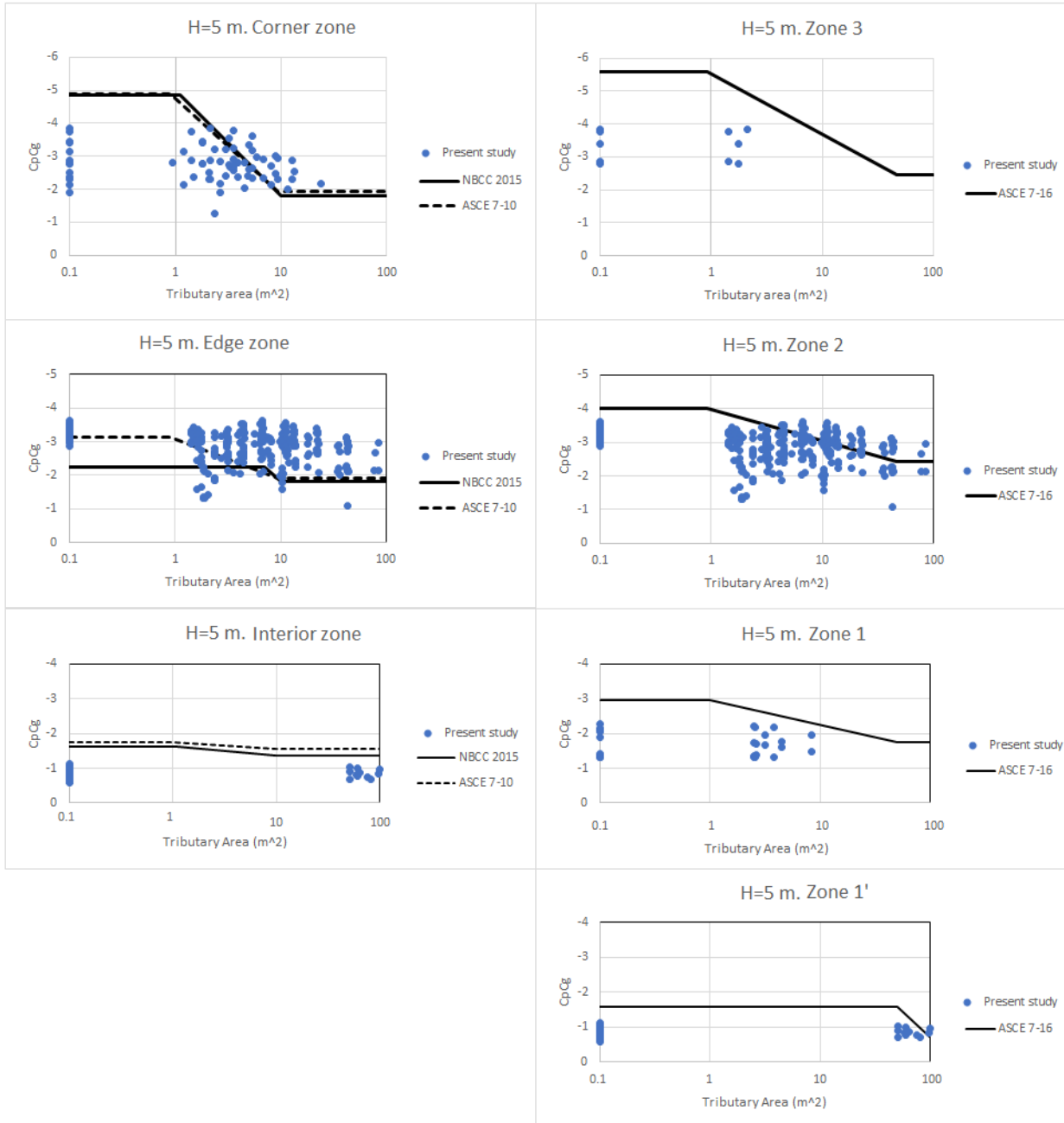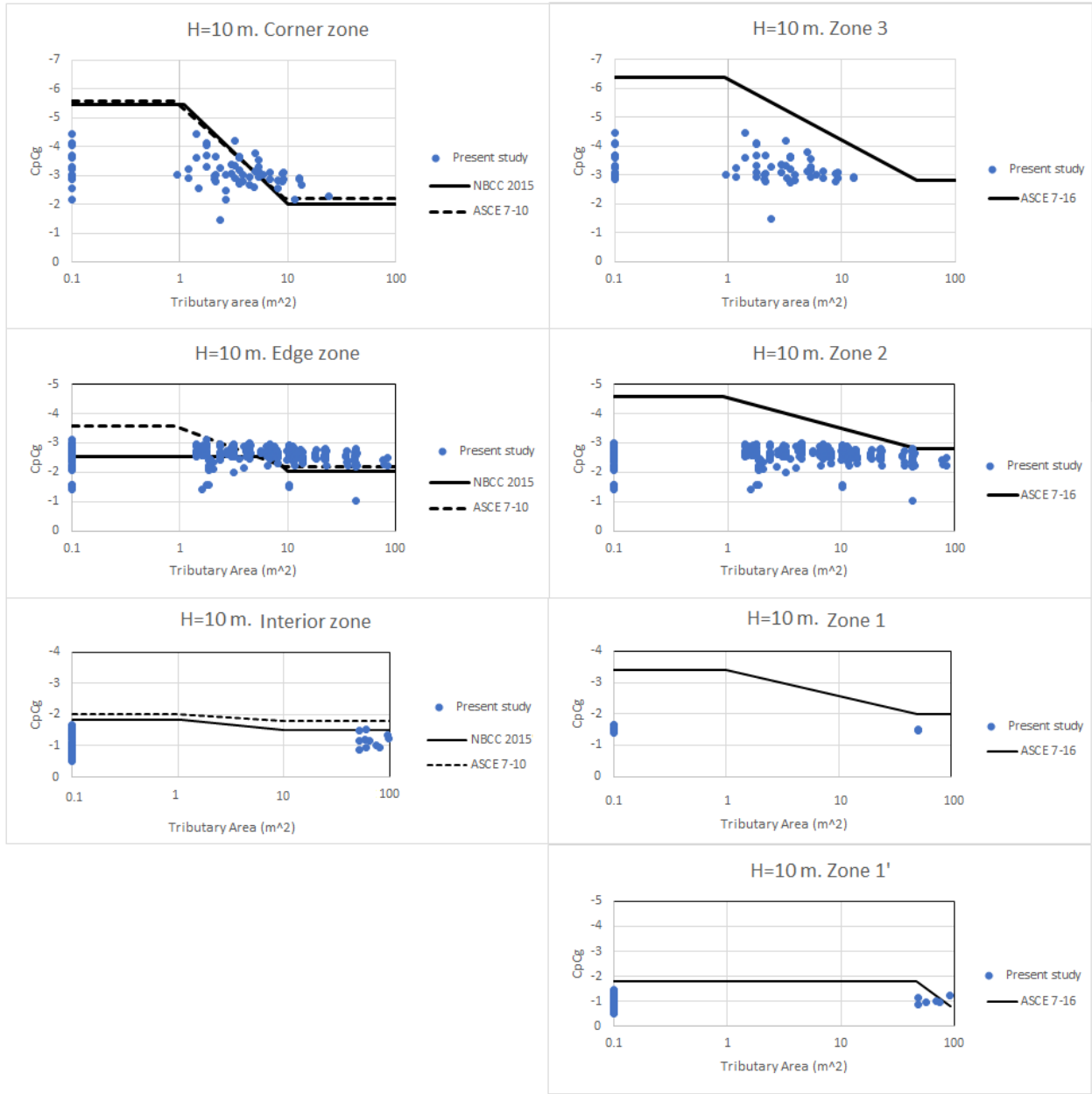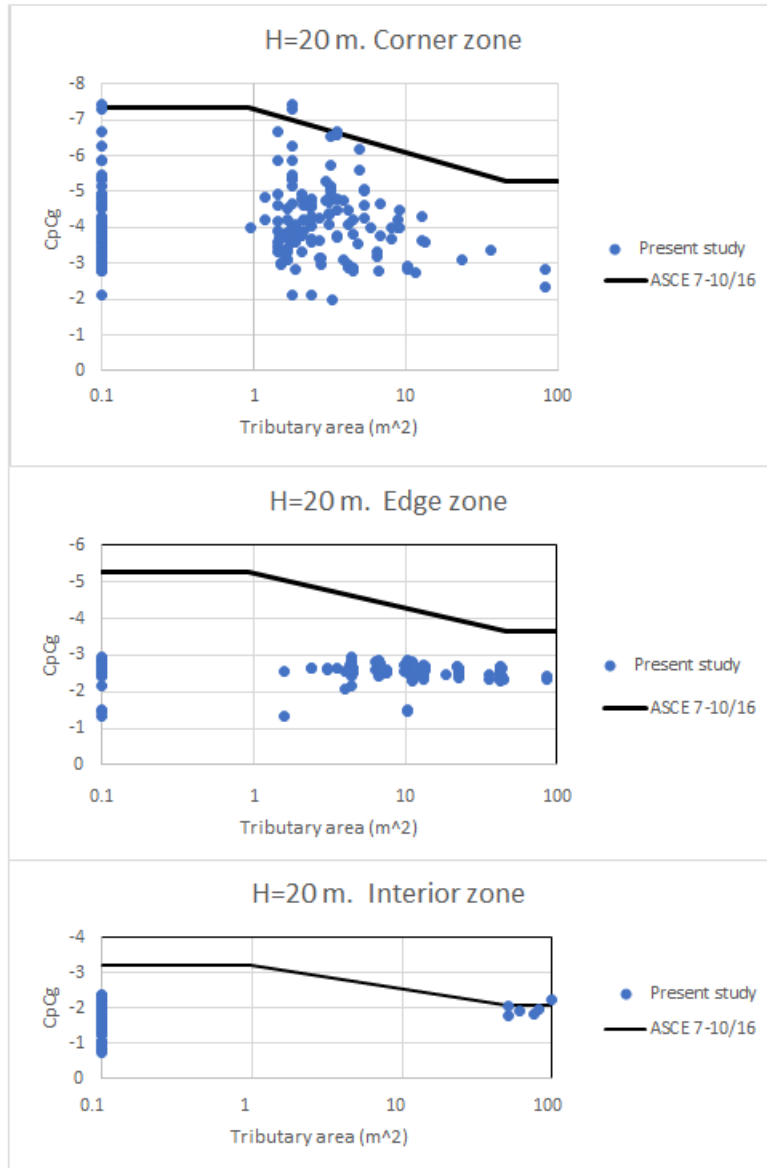
Figure 6-4: Comparison of the most critical area-averaged peak pressure coefficients, CpCg, of the present study and the values recommended by ASCE 7-10/16 (H=20 m, Exposure C).

6.2   Roof pressure zones

Comparison of the pressure zones with the North American codes can be accomplished by setting the pressure zones on the contours of the enveloped peak pressure coefficients of the three buildings in the present study, and then the pressure zones can be examined. Corner zone should capture the highest peaks in the roof corner and extend to cover an area that is subjected to wind peak pressure coefficients greater than the peak pressure coefficient provided by the code for the edge zone. On the other hand, the edge zone should not have peaks greater than those specified by the codes for the edge zone. In these comparisons, peak pressure coefficients specified in ASCE 7-10 for the edge zone will be taken as a reference to determine the suitability of the zonal systems of the North American codes.

Figure 6-5 shows the most critical peak pressure coefficients over the bottom-left quarter of the roof for the building of 5 m (16 ft) height in exposure C and exposure B, as well as, the pressure zones of the three codes. As shown, corner zones of the three codes capture the highest peak pressure coefficients in the roof corner in both exposures, however, the highest peak pressure coefficients developed on the edge zone are approximately the same as those developed on the corner zone, which are greater than the edge zone peak pressure coefficients of ASCE 7-10 for the 5 m (16 ft) height building in both exposures. In this case, corner and edge zones should be treated as a single pressure zone with the same peak pressure coefficients. Again, this will be very costly for large buildings, however, it is safe.

The pressure zones of ASCE 7-10, NBCC 2015 and ASCE 7-16; and the most critical pressure coefficients for the building of 10 m (32 ft) height in exposure C and exposure B are presented in Figure 6-6. According to ASCE 7-10, the maximum peak pressure coefficient for the edge zone and for the 32 ft height building in exposure C is -3.6, the corner zone size of NBCC 2015 and ASCE 7-10 is adequate to capture the wind peak pressure coefficients more than -3.6, whereas the corner zone of ASCE 7-16 is slightly oversized along the leading edges. It should be noted that the L-shaped corner zone of ASCE 7-16 takes the same spatial distribution of the high peaks in the roof corner; however, it extends a bit more along the leading edge, and captures peak pressure

coefficients lower than the value provided by ASCE 7-10 for the edge zone. The same scenario applies to the wind load distribution in exposure B, where the corresponding value of the edge zone peak pressure coefficient in ASCE 7-10 for exposure B is equal to -5.1. As shown in the figure, the corner zone of ASCE 7-10 and NBCC 2015 includes all pressure coefficients greater than -5, and the corner zone of ASCE 7-16 extends along the leading edge and captures relatively low-pressure coefficients. As a result, the proper corner zone for such buildings of around 10 m (32 ft) height should be sized according to NBCC 2015 or ASCE 7-10 and shaped based on ASCE 7-16 as shown in Figure 6-8.

Figure 6-7 shows most critical peak pressure coefficients for the 20 m (64 ft) height building in exposure C and Exposure B; and the pressure zones of the three codes based on the provisions of mid-rise buildings. The corner zone is very large such that it extends along the leading edge to include wind peak pressure coefficients much lower than those specified for the edge zone in ASCE 7-10.

Experimental examination of wind loads on the buildings of 5 m and 10 m heights results in two different scenarios: similar peak pressure coefficients occur in the corner and the edge zone for the 5 m height building, and the L-shaped distribution of high wind pressures in the roof corner for the 10 m height building. However, each scenario should be generalized for a set of heights rather than a specific height, for this reason, an intermediate height of 8 m (26 ft) may be selected to separate between the two scenarios. Figure 6-8 presents a proposed roof zonal system for large low-slope roofs of low-rise buildings. The proposed roof zones are based on the experimental results of the present study, and they are for buildings of height greater than 8 m (26 ft) and large plan dimensions. The size of long side of L-shaped corner is the end- zone width, z, see section 3.2, while short side size is z/3 based on the experimental data in both exposure C and B.

Figure 6-5: Contour of most critical peak pressure coefficients for the building of 5 m height in both exposure with the pressure zones of ASCE 7-16 (white lines) and NBCC 2015 and ASCE 7-10 (black lines).

Figure 6-6: Contour of most critical peak pressure coefficients for the building of 10 m height in both exposure with the pressure zones of ASCE 7-16 (white lines) and NBCC 2015 and ASCE 7-10 (black lines).
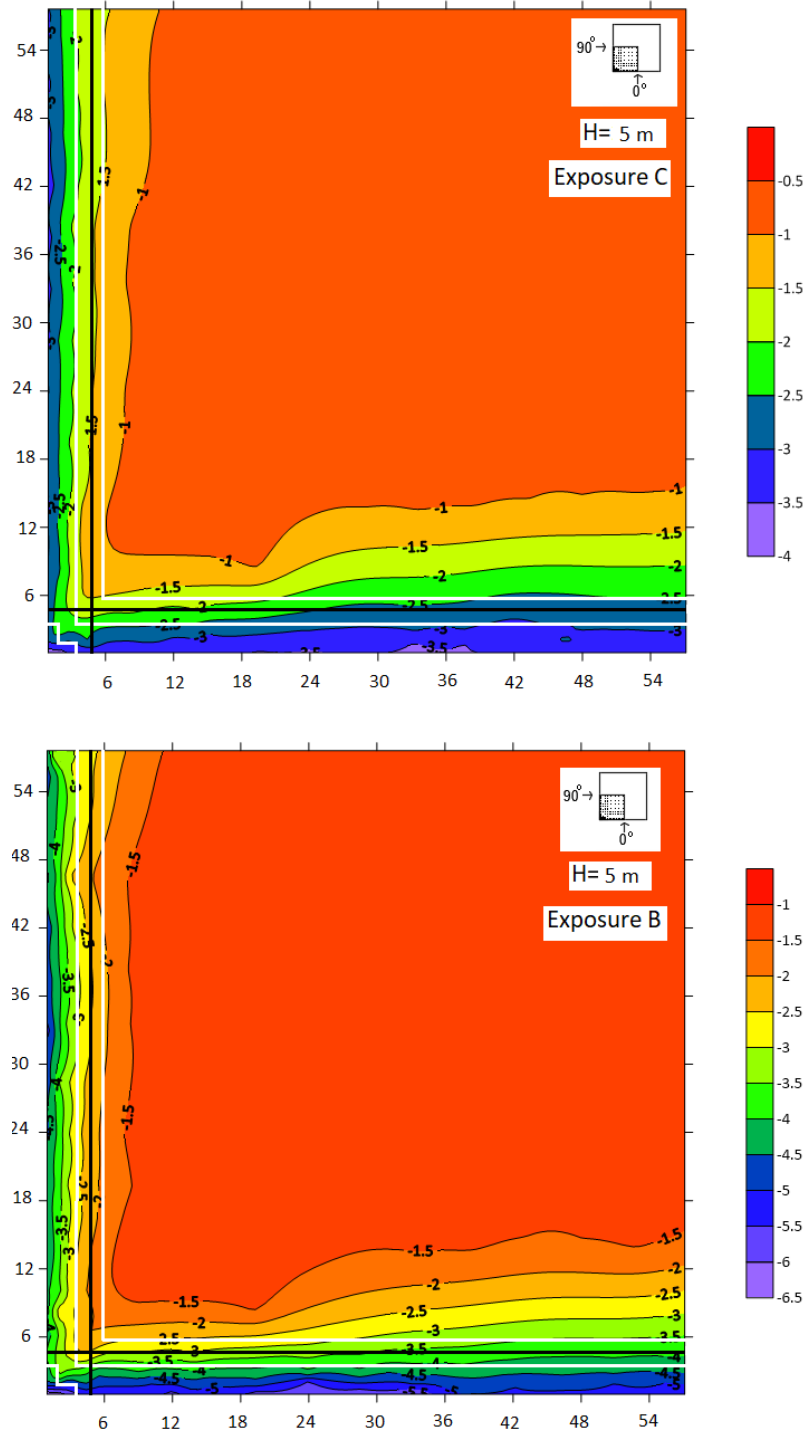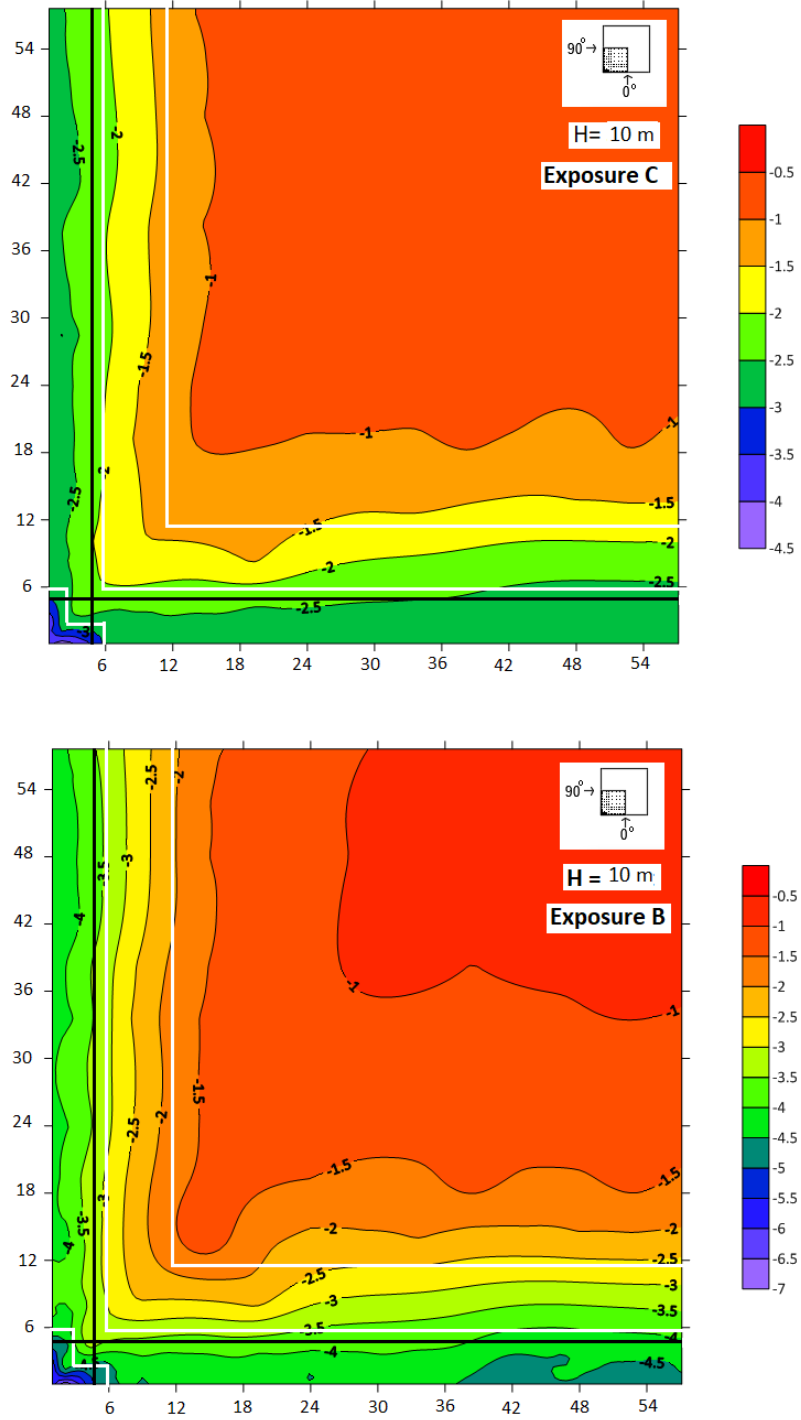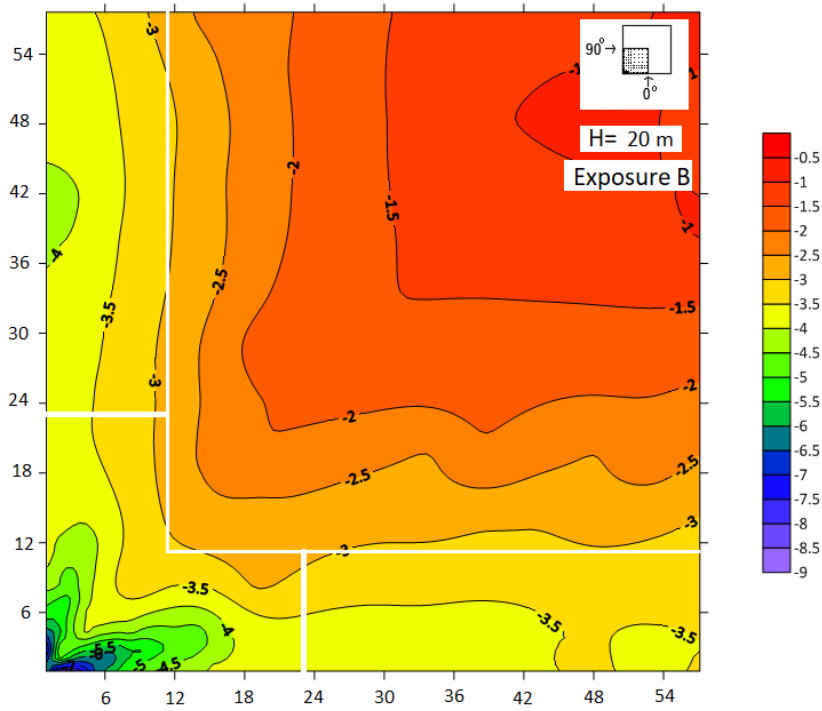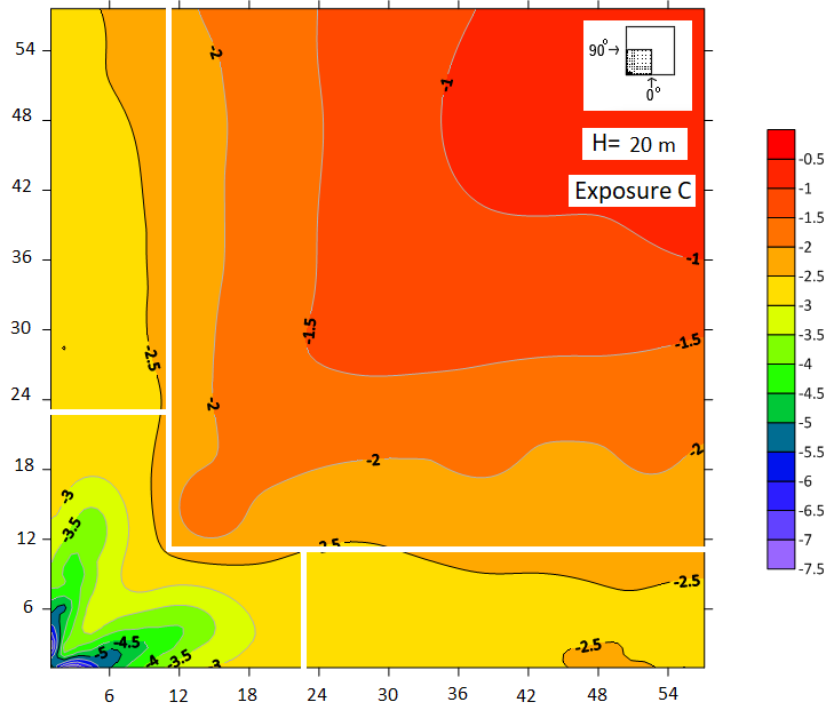
Figure 6-7: Contour of most critical peak pressure coefficients for the building of 20 m height in both exposures with the pressure zones of ASCE 7-16, NBCC 2015 and ASCE 7-10.
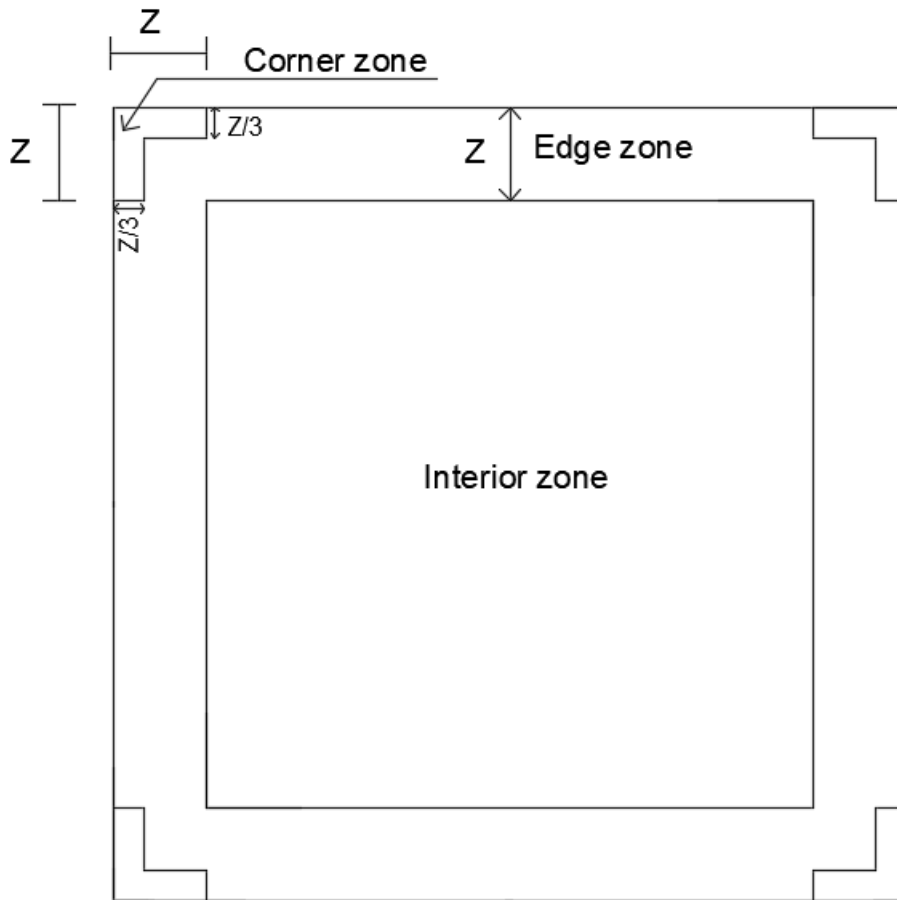
Figure 6-8: Proposed zonal system for low-slope low-rise buildings of heights more than 8 m and large geometries, z is the end-zone width defined in NBCC 2015.

Chapter 7

Conclusion and recommendations for future work

7.1 Conclusion

The necessity of examining wind loads on buildings of large plan dimensions arises since wind provisions of the North American codes were constructed based on studies conducted on buildings of regular size. This study investigated wind loads on low-slope (less than < 7°) roof buildings of large plan dimensions (more than 60 m or 200 ft) to investigate the applicability of the North American codes to such buildings.

Three building models of identical plan dimensions (118 m x 118 m) and different heights: 5 m, 10 m, and 20 m were tested in the wind tunnel for seven wind directions in two terrain exposures: open country exposure and suburban exposure. The experimental results were presented in terms of contours of most critical pressure coefficients, extreme local pressure coefficients versus wind direction, and area-averaged peak pressure coefficients. The results were compared with past studies, full-scale data, and the North American codes. The comparison with the North American codes and standards (ASCE 7-10, ASCE 7-16, and NBCC 2015) were carried out in two aspects: the magnitude of peak pressure coefficients and the roof zonal system. The following are conclusive remarks of the present study:

1. Peak pressure coefficients recommended by ASCE 7-16 for low-slope roofs are much higher than the actual wind loads on large low-slope roofs of low-rise buildings and using these peaks for large low-slope roof design is uneconomical.

2. Peak pressure coefficients of ASCE 7-10 specified for low-slope roofs are conservative and economical for large low-slope roof design.

3. Peak pressure coefficients of NBCC 2015 recommended for low-slope roofs are also applicable to large low-slope roofs except the peak pressure coefficients provided for the edge zone, they are low and should be increased to be similar to the peak pressure coefficients of ASCE 7-10.

4. For large low-slope roof low-rise buildings of low heights (less than 8 m), wind loads developed on the corner zone and the edge zone are comparable. For this case, the corner and the edge zone should be treated as a single zone with the same design peak pressure coefficients.

5. For large low-slope roof low-rise buildings of height greater than 8 m, the corner zone should have an L-shape. The size of long side of the L-shaped corner is the end- zone width, z, as defined in NBCC 2015, while short side size is z/3 – see Fig. 6-8.

6. Area-averaged wind loads on the edge zone of large roofs decrease only a little as the tributary area increases.

7. The spatial distribution of wind pressures over large roofs is similar in both open country and suburban exposures.

7.2   Recommendations for future work

- The current study concerned square roofs with one plan dimension (118 m). Thus, it is recommended to test building models with different shape and plan dimensions.

- Large mid-rise buildings have been examined by testing a 20 m high building only. Higher mid-rise buildings (30 m, 40 m) should be examined in the future.

- Two terrain exposures, open country and suburban, have been considered. It is recommended to consider urban exposure as well, in the future research.

References

Alrawashdeh, H., 2015. Wind pressures on flat roof edges and corners of large low buildings. Concordia University, Montreal, Quebec, Canada, Master's Thesis.

Alrawashdeh, H., Stathopoulos, T., 2015. Wind pressures on large roofs of low buildings and wind codes and standards. J. Wind Eng. Ind. Aerodyn. 147, 212–225.

AS/NZS 1170.2 (2011) Australian/New Zealand Standard for Structural Design Actions, part 2: Wind Actions. Sydney, New South Wales, Australia: Standards Australia and Standards New Zealand.

ASCE/SEI 7-10, 2010. Minimum Design Loads for Buildings and Other Structures. Structural Engineering Institute of ASCE, Reston, VA.

ASCE/SEI 7-16, 2017. Minimum Design Loads and associated criteria for Buildings and Other Structures. Structural Engineering Institute of ASCE, Reston, VA.

Baniotopoulos, C.C., Borri, C., Stathopoulos, T., (2011). Environmental Wind Engineering and Design of Wind Energy Structures. SpringerWeinNewYork, ISBN 978-3-7091-1120-8.

Blaabjerg, F., Ma, K., (2017). Wind energy systems. Proceedings of the IEEE. 105, 2116-2131.

Celik, I.B., (1999). Introductory Turbulence Modeling. Lectures Notes, Mechanical & Aerospace Engineering Dept., West Virginia University.

Cochran, L.S., Cermak, J.E., 1992. Full-and model-scale cladding pressures on the Texas tech experimental building. J. Wind Eng. Ind. Aerodyn. 43, 1589–1600.

Davenport, A.G., 1983. On the assessment of the reliability of wind loading on low buildings. J. Wind Eng. Ind. Aerodyn. 11, 21–37.

Davenport, A.G., Isyumov, N., (1967). The application of the boundary layer wind tunnel to the prediction of wind loading. Proc. Int. Research Seminar on Wind Effects on Buildings and Structures. 201-230.

Durst, C.S, 1960. Wind Speeds Over Short Periods of Time. Meteor. Magazine, 89, 181-187.

EN 1991-1-4, 2005. Eurocode 1, 2005: Actions on Structures-General Actions-Part 1-4: Wind Actions, European Standard.

Garret, J.R., 1994. The Atmospheric Boundary Layer, Cambridge University Press (Cambridge).

Ho, T.C.E., Surry, D., Morrish, D., Kopp, G.A., 2005. The UWO contribution to the nist aerodynamic data base for wind on low buildings: Part1. Archiving format and basic aerodynamic data. J. Wind Eng. Ind. Aerodyn. 93, 1–30.

Holmes, J.D., 1993. Wind Loads on Low-rise Buildings-A Review, CSIRO. Division of Building Research, Highett, Victoria, Australia.

Jensen, M., 1958. The model-law for phenomena in natural wind. Ingenioren, International edition 2.

Kasperski, M., 1996. Design wind loads for low-rise buildings: a critical review of wind load specifications for industrial buildings. J. Wind Eng. Ind. Aerodyn. 61, 169–179.

Kind, R.J., Wardlaw, R.L., 1979. Model studies of the wind resistance of two loose-laid roof-insulation systems. Laboratory technical report LTR-LA-234. National aeronautical establishment, National Research Council, Ottawa, Canada.

Kopp, G.A., Morrison, M.J., 2018. Component and cladding wind loads for low-slope roofs on low-rise buildings. J. Struct. Eng., 144(4).

Krishna, P., 1995. Wind loads on low rise buildings – A review. J. Wind Eng. Ind. Aerodyn.54–55, 383–396.

Lin, J.X., Surry, D., Tieleman, H.W., 1995. The distribution of pressure near roof corners of flat roof low buildings. J. Wind Eng. Ind. Aerodyn. 56, 235–265.

Lin, J.X., Surry, D., 1998. The variation of peak loads with tributary area near corners on flat low building roofs. J. Wind Eng. Ind. Aerodyn. 77–78, 185–196.

NBC2010, 2010. User's Guide-NBC 2010, Structural Commentaries (Part 4). Issued by the Canadian Commission on Buildings and Fire Codes, National Research Council of Canada.

NBC2015, 2015. User's Guide-NBC 2015, Structural Commentaries (Part 4). Issued by the Canadian Commission on Buildings and Fire Codes, National Research Council of Canada.

Oh, J.H., Kopp, G.A., Inculet, D.R., 2007. The UWO contribution to the NIST aerodynamic database for wind on low buildings: Part3. Internal pressures. J. Wind Eng. Ind. Aerodyn. 95, 755–779.

Pierre St., L.M., Kopp, G.A., Surry, D., Ho, T.C.E., 2005. The UWO contribution to the nist aerodynamic database for wind on low buildings: Part2. Comparison of data with wind load provisions. J. Wind Eng. Ind. Aerodyn. 93, 31–59.

Prandtl, L., 1905. Verhandlungen des dritten internationalen Mathematiker-Kongresses in Heidel berg 1904, Krazer, A. (ed.), Leipzig: Teubner, p. 484. English trans. Ackroyd, J. A. K., Axcell, B. P., Ruban, A. I. (eds.) 2001. Early Developments of Modern Aerodynamics. Oxford: Butterworth-Heinemann, p. 77.

Stathopoulos, T., 1979. Turbulent Wind Action on Low-rise Buildings. The University of Western Ontario, London, Ontario, Canada, Ph.D. Thesis.

Stathopoulos, T., 1984. Design and fabrication of a wind tunnel for building aerodynamics. J. Wind Eng. Ind. Aerodyn. 16, 361–376.

Stathopoulos, T., 1984. Wind loads on low-rise buildings – A review of the state of the art. Eng. Struct. 6, 119–135.

Stathopoulos, T., 1987. Wind pressures on flat roof edges and corners, in: Proc. 7th Int. Conf. on Wind Engineering, Aachen, Germany.

Stathopoulos, T., 2003. Wind loads on low buildings: in the wake of Alan Davenport's contribution. J. Wind Eng. Ind. Aerodyn. 91, 1565–1585.

Stathopoulos, T., Davenport, A.G., Surry, D., 1981. Effective wind loads on flat roofs. Journal of the Structural Division. 107 (2), 281-298.

Stathopoulos, T., Surry, D., 1983. Scale effects in wind tunnel testing of low buildings. J. Wind Eng. Ind. Aerodyn. 13, 313–326.

Stathopoulos, T., Baniotopoulos, C.C., (2007). Wind Effects on Buildings and Design of Wind-Sensitive Structures. SpringerWeinNewYork, ISBN 978-3-211-73075-1.

Surry, D., Stathopoulos, T., 1978. An experimental approach to the economical measurements of spatially averaged wind loads. J. Wind Eng. Ind. Aerodyn. 2 (4), 385–397.

Tamura, Y., Kareem, A., 2013. Advance structural wind engineering. SpringerJapan, ISBN 978-4-431-54719-8.

Taylor, G. I., 1937. The Statistical Theory of Isotropic Turbulence. Journal of the Aeronautical Sciences. 4 (8), 311-315.

Uematsu, Y., Isyumov, N., 1999. Wind pressures acting on low-rise buildings. J. Wind Eng. Ind. Aerodyn. 82, 1–25.

Van der Hoven, I. (1957). Power spectrum of wind velocities fluctuations in the frequency range from 0.0007 to 900 cycles per hour. Journal of Meteorology. 14, 1254-1255.

Appendix A

Components and cladding external peak pressure coefficients in the North American codes.
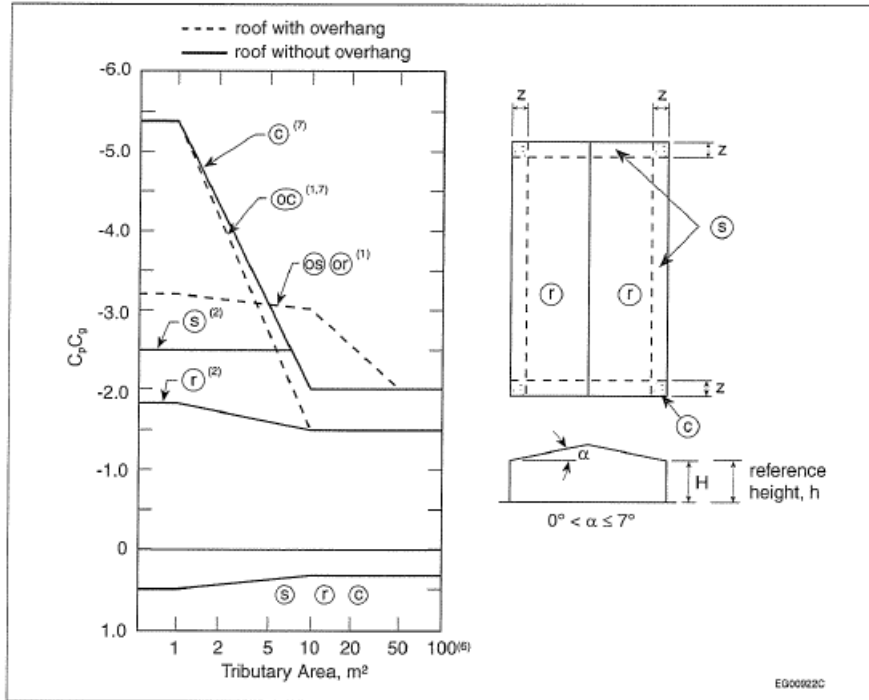
Appendix A 1: NBCC 2015 (H ≤ 20 m)

Appendix A 2: ASCE 7-10 (H ≤ 60 ft)

Appendix A 3: ASCE 7-16 (H ≤ 60 ft)

Appendix A 4: ASCE 7-10 (H > 60 ft)

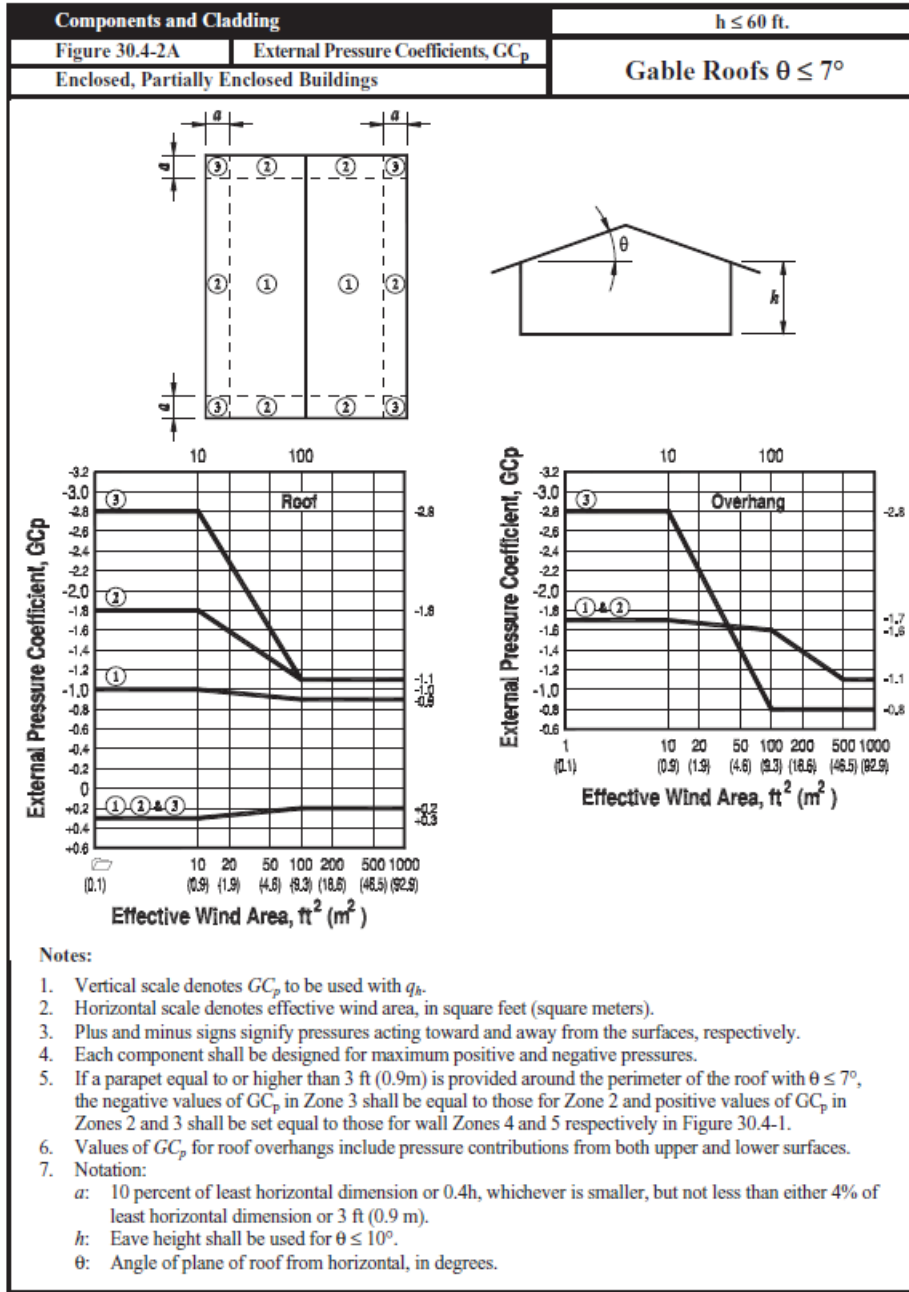**Appendix A 5:** ASCE 7-16 (H > 60 ft)

Appendix A 1: External peak pressure coefficients on roofs with a slope less than 7° in NBCC 2015 for the design of components and cladding, (Figure 4.1.7.6.-C in NBCC 2015).

Notes to Figure 4.1.7.6.-C:

(1) Coefficients for overhung roofs have the prefix "o" and refer to the same roof areas as referred to by the corresponding symbol without a prefix. They include contributions from both upper and lower surfaces. In the case of overhangs, the walls are inboard of the roof outline.

(2) s and r apply to both roofs and upper surfaces of canopies.

(3) End-zone width z is the lesser of 10% of the least horizontal dimension and 40% of height, H, but not less than 4% of the least horizontal dimension or 1 m.

(4) Combinations of external and internal pressures must be evaluated to obtain the most severe loading.

(5) Positive coefficients denote forces toward the surface, whereas negative coefficients denote forces away from the surface. Each structural element must be designed to withstand forces of both signs.

(6) For calculating the uplift forces on tributary areas larger than 100 m² on unobstructed nearly-flat roofs with low parapets, and where the centre of the tributary area is at least twice the height of the *building* from the nearest edge, the value of C_pC_g may be reduced from −1.5 to −1.1 at x/H = 2 and further reduced linearly to −0.6 at x/H = 5, where x is the distance to the nearest edge and H is the height of the *building*.

(7) For roofs having a perimeter parapet with a height of 1 m or greater, the corner coefficients C_pC_g for tributary areas less than 1 m² can be reduced from −5.4 to −4.4.

Components and Cladding		h ≤ 60 ft.
Figure 30.4-2A	External Pressure Coefficients, GC_p	Gable Roofs θ ≤ 7°
Enclosed, Partially Enclosed Buildings		

Notes:

1. Vertical scale denotes GC_p to be used with q_h.
2. Horizontal scale denotes effective wind area, in square feet (square meters).
3. Plus and minus signs signify pressures acting toward and away from the surfaces, respectively.
4. Each component shall be designed for maximum positive and negative pressures.
5. If a parapet equal to or higher than 3 ft (0.9m) is provided around the perimeter of the roof with θ ≤ 7°, the negative values of GC_p in Zone 3 shall be equal to those for Zone 2 and positive values of GC_p in Zones 2 and 3 shall be set equal to those for wall Zones 4 and 5 respectively in Figure 30.4-1.
6. Values of GC_p for roof overhangs include pressure contributions from both upper and lower surfaces.
7. Notation:
   - a: 10 percent of least horizontal dimension or 0.4h, whichever is smaller, but not less than either 4% of least horizontal dimension or 3 ft (0.9 m).
   - h: Eave height shall be used for θ ≤ 10°.
   - θ: Angle of plane of roof from horizontal, in degrees.

Appendix A 3: External peak pressure coefficients on roofs with a slope less than 7° in ASCE 7-16

(Height ≤ 60 ft)

Diagrams

ELEVATION

PLAN

Notation

B = Horizontal dimension of building measured normal to wind direction, in ft (m).
h = Eave height shall be used for $\theta = 10°$.
θ = Angle of plane of roof from horizontal, in degrees.

External Pressure Coefficients

Roof

Overhang

External Pressure Coefficient, (GC_p)

Effective Wind Area, ft^2(m^2)

Notes

1. Vertical scale denotes (GC_p) to be used with q_h.
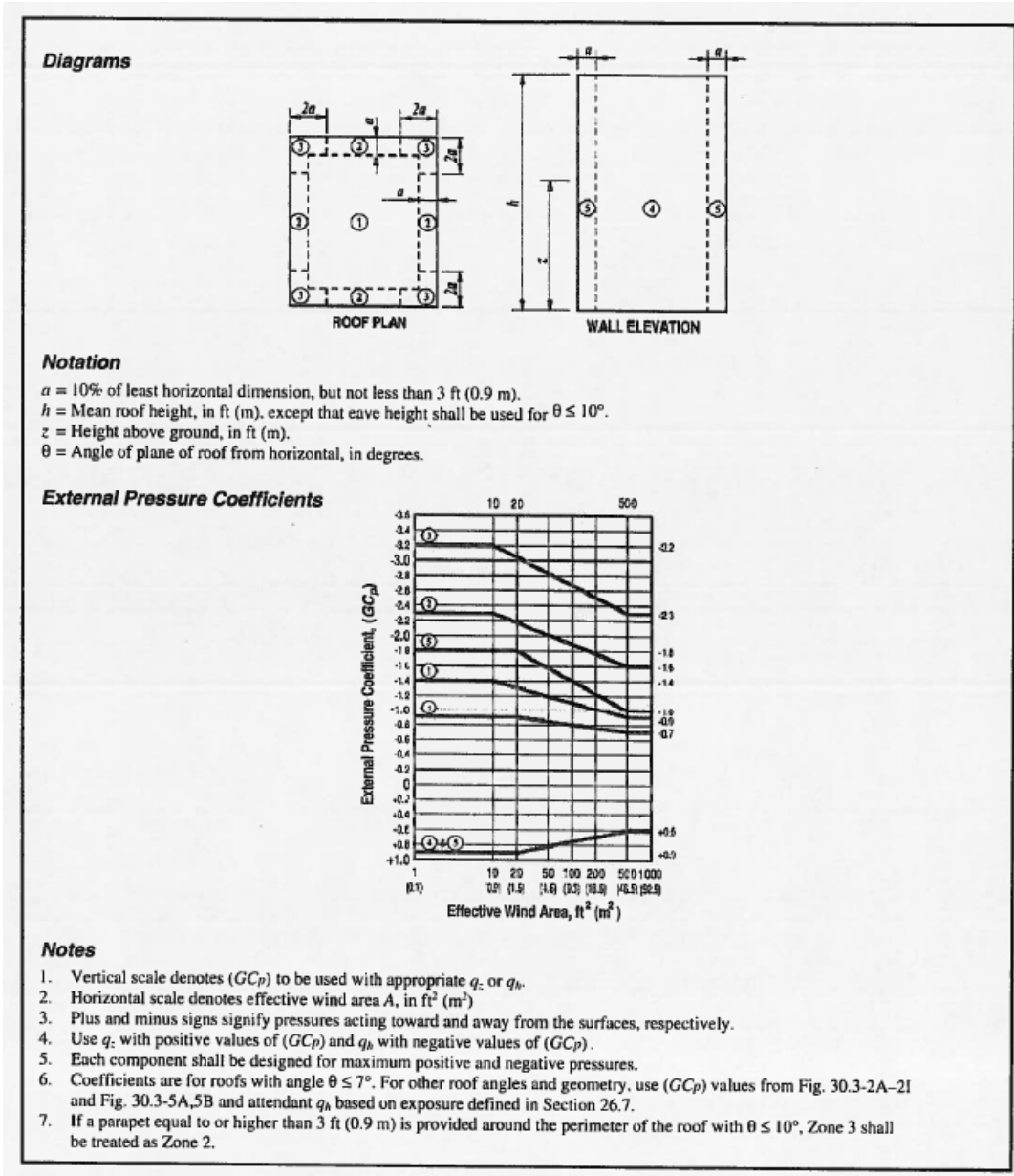2. Horizontal scale denotes effective wind area, in ft^2 (m^2).
3. Plus and minus signs signify pressures acting toward and away from the surfaces, respectively.
4. Each component shall be designed for maximum positive and negative pressures.
5. If a parapet equal to or higher than 3 ft (0.9 m) is provided around the perimeter of the roof with $\theta \leq 7°$, the negative values of (GC_p) in Zone 3 shall be equal to those for Zone 2, and positive values of (GC_p) in Zones 2 and 3 shall be set equal to those for wall Zones 4 and 5, respectively, in Fig. 30.3-1.
6. Values of (GC_p) for roof overhangs include pressure contributions from both upper and lower surfaces.
7. If overhangs exist, the lesser horizontal dimension of the building shall not include any overhang dimension, but the edge distance, a, shall be measured from the outside edge of the overhang.

Appendix A 4: External peak pressure coefficients in ASCE 7-10 (Height > 60 ft)

Components and Cladding — **h > 60 ft.**

Figure 30.6-1 — **External Pressure Coefficients, GCp**

Enclosed, Partially Enclosed Buildings — **Walls & Roofs**

ROOF PLAN

WALL ELEVATION

External Pressure Coefficient, GCp

Effective Wind Area, ft^2 (m^2)

Notes:
1. Vertical scale denotes GC_p to be used with appropriate q_z or q_h.
2. Horizontal scale denotes effective wind area A, in square feet (square meters).
3. Plus and minus signs signify pressures acting toward and away from the surfaces, respectively.
4. Use q_z with positive values of GC_p and q_h with negative values of GC_p.
5. Each component shall be designed for maximum positive and negative pressures.
6. Coefficients are for roofs with angle $\theta \le 10°$. For other roof angles and geometry, use GC_p values from Fig. 30.4-2A, B and C and attendant q_h based on exposure defined in Section 26.7.
7. If a parapet equal to or higher than 3 ft (0.9m) is provided around the perimeter of the roof with $\theta \le 10°$, Zone 3 shall be treated as Zone 2.
8. Notation:
   a: 10 percent of least horizontal dimension, but not less than 3 ft (0.9 m).
   h: Mean roof height, in feet (meters), except that eave height shall be used for $\theta \le 10°$.
   z: height above ground, in feet (meters).
   θ: Angle of plane of roof from horizontal, in degrees.

Appendix A 5: External peak pressure coefficients on roofs and walls in ASCE 7-16 (Height > 60 ft)

Diagrams

ROOF PLAN   WALL ELEVATION

Notation

a = 10% of least horizontal dimension, but not less than 3 ft (0.9 m).
h = Mean roof height, in ft (m). except that eave height shall be used for $\theta \leq 10°$.
z = Height above ground, in ft (m).
θ = Angle of plane of roof from horizontal, in degrees.

External Pressure Coefficients

Notes

1. Vertical scale denotes (GC_p) to be used with appropriate q_z or q_h.
2. Horizontal scale denotes effective wind area A, in ft^2 (m^2)
3. Plus and minus signs signify pressures acting toward and away from the surfaces, respectively.
4. Use q_z with positive values of (GC_p) and q_h with negative values of (GC_p).
5. Each component shall be designed for maximum positive and negative pressures.
6. Coefficients are for roofs with angle $\theta \leq 7°$. For other roof angles and geometry, use (GC_p) values from Fig. 30.3-2A–2I and Fig. 30.3-5A,5B and attendant q_h based on exposure defined in Section 26.7.
7. If a parapet equal to or higher than 3 ft (0.9 m) is provided around the perimeter of the roof with $\theta \leq 10°$, Zone 3 shall be treated as Zone 2.

112

Appendix B

Contours of mean and peak pressure coefficients of the 5 m (16 ft) height building for all wind directions

Appendix B 1: 0° wind direction in exposure C and exposure B.

Appendix B 2: 15° wind direction in exposure C and exposure B.

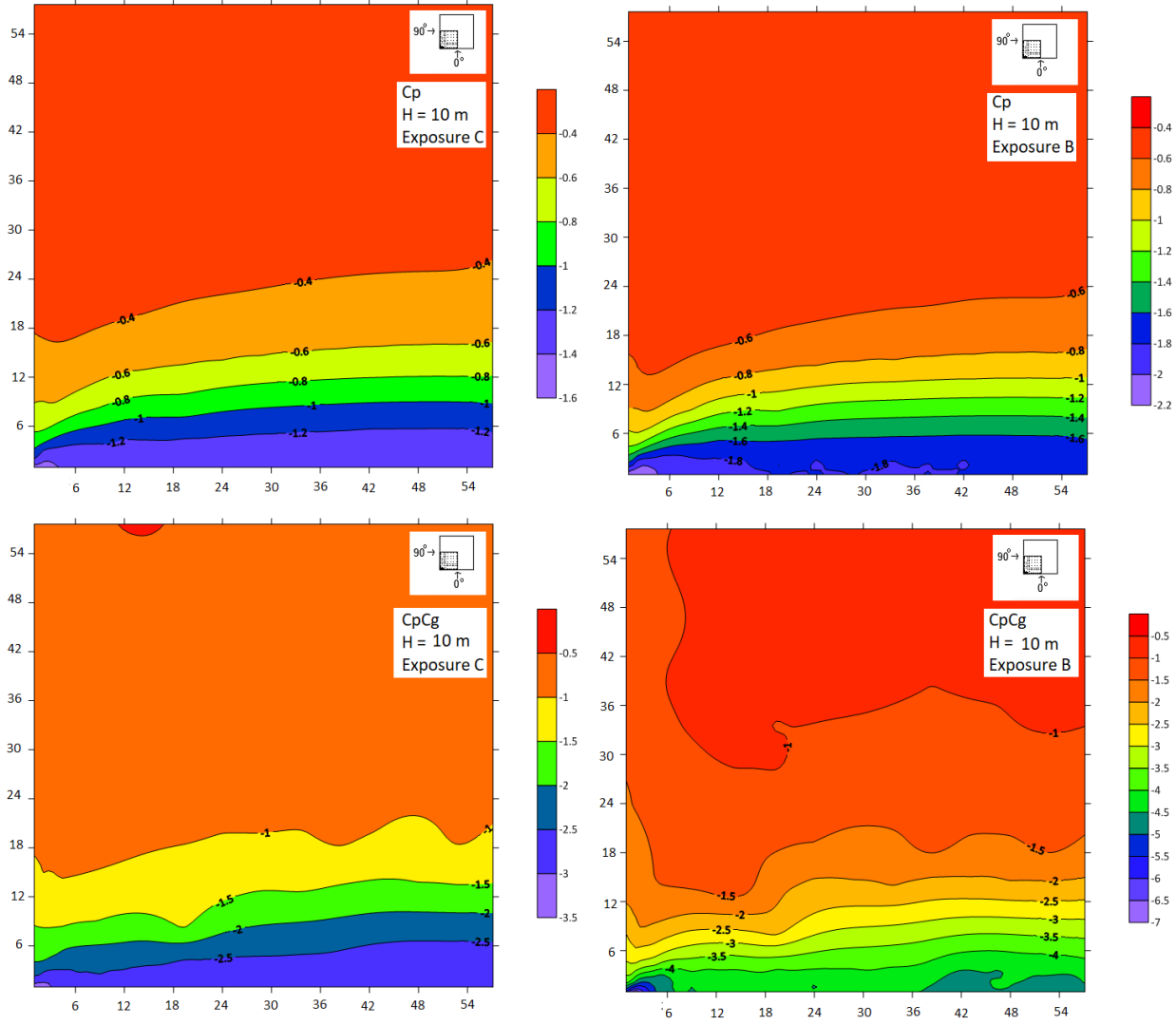**Appendix B 3:** 30° wind direction in exposure C and exposure B.

Appendix B 4: 45° wind direction in exposure C and exposure B.

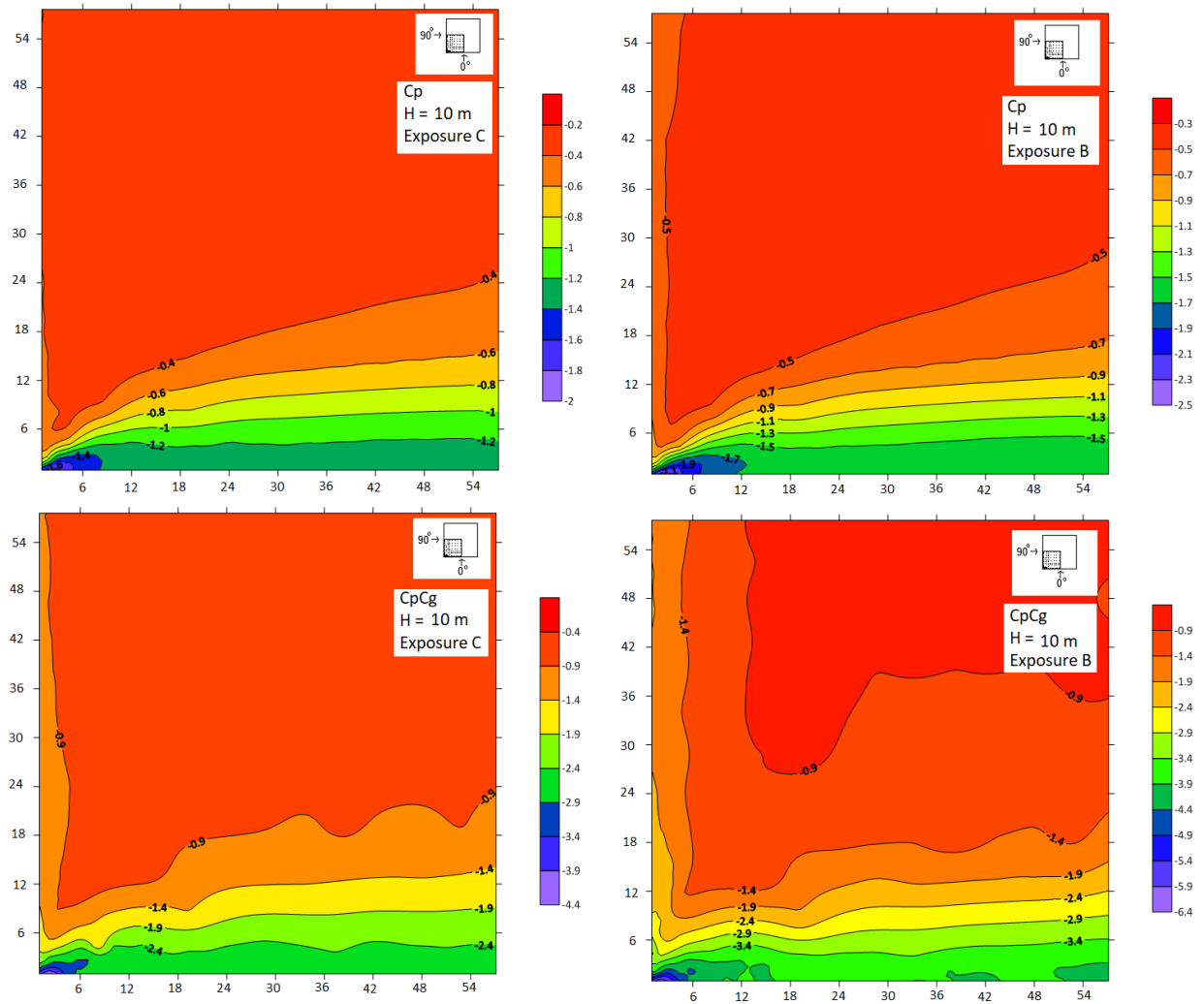**Appendix B 5:** 60° wind direction in exposure C and exposure B.

Appendix B 6: 75° wind direction in exposure C and exposure B.

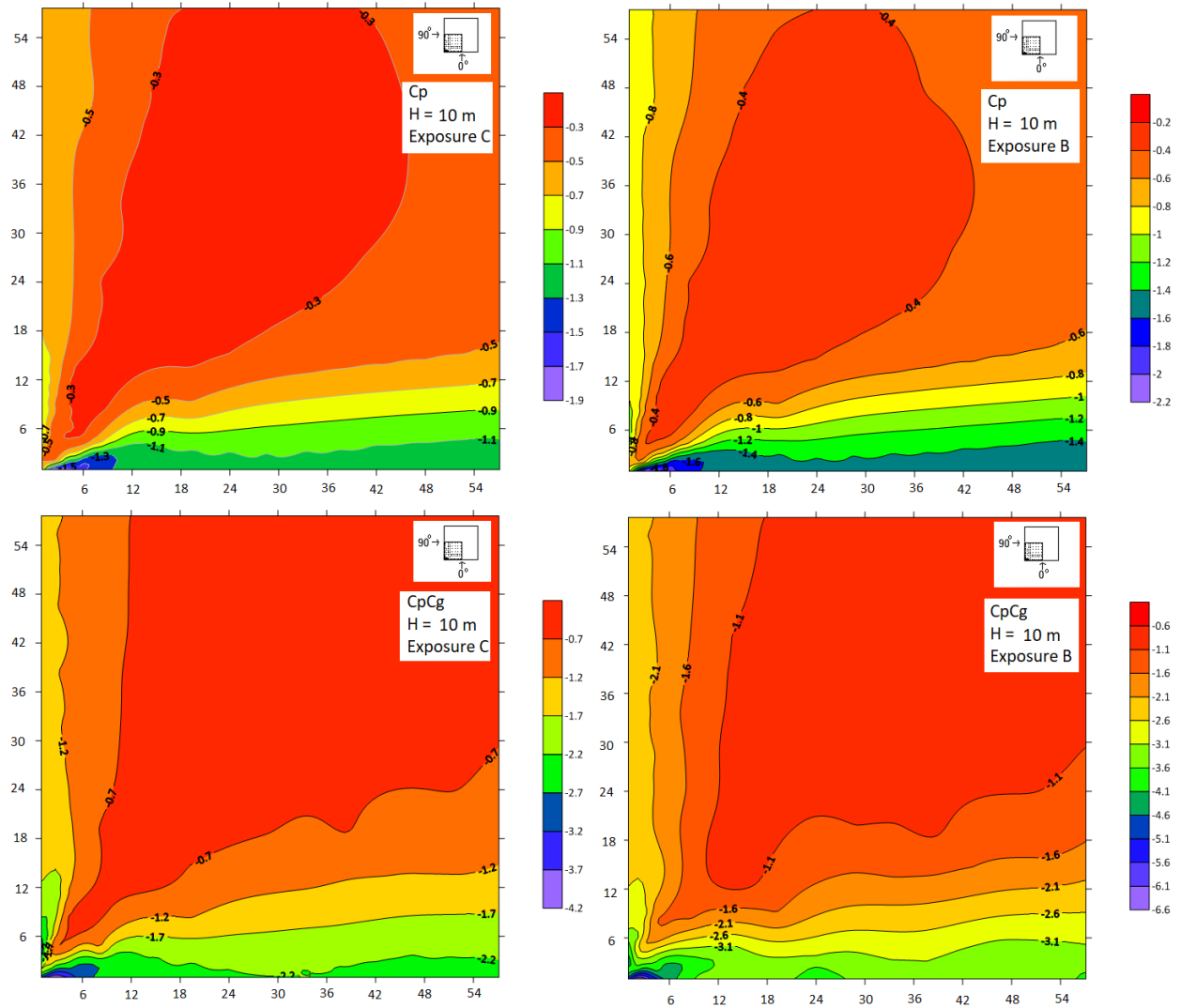**Appendix B 7:** 90° wind direction in exposure C and exposure B.

Appendix B 1: Contours of mean and peak pressure coefficients for 0° wind direction in exposure C and exposure B.

114
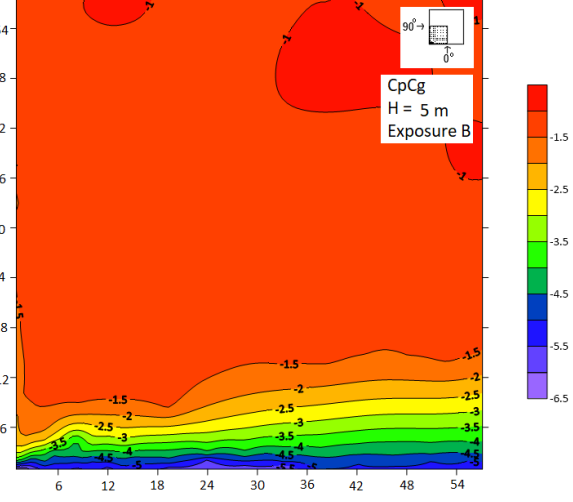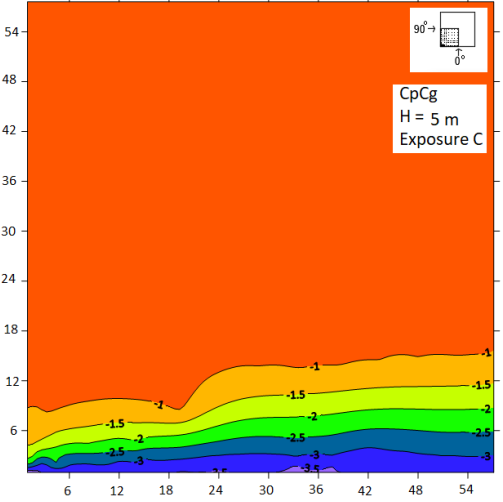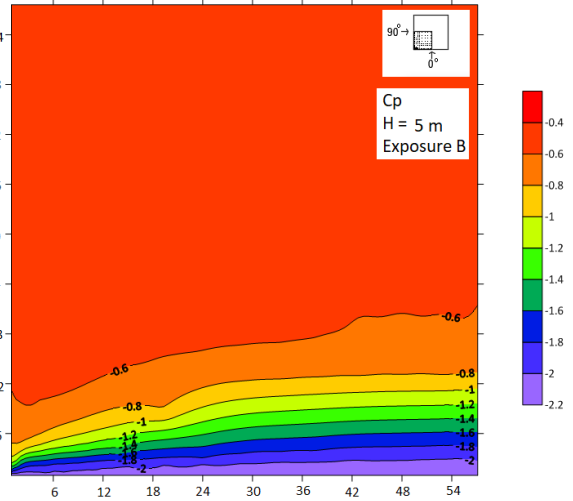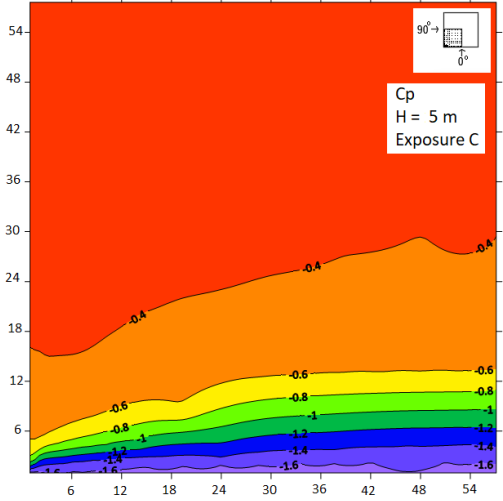
Appendix B 2: Contours of mean and peak pressure coefficients for 15° wind direction in exposure C and exposure B.
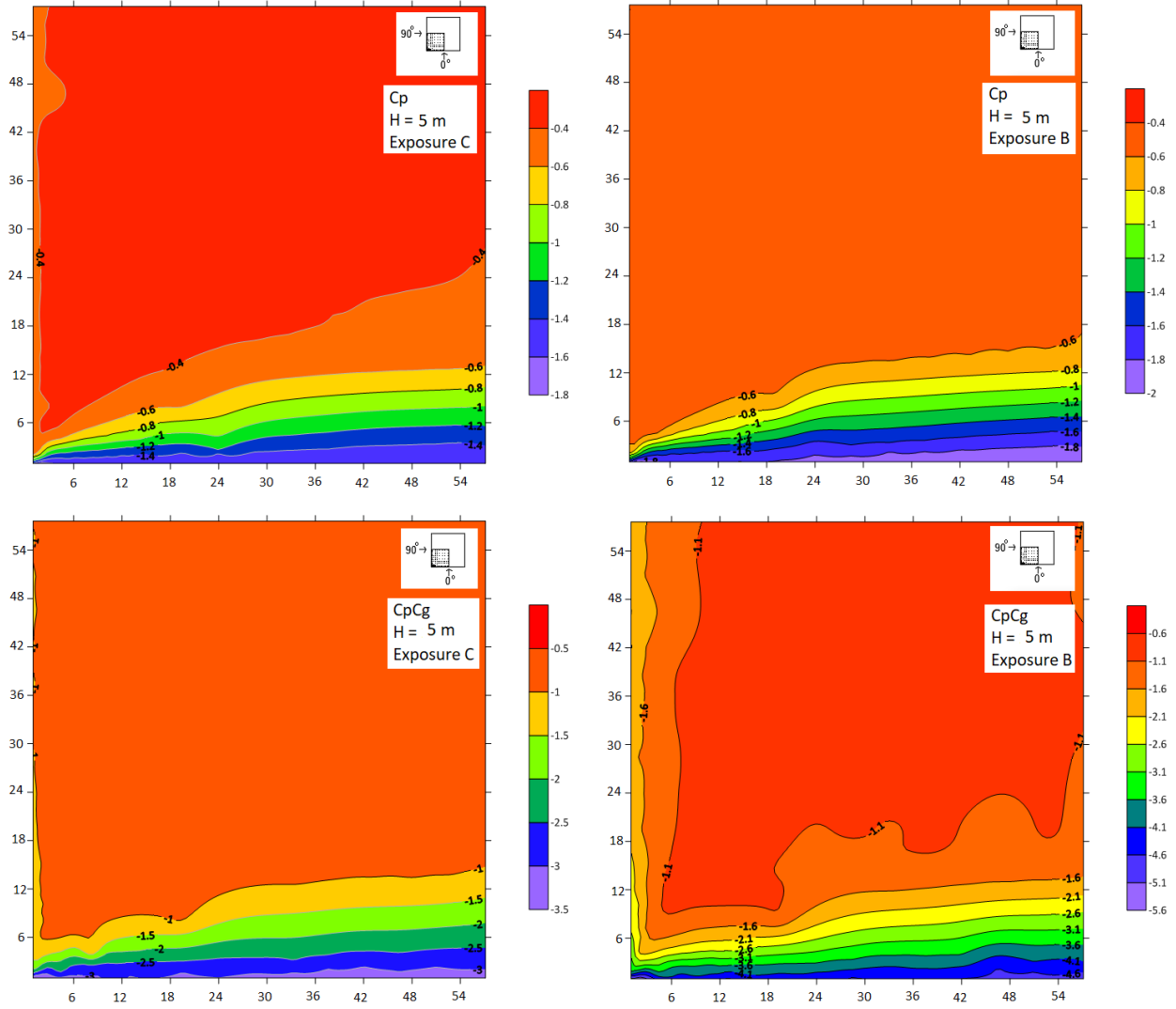
Appendix B 3: Contours of mean and peak pressure coefficients for 30° wind direction in exposure C and exposure B.
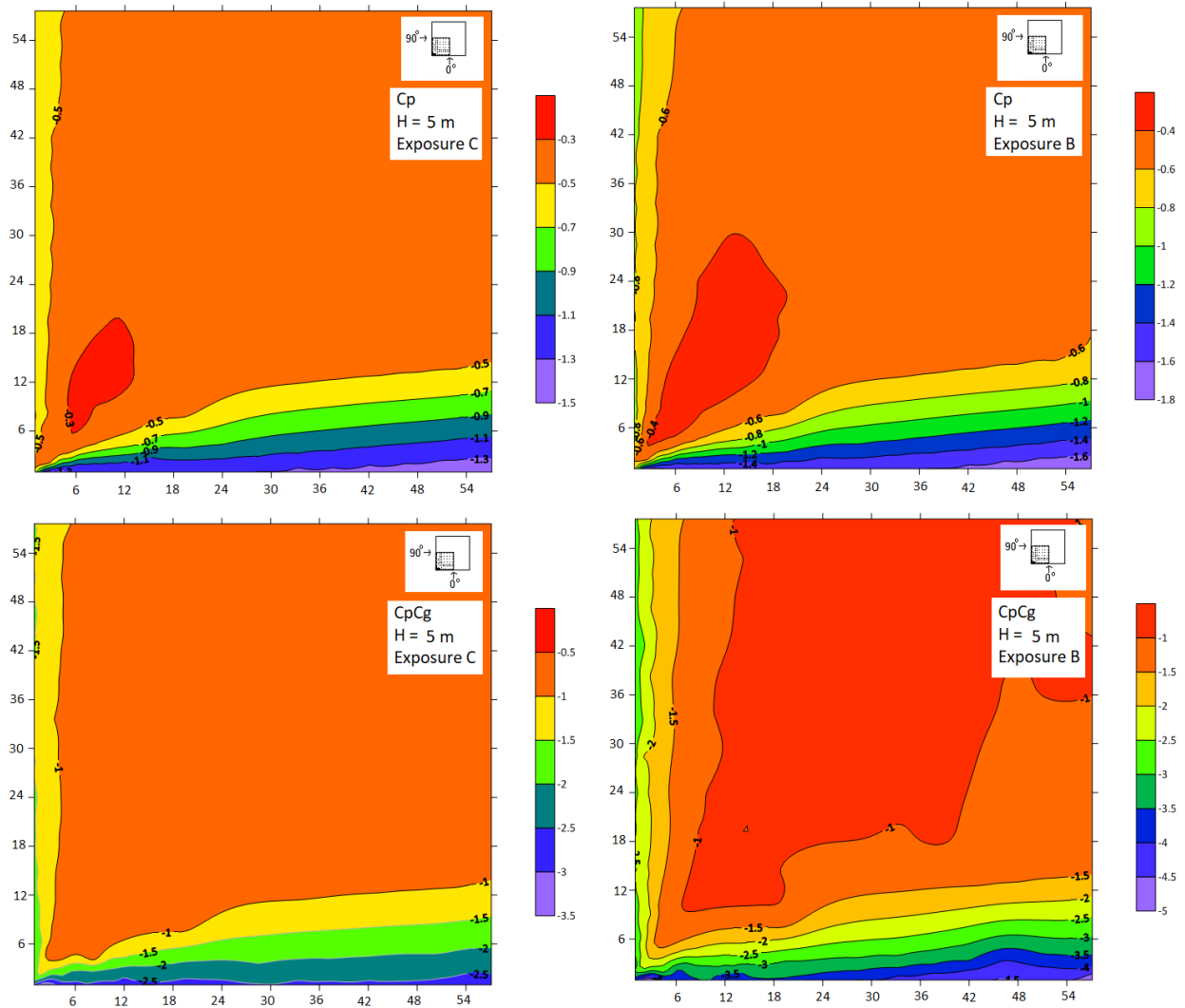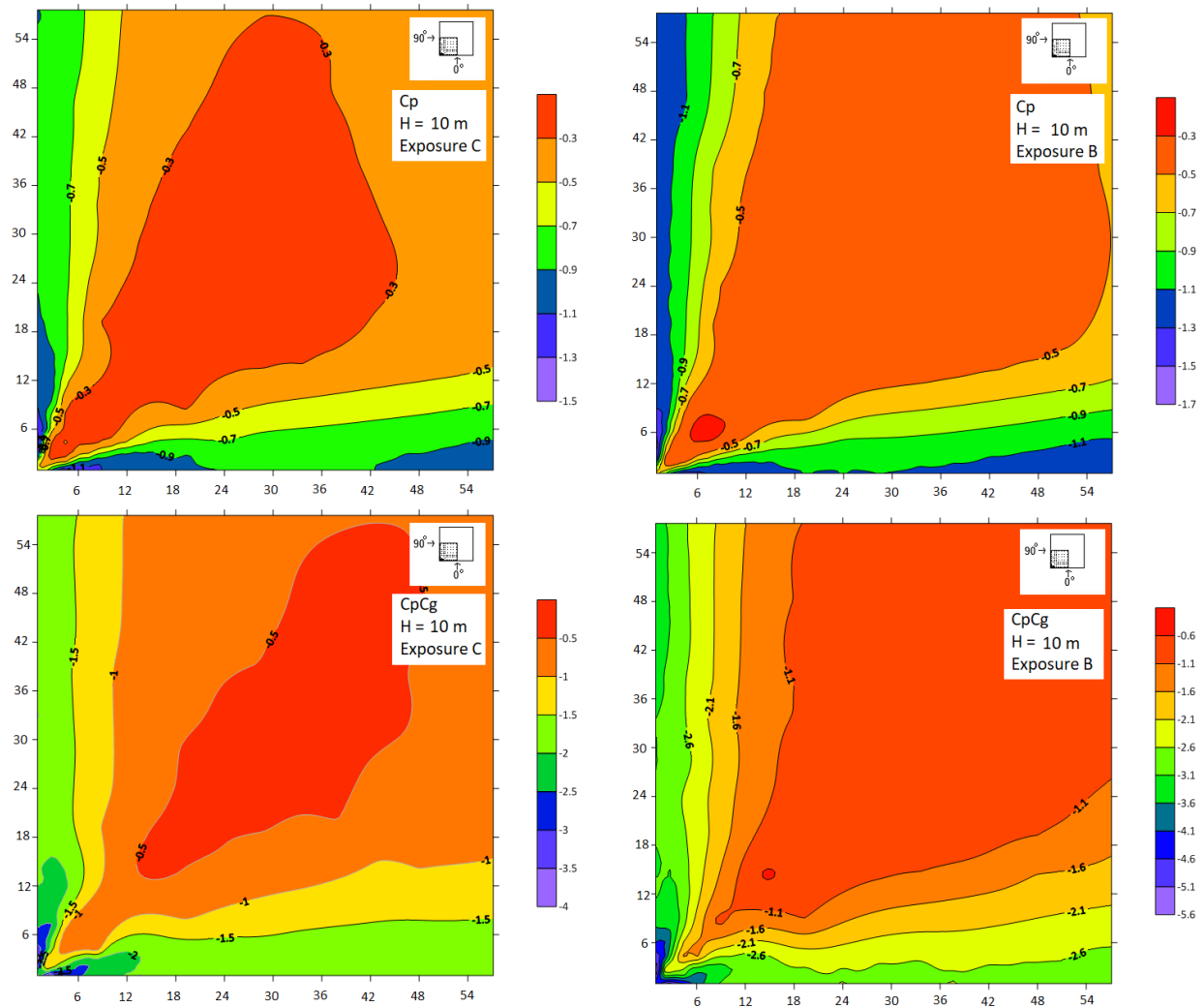
Appendix B 4: Contours of mean and peak pressure coefficients for 45° wind direction in exposure C and exposure B.
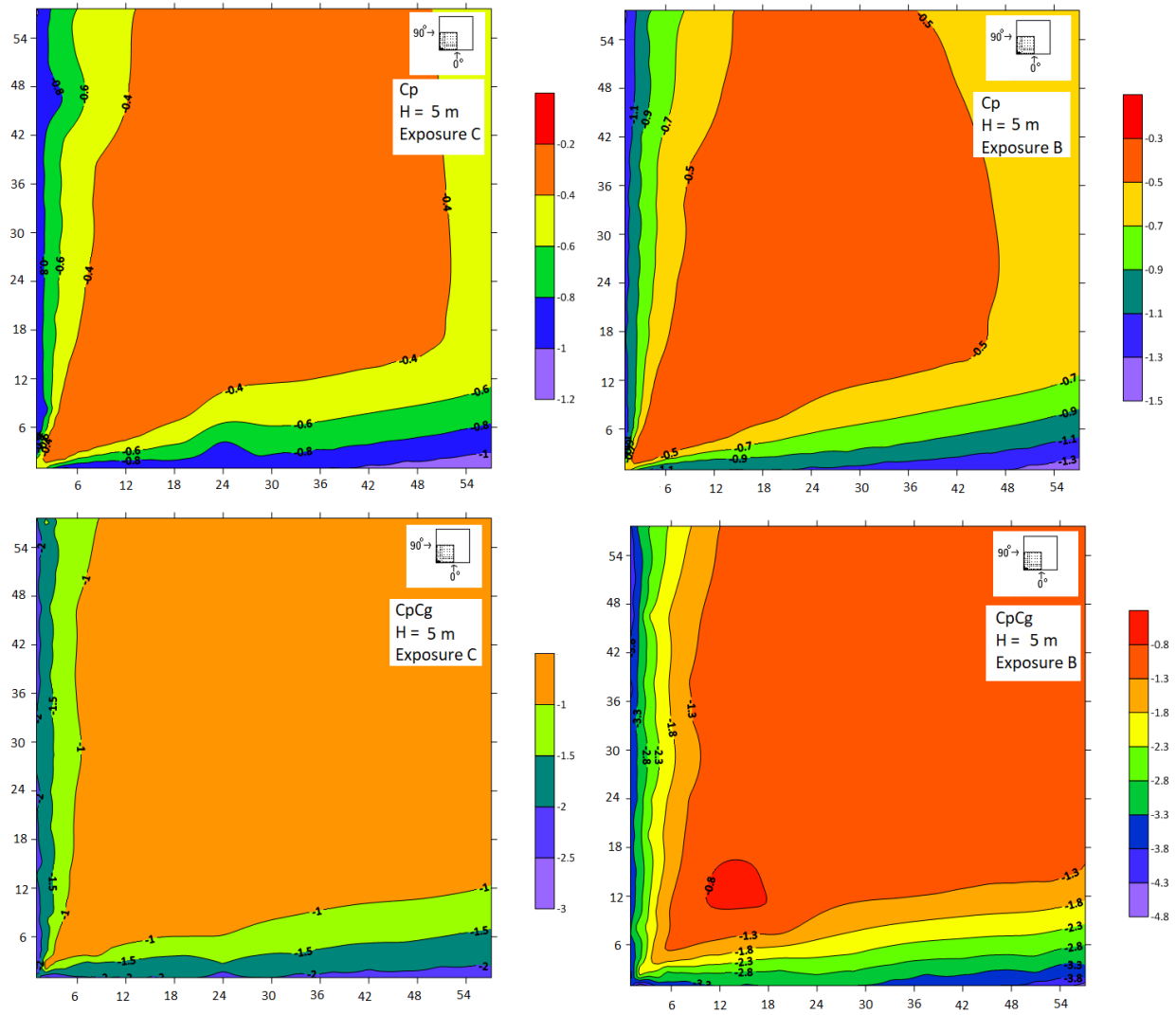
Appendix B 5: Contours of mean and peak pressure coefficients for 60° wind direction in exposure C and exposure B.
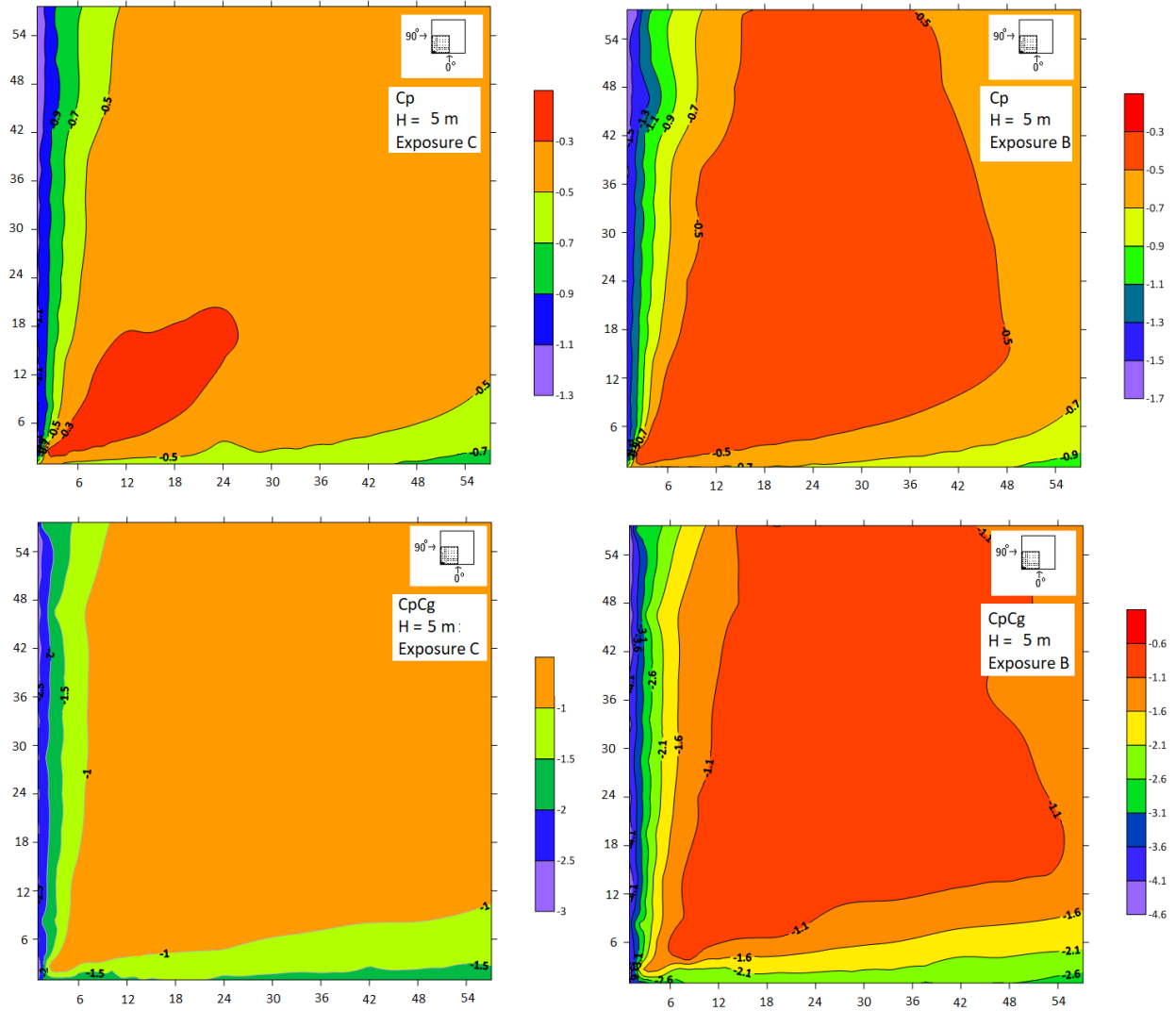
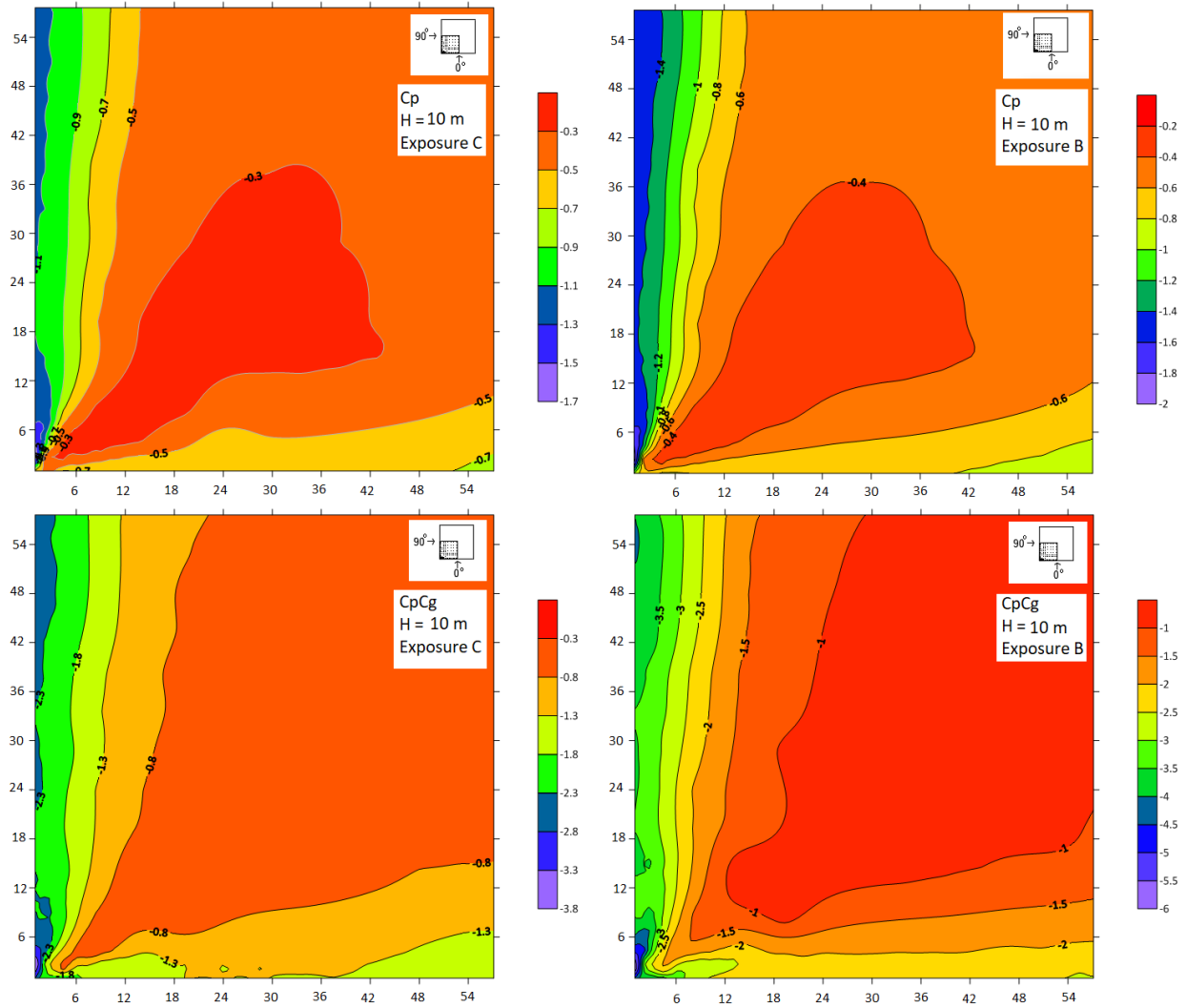Appendix B 6: Contours of mean and peak pressure coefficients for 75° wind direction in exposure C and exposure B.
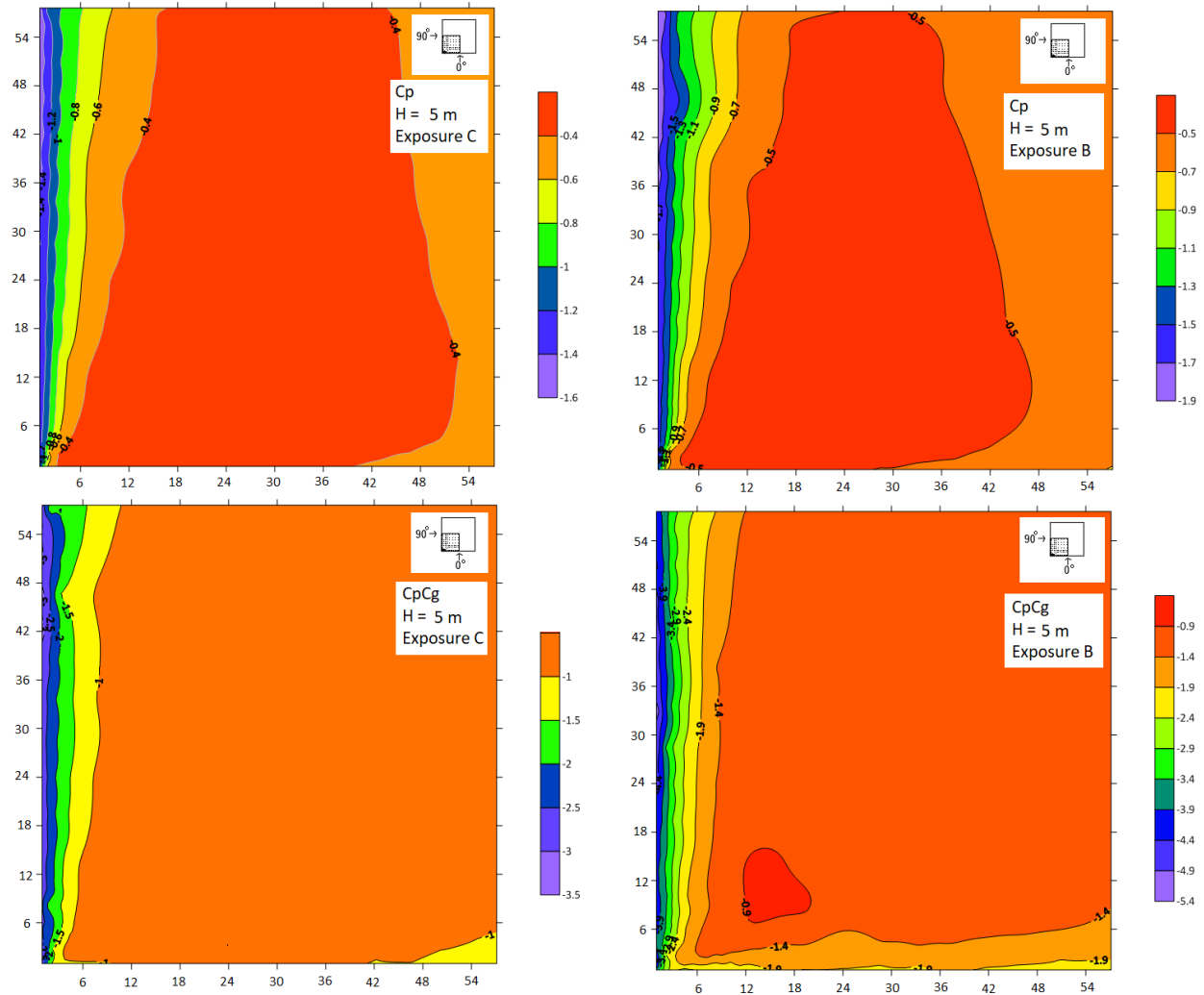
Appendix B 7: Contours of mean and peak pressure coefficients for 90° wind direction in exposure C and exposure B.
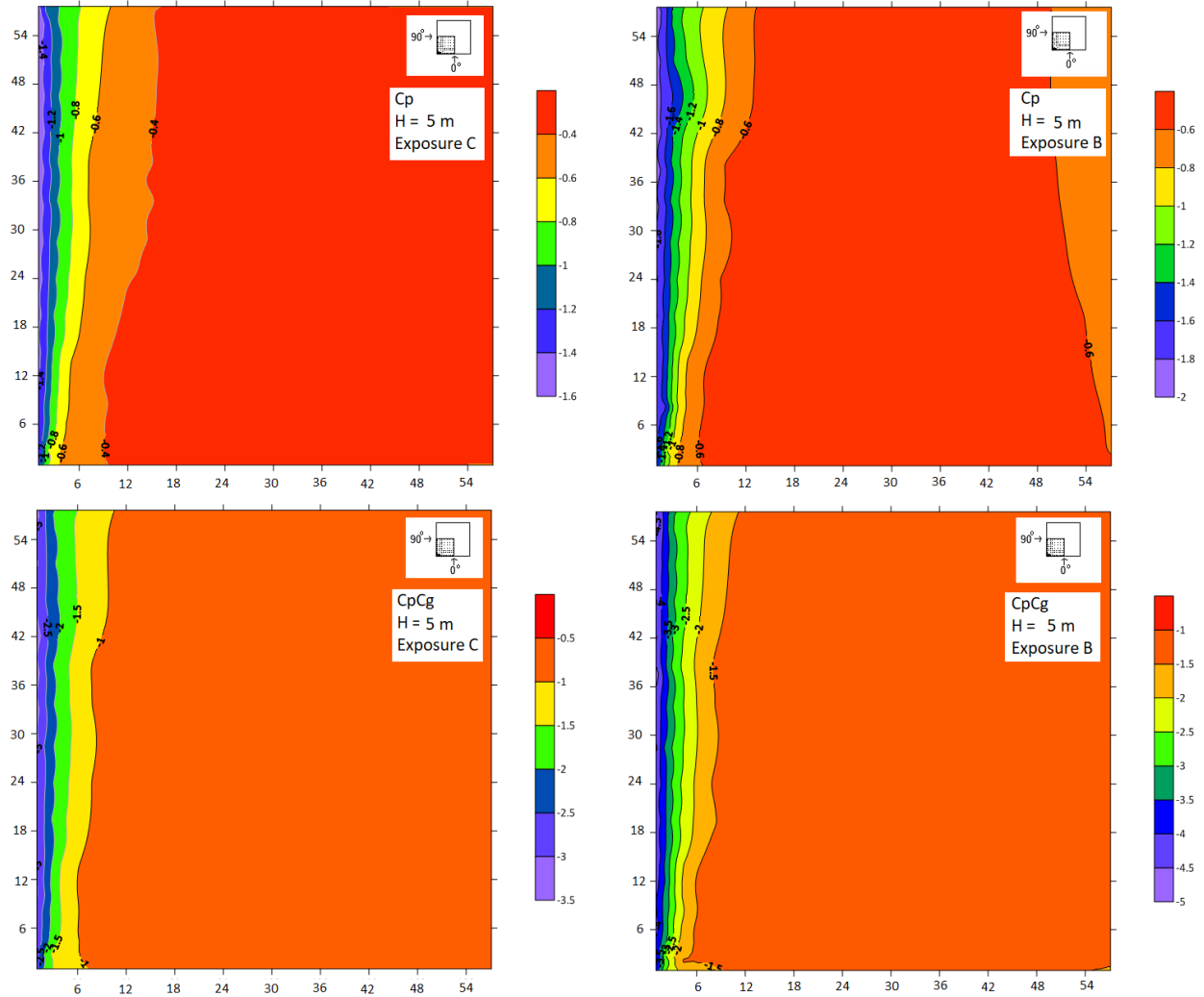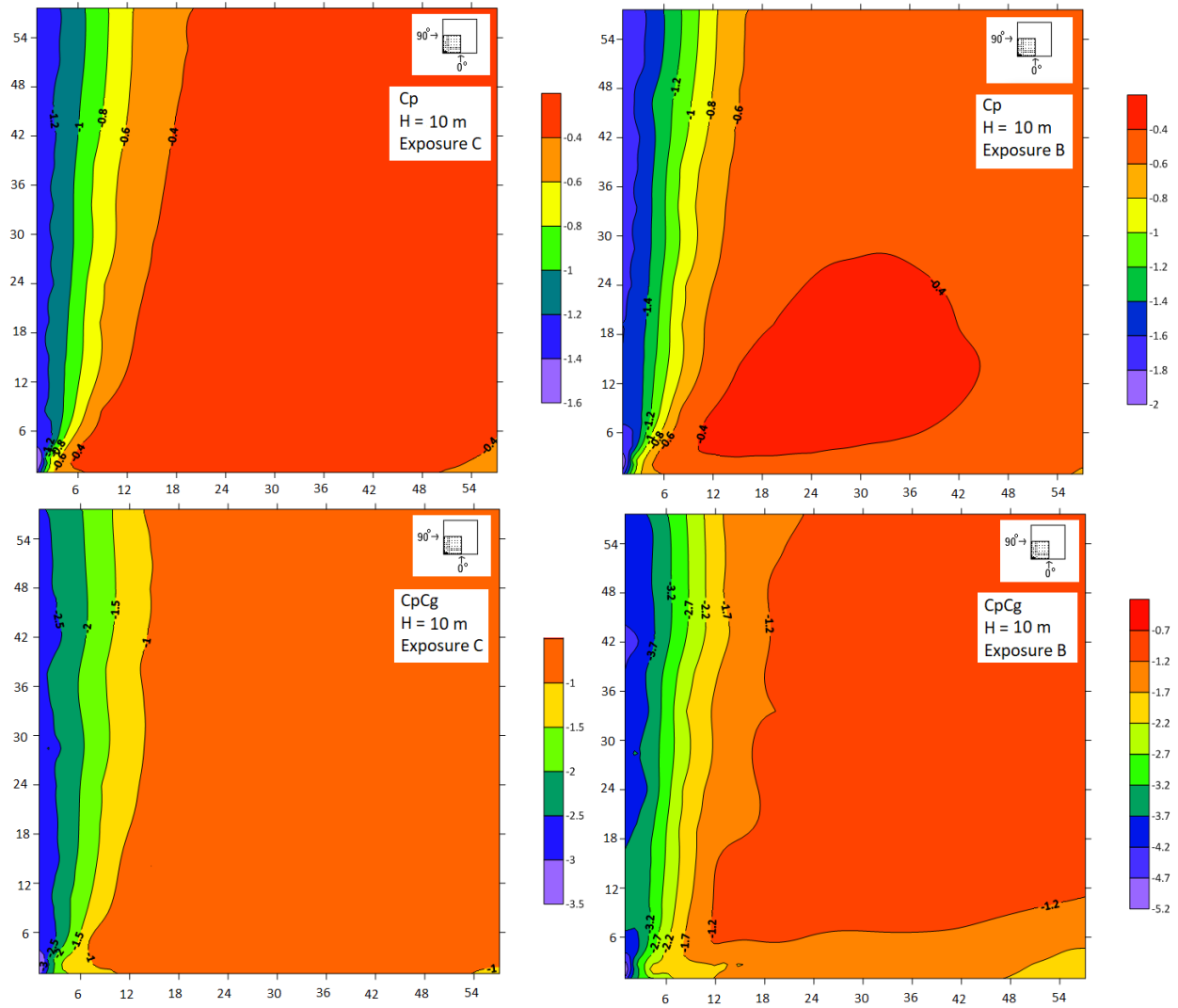
Appendix C

Contours of mean and peak pressure coefficients of the 10 m (32 ft) height building for all wind directions

Appendix C 1: 0° wind direction in exposure C and exposure B.

Appendix C 2: 15° wind direction in exposure C and exposure B.

Appendix C 3: 30° wind direction in exposure C and exposure B.

Appendix C 4: 45° wind direction in exposure C and exposure B.

Appendix C 5: 60° wind direction in exposure C and exposure B.

Appendix C 6: 75° wind direction in exposure C and exposure B.

Appendix C 7: 90° wind direction in exposure C and exposure B.

Appendix C 1: Contours of mean and peak pressure coefficients for 0° wind direction in exposure C and exposure B.

Appendix C 2: Contours of mean and peak pressure coefficients for 15° wind direction in exposure C and exposure B.
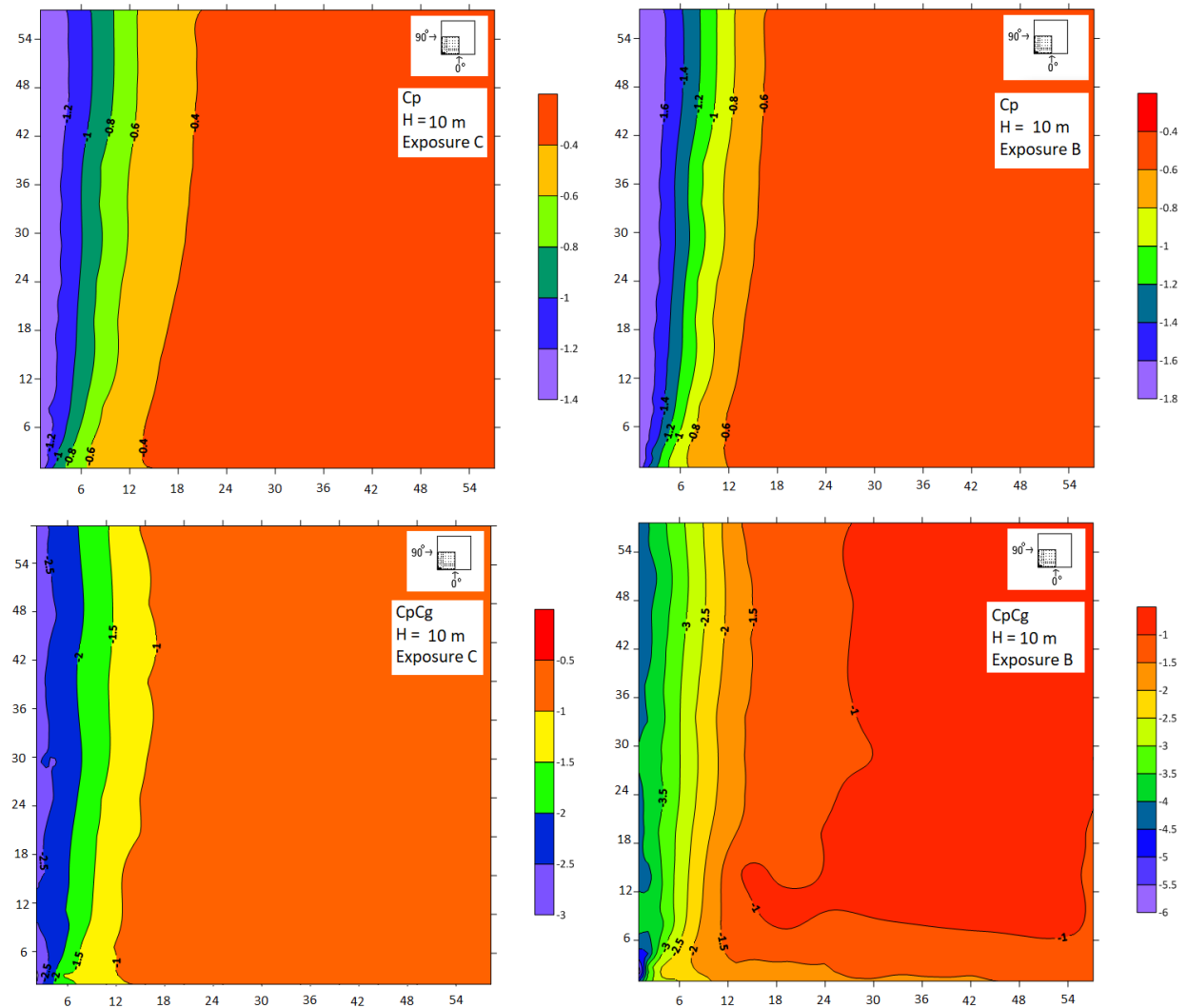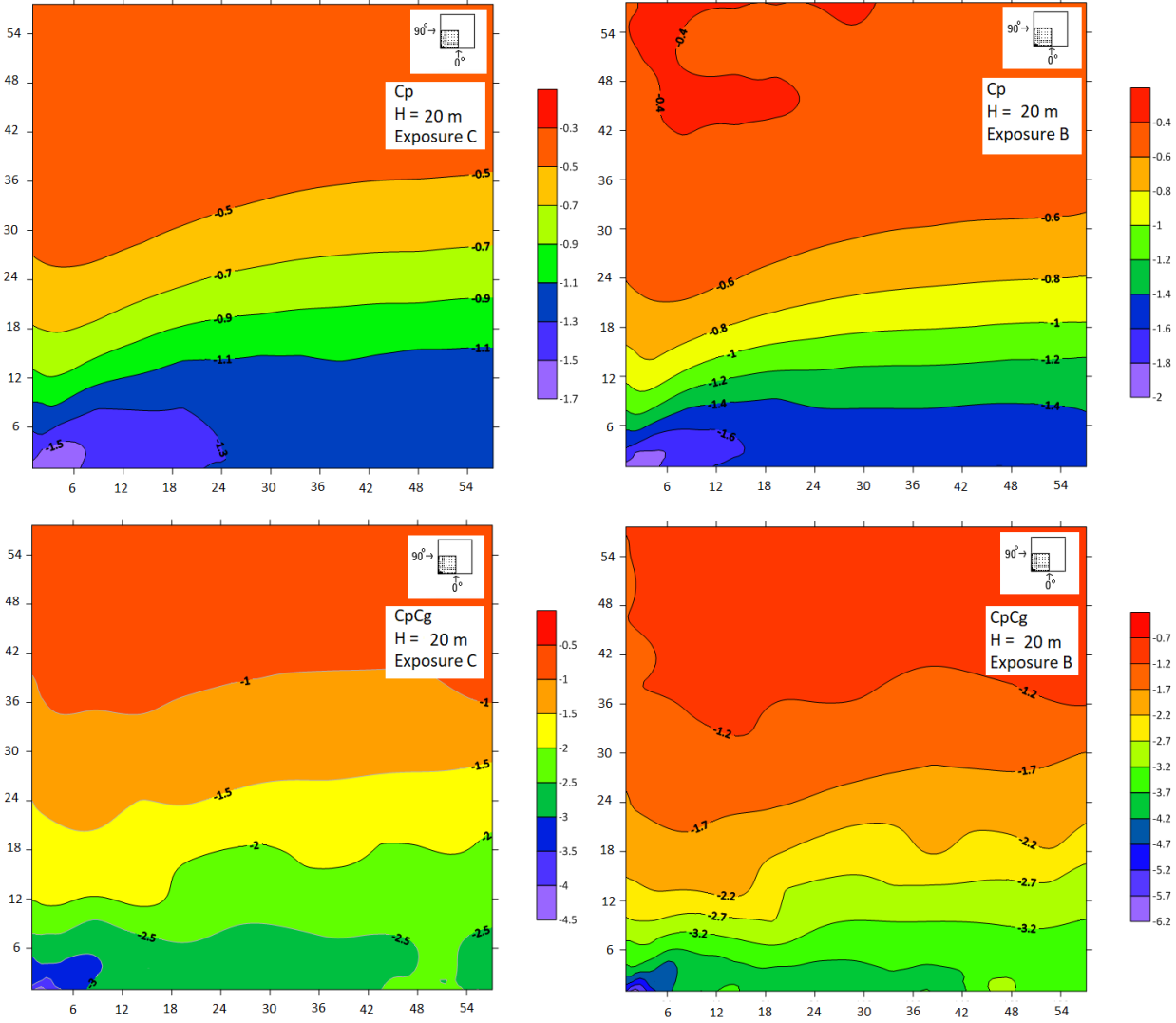
Appendix C 3: Contours of mean and peak pressure coefficients for 30° wind direction in exposure C and exposure B.

Appendix C 4: Contours of mean and peak pressure coefficients for 45° wind direction in exposure C and exposure B.

Appendix C 5: Contours of mean and peak pressure coefficients for 60° wind direction in exposure C and exposure B.

Appendix C 6: Contours of mean and peak pressure coefficients for 75° wind direction in exposure C and exposure B.

Appendix C 7: Contours of mean and peak pressure coefficients for 90° wind direction in exposure C and exposure B.

Appendix D

Contours of mean and peak pressure coefficients of the 20 m (64 ft) height building for all wind directions

Appendix D 1: 0° wind direction in exposure C and exposure B.

Appendix D 2: 15° wind direction in exposure C and exposure B.

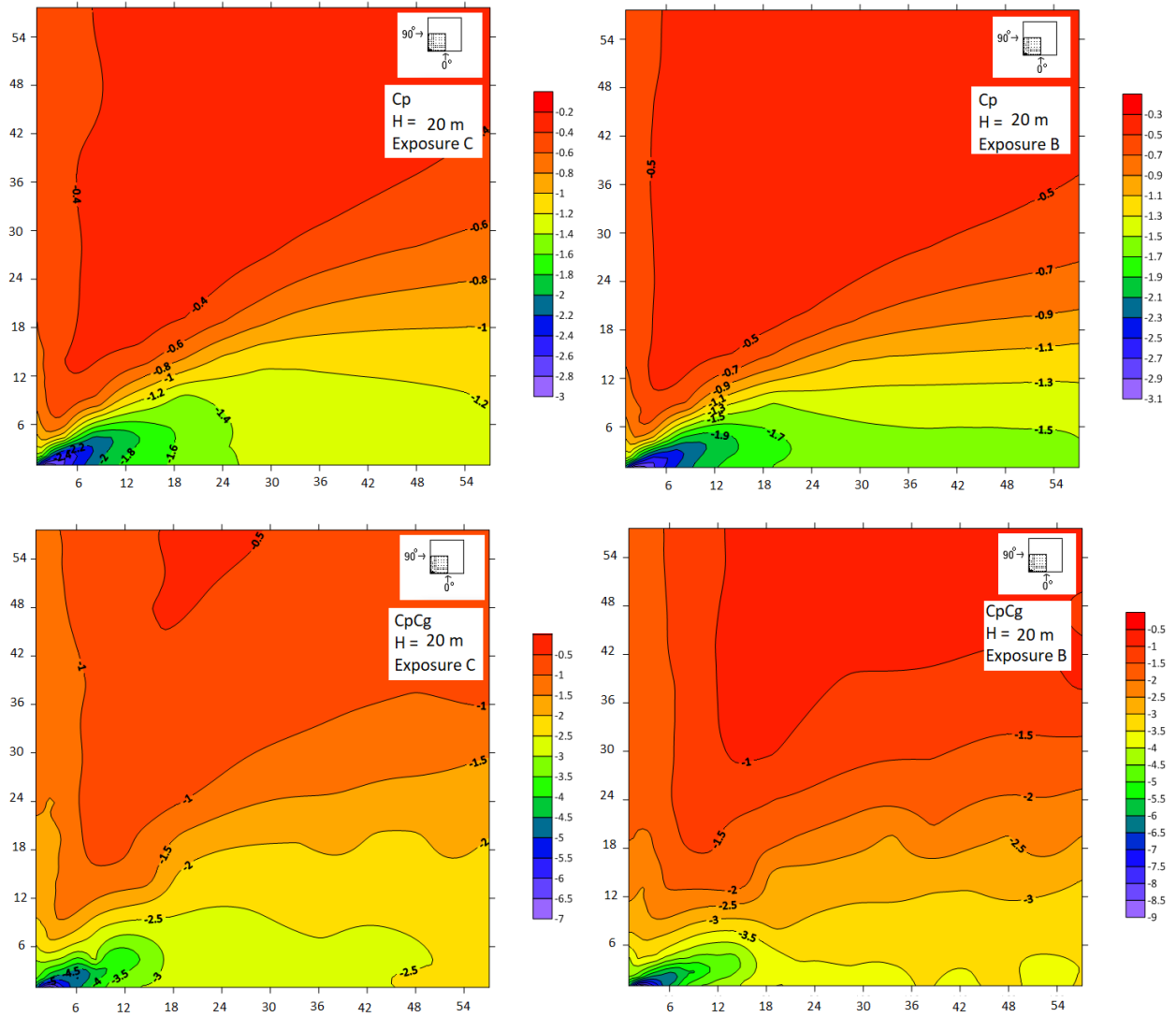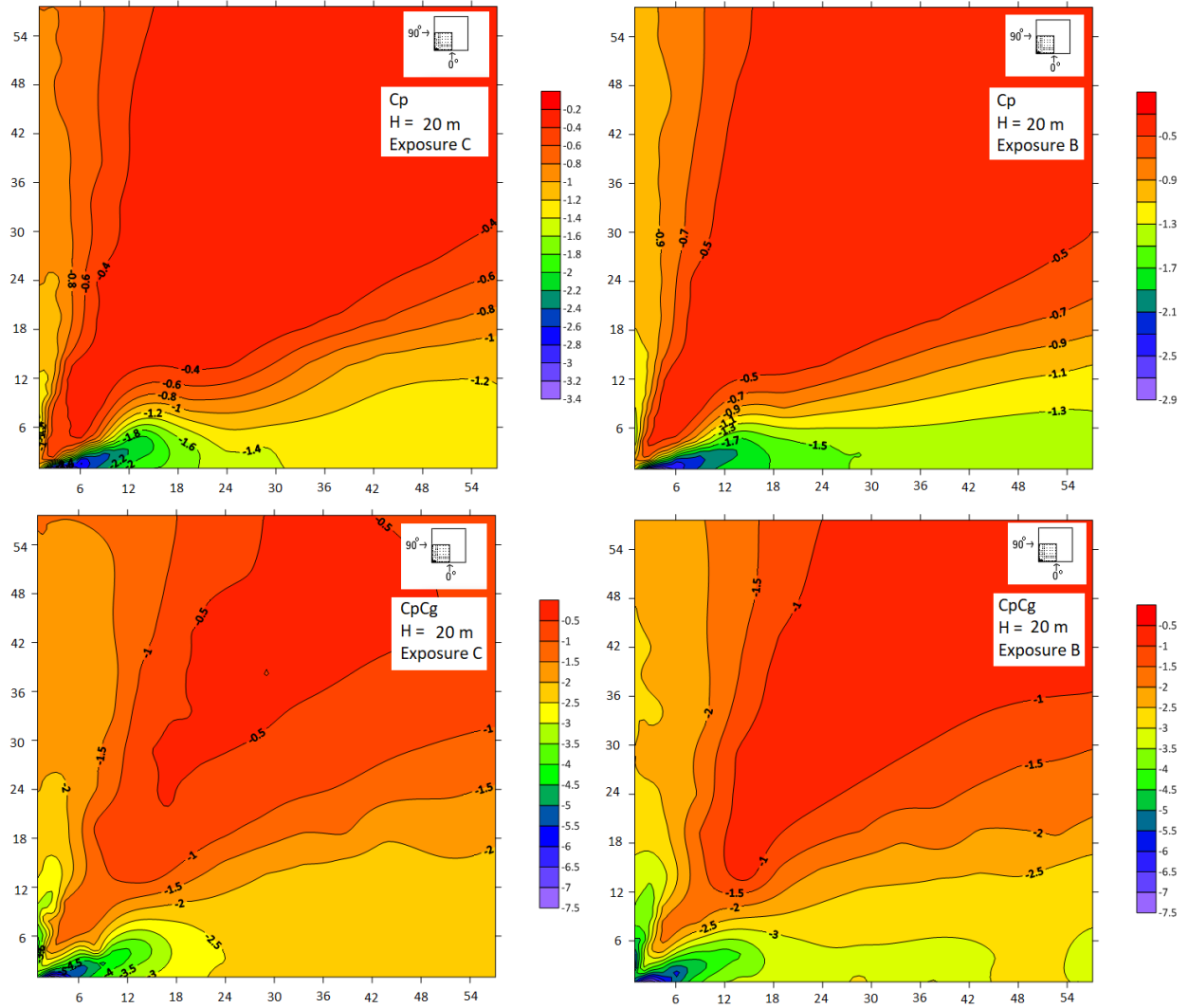**Appendix D 3:** 30° wind direction in exposure C and exposure B.

Appendix D 4: 45° wind direction in exposure C and exposure B.

Appendix D 5: 60° wind direction in exposure C and exposure B.

Appendix D 6: 75° wind direction in exposure C and exposure B.

Appendix D 7: 90° wind direction in exposure C and exposure B.

Appendix D 1: Contours of mean and peak pressure coefficients for 0° wind direction in exposure C and exposure B.
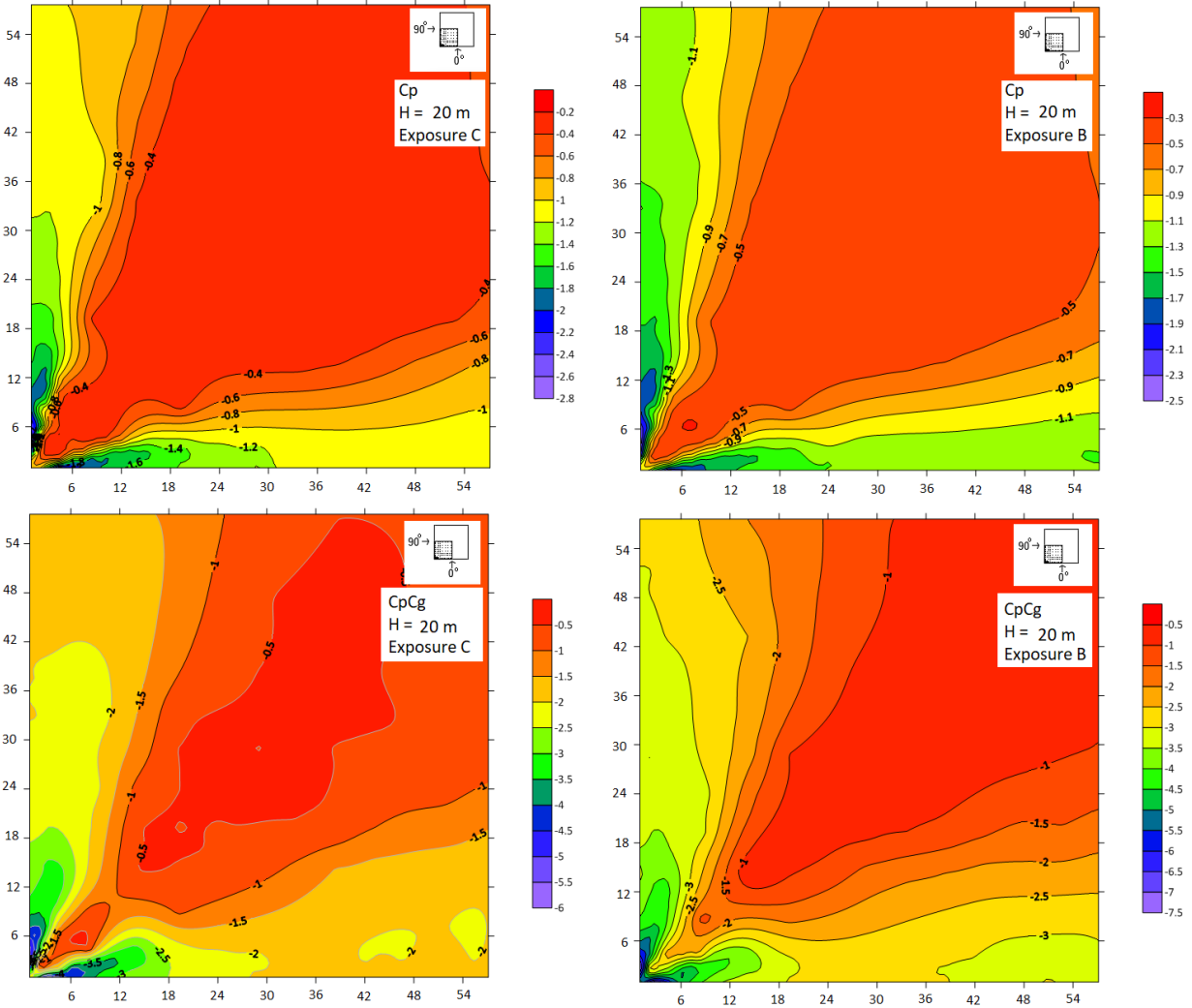
Appendix D 2: Contours of mean and peak pressure coefficients for 15° wind direction in exposure C and exposure B.
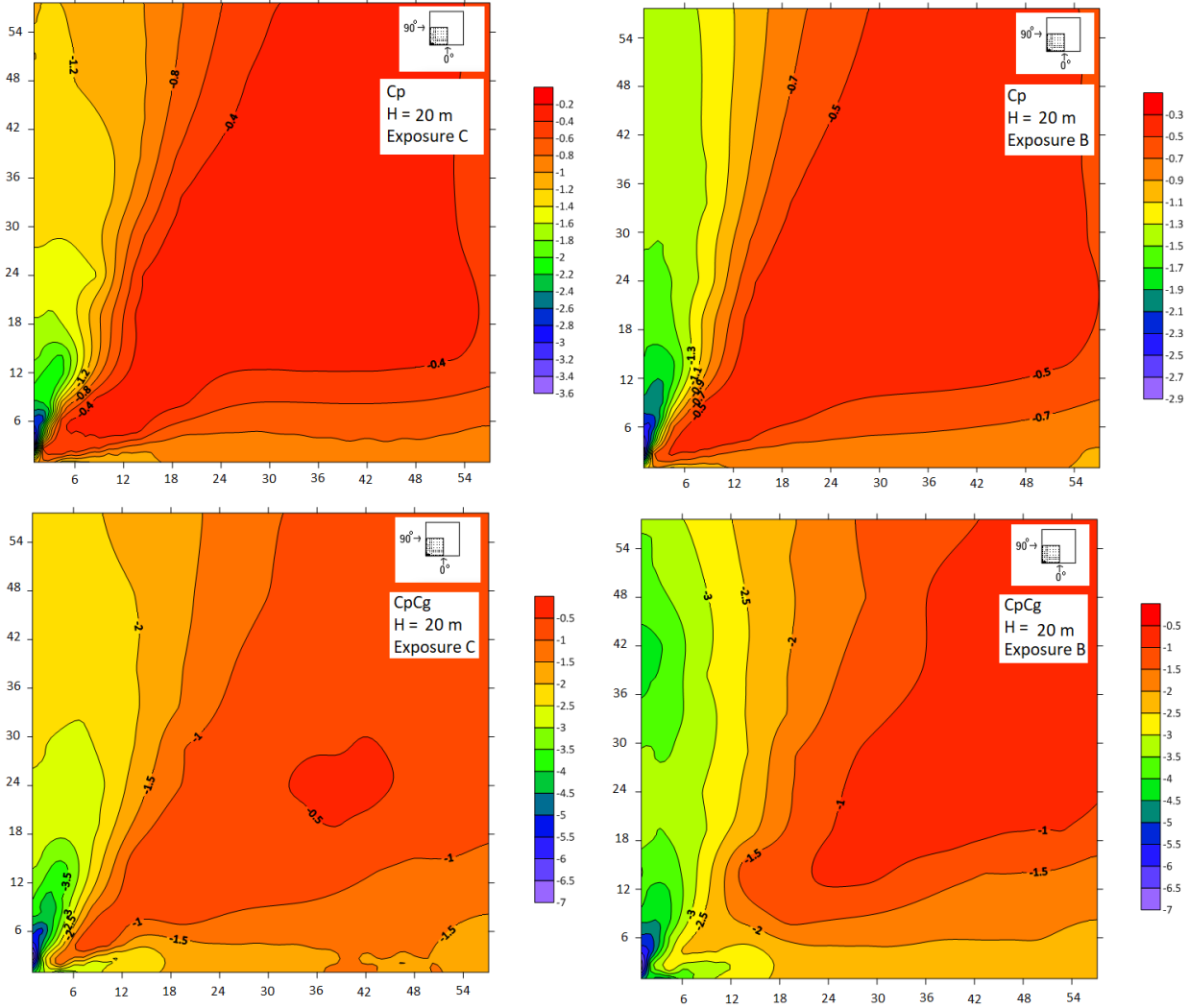
Appendix D 3: Contours of mean and peak pressure coefficients for 30° wind direction in exposure C and exposure B.
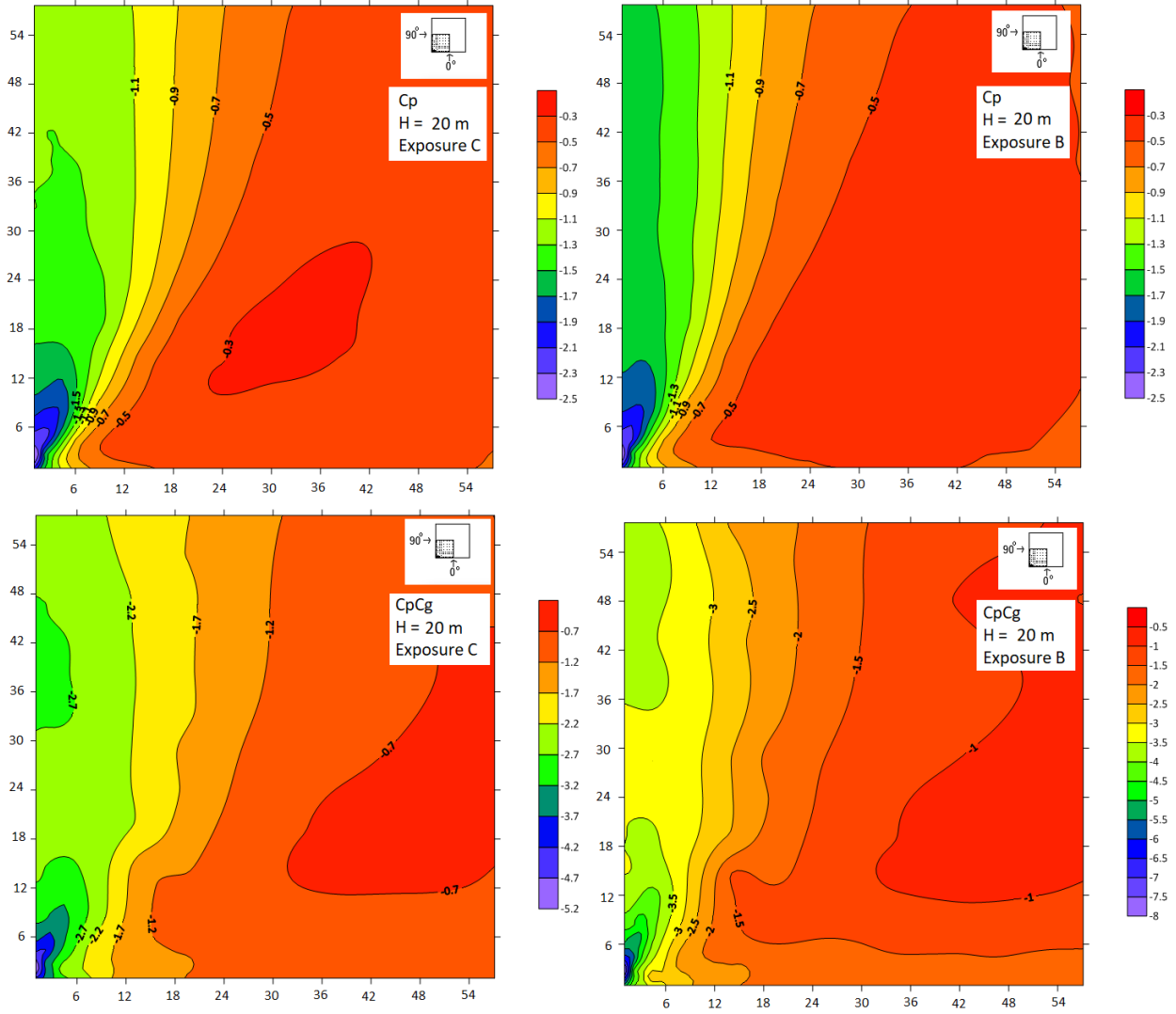
Appendix D 4: Contours of mean and peak pressure coefficients for 45° wind direction in exposure C and exposure B.

Appendix D 5: Contours of mean and peak pressure coefficients for 60° wind direction in exposure C and exposure B.

Appendix D 6: Contours of mean and peak pressure coefficients for 75° wind direction in exposure C and exposure B.

Appendix D 7: Contours of mean and peak pressure coefficients for 90° wind direction in exposure C and exposure B.